ฟลูออเรสเซนต์เซ็นเซอร์จากไดเฟนิลแอเซทิลีนแบบกิ่ง

นางสาวณัฐพร กิมพิทักษ์

วิทยานิพนธ์นี้เป็นส่วนหนึ่งของการศึกษาตามหลักสูตรปริญญาวิทยาศาสตรมหาบัณฑิต
สาขาวิชาปิโตรเคมีและวิทยาศาสตร์พอลิเมอร์
คณะวิทยาศาสตร์ จุฬาลงกรณ์มหาวิทยาลัย
ปีการศึกษา 2554

FLUORESCENT SENSORS FROM BRANCHED DIPHENYLACETYLENES

Miss Nattaporn Kimpitak

A Thesis Submitted in Partial Fulfillment of the Requirements
for the Degree of Master of Science Program in Petrochemistry and Polymer Science
Faculty of Science
Chulalongkorn University
Academic Year 2011

Thesis Title	FLUORESCENT SENSORS FROM BRANCHED DIPHENYLACETYLENES
By	Miss Nattaporn Kimpitak
Field of Study	Petrochemistry and Polymer Science
Thesis Advisor	Associate Professor Mongkol Sukwattanasinitt, Ph.D.
Thesis Co-advisor	Assistant Professor Paitoon Rashatasakhon, Ph.D.

Accepted by the Faculty of Science, Chulalongkorn University in Partial Fulfillment of the Requirements for the Master's Degree

…….. Dean of the Faculty of Science
(Professor Supot Hannongbua, Dr.rer.nat.)

THESIS COMMITTEE

…….. Chairman
(Assistant Professor Warinthorn Chavasiri, Ph.D.)

…….……. Thesis Advisor
(Associate Professor Mongkol Sukwattanasinitt, Ph.D.)

…….……. Thesis Co-advisor
(Assistant Professor Paitoon Rashatasakhon, Ph.D.)

…….. Examiner
(Associate Professor Nuanphun Chantarasiri, Ph.D.)

…….. External Examiner
(Gamolwan Tumcharern, Ph.D.)

ณัฐพร กิมพิทักษ์ : ฟลูออเรสเซนต์เซ็นเซอร์จากไดเฟนิลแอเซทิลีนแบบกิ่ง (FLUORESCENT SENSORS FROM BRANCHED DIPHENYLACETYLENES) อ.ที่ปรึกษาวิทยานิพนธ์หลัก : รศ.ดร.มงคล สุขวัฒนาสินทธิ์, อ.ที่ปรึกษาวิทยานิพนธ์ร่วม : ผศ.ดร.ไพฑูรย์ รัชตะสาคร, 96 หน้า.

ฟลูออโรฟอร์ใหม่ 5 ตัว ที่ประกอบด้วยกิ่งฟีนิลลีนเอไทนิลีน มีหมู่ปลายเป็นซาลิไซลิกแอซิด (F2-F5) และไทรเมทิลแอมโมเนียม (4N$^+$Cl$^-$) ได้ถูกสังเคราะห์ขึ้น เพื่อนำมาใช้เป็นตัวตรวจวัดสารเคมีและสารทางชีวโมเลกุล ฟลูออโรฟอร์ที่มีหมู่ซาลิไซลิกแอซิด 3 หมู่ (F4) แสดงการตอบสนองต่อการระงับสัญญาณการเรืองแสงโดยไอออนของทองแดงได้ดีที่สุดในระบบน้ำ และมีค่าคงที่ของการระงับการเรืองแสง (K_{SV}) เท่ากับ 5.79 × 10^6 M^{-1} การเตรียมตัวตรวจวัดไอออนของทองแดงบนพื้นผิวของกระดาษที่มีฟลูออโรฟอร์ดังกล่าว สามารถตรวจวัดไอออนของทองแดงในระดับพิโคโมลได้ด้วยตาเปล่า โมเลกุลเรืองแสงที่ประกอบด้วยหมู่ไทรเมทิลแอมโมเนียม 4 หมู่ (4N$^+$Cl$^-$) มีอันตรกิริยากับสายดีเอ็นเอในสารละลายบัฟเฟอร์ ที่มีค่า pH 7.4 ฟลูออโรฟอร์มีสัญญาณการเรืองแสงเพิ่มขึ้นเมื่อเกิดอันตรกิริยากับสายดีเอ็นเอ เนื่องจากการลดลงของกระบวนการจีโอเมทริคัลรีแลกซีชัน และกระบวนการคอลลิชันนอลเซลฟ์เควนชิ่ง อันตรกิริยาระหว่างฟลูออโรฟอร์และสายดีเอ็นเอ จะเกิดผ่านการถ่ายเทพลังงานแบบฟอร์สเตอร์เรโซแนนส์ระหว่างฟลูออโรฟอร์และสายดีเอ็นเอ เมื่อในระบบมีสีย้อมเรืองแสงทางการค้า (SyBrGreen)

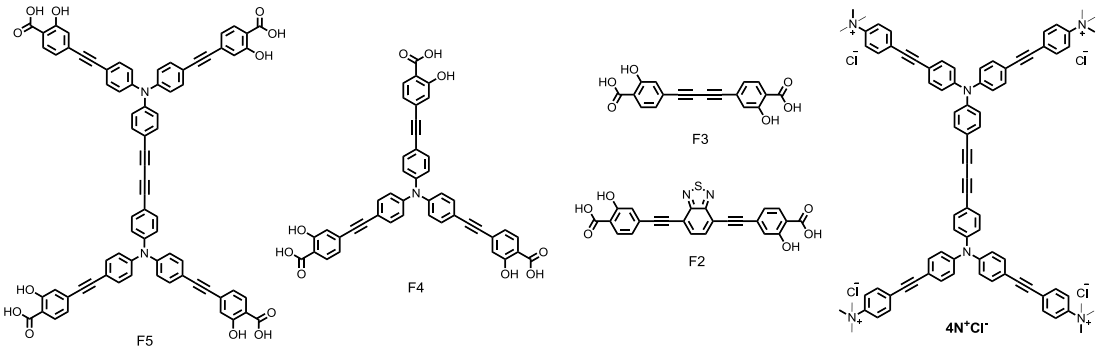

สาขาวิชาปิโตรเคมีและวิทยาศาสตร์พอลิเมอร์ ลายมือชื่อนิสิต .....

ปีการศึกษา 2554 ลายมือชื่อ อ.ที่ปรึกษาวิทยานิพนธ์หลัก .....

ลายมือชื่อ อ.ที่ปรึกษาวิทยานิพนธ์ร่วม .....

5273415423 : MAJOR PETROCHEMISTRY AND POLYMER SCIENCE
KEYWORDS : METAL SENSOR / DIPHENYLACETYLENE

NATTAPORN KIMPITAK: FLUORESCENT SENSORS FROM BRANCHED DIPHENYLACETYLENES. ADVISOR: ASSOC. PROF. MONGKOL SUKWATTANASINITT, Ph.D. CO-ADVISOR: ASSIS. PROF. PAITOON RASHATASAKHON, Ph.D., 96 pp.

Five new fluorophores containing phenylene-ethynylene branches with salicylic acid (**F2**-**F5**) and trimethylammonium (**4N$^+$Cl$^-$**) termini were synthesized and evaluated as chemical and biological sensors. The tribranched fluorophore (**F4**) with salicylic acid termini exhibited the highest Cu^{2+} quenching sensitivity in aqueous solution; $K_{sv} = 5.79 \times 10^6\ M^{-1}$. The paper-based sensor fabricated from this compound allows picomole detection of Cu^{2+} by naked eye. The tetrabranched fluorophore (**4N$^+$Cl$^-$**) with trimethylammonium termini can bind with DNA in aqueous buffered solution pH 7.4. Upon DNA binding, the fluorescent signal of the fluorophore increases presumably due to the reduction of geometrical relaxation and collisional self-quenching processes. The interaction between the fluorophore and DNA were useful for FRET detection of DNA sequences via DNA/DNA hybridization in the presence of SyBrGreen commercial fluorescence dye.

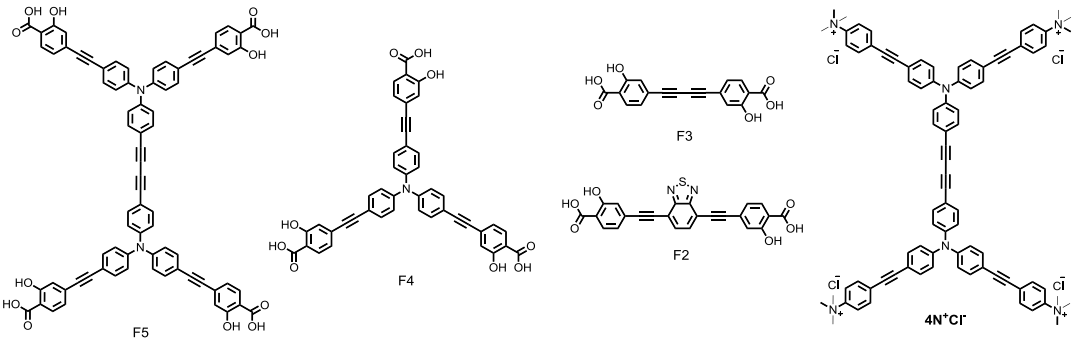

Field of Study : Petrochemistry and Polymer Science Student's Signature .....

Academic Year : 2011 Advisor's Signature .....

Co-advisor's Signature .....

ACKNOWLEDGEMENTS

I wish to express my deep gratitude to my advisor, Associate Professor Dr. Mongkol Sukwattanasinitt, my co-advisor Assistant Professor Dr. Paitoon Rashatasakhon for their generous advice, invaluable guidance and encouragement throughout the course of this research.

I would like to gratefully acknowledge the committee, Assistant Professor Dr. Warinthorn Chavasiri, Associate Professor Dr. Nuanphun Chantarasiri and Dr. Gamolwan Tumcharern for their comments, guidance and extending cooperation over my presentation. I would like to thank Dr. Anawat Ajavakom and Assistant Professor Dr. Sumrit Wacharasindhu for their attention and suggestions during our research group meeting. I would like to express my gratitude to Material Advancement via Proficient Synthesis (MAPS Group), Department of Chemistry, Faculty of Science, Chulalongkorn University for providing the chemicals and facilities throughout the course of study.

A deep affectionate gratitude is acknowledged to my beloved family for their understanding, encouragement and support throughout the education course. I especially thank Dr. Nakorn Niamnont, Ms. Warathip Siripornnoppakhun, Ms. Kanokthorn Boonkitpatarakul and Mr. Akachai Khumsri for their suggestions and guidance. I would like to thank all of my friends for their friendship, especially Mr. Watcharin Ngampueng, Ms. Wanwisa Thongmalai, Ms. Daranee Homraruen, Ms. Wannapa Yuanboonlim and Mr. Pharkphoom Auttapornpitak for their help during the course of my graduate research. Moreover, I would like to thank Mr. Chaiwat Phollookin, Ms. Suricha Pumtang and Ms. Yamonporn Yodta for their suggestions and encouragement.

I would like to thanks Center for Petroleum, Petrochemicals and Advanced Materials, ADB under the Petroleum & Petrochemical Technology Consortium and 100th Anniversary of Chulalongkorn University Fund.

Finally, I would like to express my thankfulness to my beloved parents who always stand by my side during both of my pleasant and hard time.

CONTENTS

CHAPTER **Page**

Page

LIST OF TABLES

LIST OF FIGURES

Figure **Page**

LIST OF SCHEMES

LIST OF ABBREVIATIONS

A	acceptor
Ar	aromatic
calcd	calculated
^{13}C NMR	carbon-13 nuclear magnetic resonance
$CDCl_3$	deuterated chloroform
D	donor
d	doublet (NMR)
dd	doublet of doublet (NMR)
ESIMS	electrospray ionization mass spectrometry
equiv	equivalent (s)
FT-IR	fourier transform infrared spectroscopy
g	gram (s)
^{1}H NMR	proton nuclear magnetic resonance
Hz	Hertz
HRMS	high resolution mass spectrum
h	hour (s)
ICT	internal charge transfer
IR	infrared
J	coupling constant
mg	milligram (s)
mL	milliliter (s)
mmol	millimole (s)
m/z	mass per charge
m	multiplet (NMR)
mp	melting point
MW	molecular weight
M	molar
MHz	megahertz
rt	room temperature
s	singlet (NMR)

THF	tetrahydrofuran
UV	ultraviolet
δ	chemical shift
°C	degree Celsius
µL	microliter (s)
µM	micromolar (s)
Φ	quantum yield
% yield	percentage yield

CHAPTER I

INTRODUCTION

1.1 Fluorescence

The fluorescence is an emission process occurring after a molecule absorbs light energy, which could be depicted using the Jablonski diagram (Figure. 1) [1]. When the molecule is given a certain amount of light energy or photons (orange arrows), its energy level increases to reach a state called “excited state”. The excited molecule is unstable and will rapidly relax or release the energy in order to return to the lower electronic state (green arrows). The energy can be discharged in a form of thermal (heat) or kinetic energy (molecular rotation and vibration). These non-radiative processes are called “internal conversion”, which do not result in emission of light. For fluorescent compounds, the excited molecule will temporarily reside at the lowest electronic excited state (S_1) known as a semi-stable state. Eventually, an amount of energy in a form of light will be released as the fluorescence signal (blue arrows).

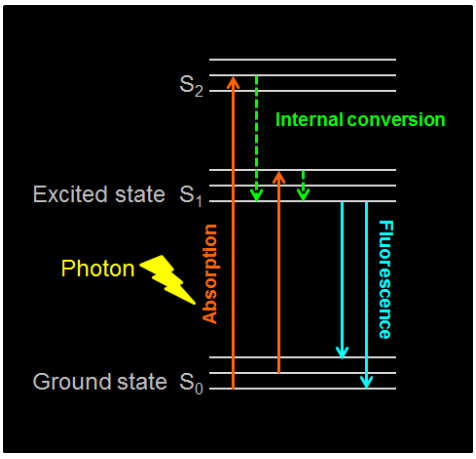

Figure 1.1 Jablonski diagram

1.2 Fluorescent chemosensor

Fluorescence phenomenon is used as a detection method in many chemical, biological, and medical researches. It provides several advantages over other spectroscopic methods such as simplicity, high selectivity, and sensitivity. Nowadays, ion recognition plays an important role in a wide range of biological metabolisms. For the purpose of detection and quantitative determination of ions, much effort has been devoted to develop the appropriate chemosensors. Most of the fluorescence ion sensors are composed of an ion recognition unit (ionophore) for selective binding of the substrate, while the fluorogenic unit (fluorophore) provides the means of signaling this binding, whether by fluorescence quenching or enhancement. The combination of these two sensory units leads to a term "fluoroionophore". The mechanism which controls the quenching response of a fluoroionophore to substrate binding includes photo-induced electron transfer (PET), photo-induced charge transfer (PCT), fluorescence (Förster) resonance energy transfer (FRET), and excimer/exciplex formation or extinction.

1.3 Fluorescence quenching

Fluorescence quenching refers to any process that decreases the fluorescence intensity of a sample. There are a wide variety of quenching processes that include excited state reactions, molecular rearrangements, ground state complex formation, and energy transfer. Generally, fluorescence quenching has two main different mechanisms, dynamic quenching and static quenching [1]. Dynamic quenching, also called collisional quenching, is controlled by the diffusion rate of the fluorophore and quencher. As shown in **Figure 1.2A top**, dynamic quenching occurs when the excited fluorophore (F*) is deactivated upon a diffusive encounter of quencher (Q) and return to S_0 without emission of a photon, while Q is not chemically altered in the process. On the other hand, **Figure 1.2B top** illustrates the static quenching which results from a formation of non-fluorescent complex between the F and Q (F·Q). When this complex absorbs light, it immediately returns to the ground state without emitting fluorescence. The static quenching occurs in the ground state and its efficiency is related to the association

constant (K_a) for F·Q complexation. Results from experiments at various temperatures could indicate the mode of quenching. For the collisional mode of quenching, the efficiency will be enhanced as the temperature increases since molecule will diffuse at a higher rate (Figure 1.2A bottom). In contrast, the elevated temperature will cause the dissociation of F.Q complex, which results in a lower efficiency for static quenching at higher temperature.

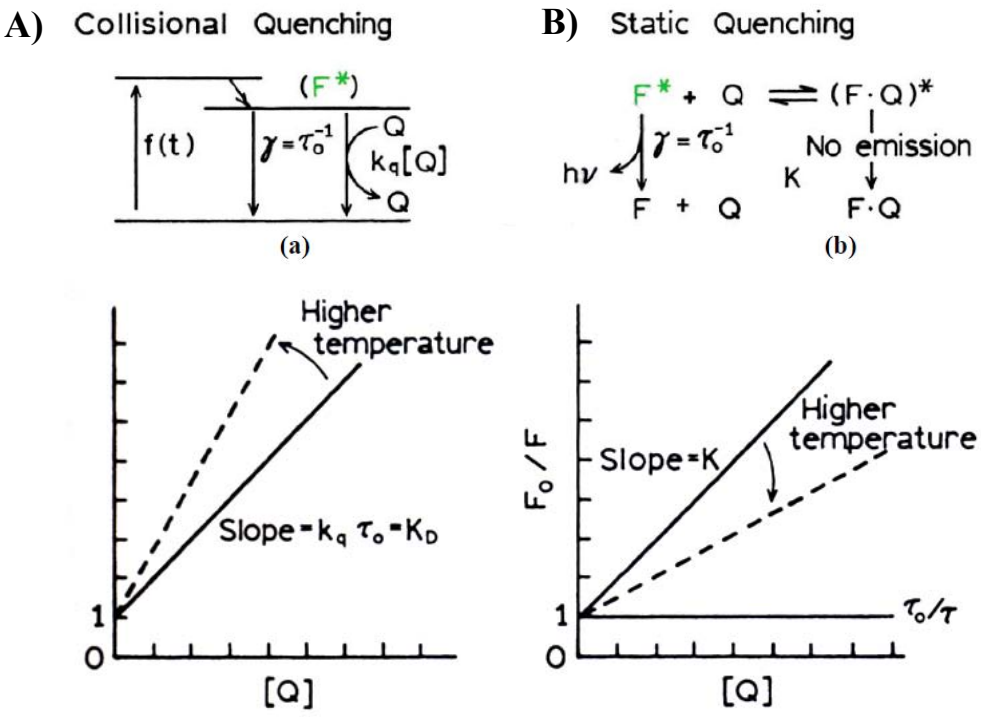

Figure 1.2. Mechanism of fluorescence quenching. A) Dynamic quenching. B) Static quenching [1].

Stern-Volmer equation

Both dynamic quenching and static quenching are described by Stern-Volmer (SV) equation which is given by

$$\frac{I_0}{I} = 1 + K_{SV}[Q]$$

, where I_0 and I are the fluorescence intensities observed in the absence and presence of quencher, respectively. [Q] is the quencher concentration and K_{SV} is the Stern-Volmer constant – a parameter that determines the efficiency of quenching process. A linear relationship of I_0/I and [Q] may indicate either a dynamic or static quenching process. The moderate to large binding constants give rise to Stern-Volmer constants (K_{SV}) that exceed the rate achievable at the diffusion limit, and hence, static quenching can be inferred. Another method to determine if the quenching process is dynamic or static is to determine the dependence of the lifetime on the quencher concentration [Q].

The dynamic quenching shortens the lifetime of the fluorescence according to the equation shown below; where k_q is the bimolecular rate constant of fluorescence quenching, τ_0 is the lifetime without added quencher, and τ is the lifetime upon addition quencher at molar concentration of [Q]. For pure dynamic quenching, k_q must be smaller than the diffusion limit k_d which can be determined from Stroke-Einstein equation; $k_d = 8RT/3\eta$ where R is the universal gas constant, T is the absolute temperature and η is the solution viscosity.

$$\tau_0/\tau = (1 + k_q \tau_0[Q])$$

In the case of static quenching, a fluorophore bound to a quencher is in a dark or non-emissive state. The unbound fluorophores exhibit the same lifetimes, and τ is thus independent to [Q] giving constant τ_0/τ at 1.

1.4 Fluorescence resonance energy transfer (FRET)

Fluorescence (or Förster) Resonance Energy Transfer (FRET) has become widely used in all applications of fluorescence, including medical diagnostic, optical imaging and DNA analysis. FRET occurs between a donor (D) molecule in the excited state and an acceptor (A) molecule in the ground state. If the emission spectrum of donor molecules overlaps with the absorption spectrum of the acceptor, the energy transfer will

occur as the result of long-range dipole-dipole interactions between the donor and acceptor. The emission signal of the acceptor (solid yellow arrow, **Figure 1.3**) occurs through the excitation of the donor molecule (solid purple arrow), while the emission of the donor molecule is reduced (dashed blue arrow). The donor fluorescence (solid blue arrow) is diminished during the transition to a lower quantum state. The efficiency of the transferred energy depends on the molecular distance between 1-10 nm, the extent of spectral overlap of the emission spectrum of the donor with the absorption spectrum of the acceptor, the quantum yield of the donor, the relative orientation of the donor and acceptor transition dipoles, and the distance between the donor and acceptor molecules [2].

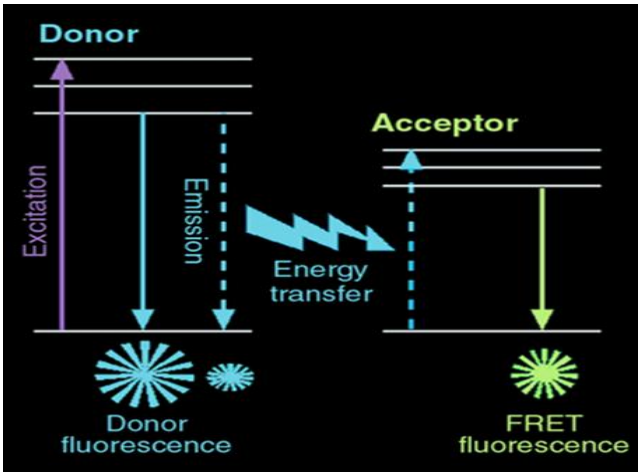

Figure 1.3 Jablonski diagram showing the energy levels of the fluorescent dyes and the rates and states involved in FRET [2].

1.5 Conjugated polyelectrolytes (CPE)

Over the past decade, CPEs have extensively been studied as optical sensors for various analytes [3], including small ions or biomolecules such as proteins and nucleic acids. The unique structural and optical properties of CPEs provide several advantages over the routine sensor methods. The multiple-charged structure of CPEs facilitates the water solubility, which is essential for carrying out biological assays in aqueous media. In addition, the CPE-based optical sensors provide a homogeneous approach, which is less

labor-intensive and less time-consuming compared with heterogeneous assay such as enzyme-linked immunosorbent assay (ELISA). As a result, the CPE-based assay is simpler, faster, and can readily be adapted to a fluorescence-based high-throughput screening (HTS) format [4]. Most importantly, signal amplification based on sensitive and collective response of CPEs to analytes can be achieved even in the presence of a very small amount of quenchers (amplified quenching effect) and minor changes in aggregation or conformation. Therefore, the CPE-based optical sensors show superior sensitivity with typical detection limits in nanomolar [5] or even in zeptomolar concentration range [6].

CPE-based optical sensors have been realized in two detection modes, colorimetric and fluorometric. Colorimetric detection is based on a change in absorption wavelength of CPEs; while the fluorometric assay affords inherent high sensitivity as well as versatility in detection of various signals, which include the changes in intensity, wavelength and lifetime. In most of the CPE-based sensors that have been developed, the fluorescence can be either enhanced to give a turn-on signal or quenched to give a turn-off signal upon direct or indirect interaction with targets. Both the turn-on and turn-off approaches are realized by three mechanisms, i.e. photoinduced electron transfer (PeT) mechanism, photoinduced energy transfer (PET) via fluorescence resonance energy transfer (FRET), Internal charge transfer (ICT), geometrical relaxation and conformational change mechanism [7]. It is important to point out that these three mechanisms are not exclusive. It is some already developed CPE-based sensors utilize more than one or even all of them in one assay.

1.6 Metal ion sensor

In 2005, Bunz et al. [8] reported a sensitive and selective lead(II) ion (Pb^{2+}) sensor which was based on the heavy metal induced fluorescence quenching of a carboxylated PPE **8** (**Figure 1.4**). The high sensitivity of this sensor was attributed to the combination of multivalent effect between **8** and Hg^{2+}, as well as the exciton migration (amplified quenching effect) along the polymer chain. More recently, the same group

employed the same polymer and developed selective sensor for mercury (II) ion (Hg^{2+}) [9]. The assay was based on a formation of an electrostatic complex between **8** and papain, a cationic cysteine-rich protease. As shown in Figure 1.4, the **8**-papain complex displays selective fluorescence quenching response only to Hg^{2+} over 9 other control metal ions (i.e., Zn^{2+}, Cd^{2+}, Pb^{2+}, Fe^{2+}, Ni^{2+}, Co^{2+}, Cu^{2+}, Ca^{2+} and Mg^{2+}). The authors proposed an agglutination mechanism to explain this selectivity as shown in **Figure 1.5**. Papain with free thiol groups is known to bind Hg^{2+}. In the 8-papain complex, the protein chains are strongly cross-linked by the anionic polymer, forming a supramolecular structure which is more sensitive towards agglutination than either **8** or papain alone. As a result, a weak emissive precipitation and a non-fluorescent solution were observed after adding Hg^{2+} to the **8**-papain complex solution.

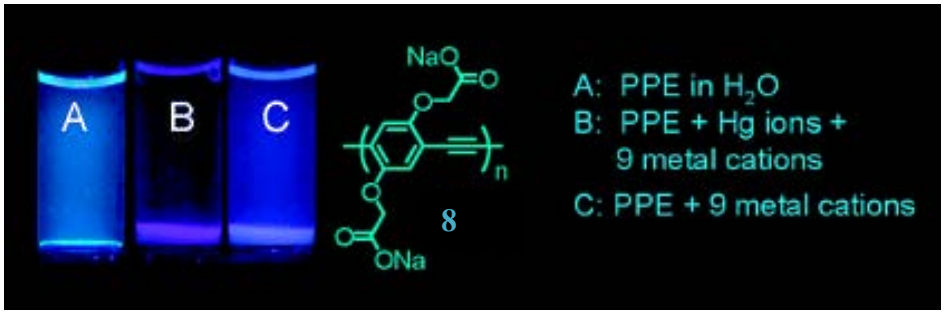

Figure 1.4. Structure of carboxylated PPE **8** and pictures taken under a hand-held UV light to show the fluorescence under different situations: A) **8**-papain complex ([**8**] = 5 μM, [papain] = 5 μM). B) All 10 metal ions added to **8**-papain complex ([metal ion] = 0.4 mM). C) All ions except Hg^{2+} add to **8**.

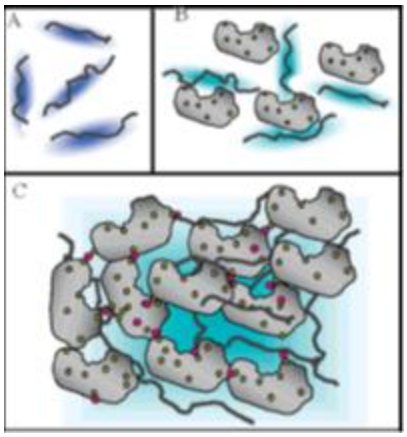

Figure 1.5. Qualitative interpretation of the Hg^{2+}-induced agglutination of the **8**-papain complex. A) PPE **8** alone. B) Electrostatic complex of **8** and papain. C) The addition of Hg^{2+} to **8**-papain complex leads to its precipitation by cross-linking of the papain molecules through Hg^{2+}.

In 2008, Tolosa and coworkers [10] synthesized water soluble fluorescent cruciforms **V-VII**. The emission spectra of these compounds shifted differently upon the addition of metal ions such as Mg^{2+}, Ca^{2+}, Al^{3+}, Hg^{2+}, Zn^{2+}, Fe^{2+} and Cu^{2+}. This responsive property was developed into a sensor array for metal ions.

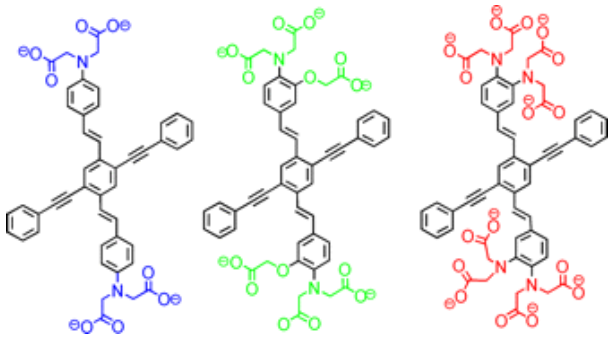

V **VI** **VII**

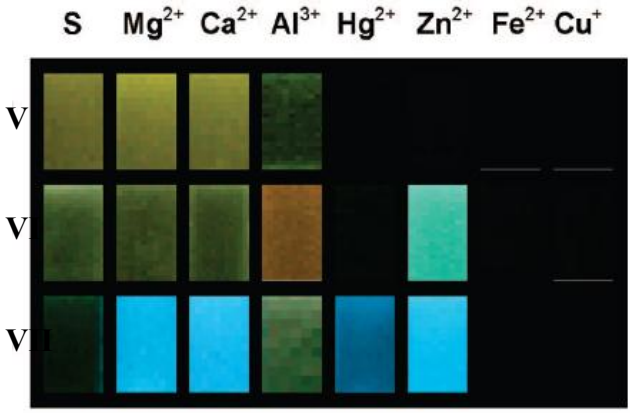

Figure 1.6 Fluorogenic responses of **V**-**VII** in the presence of metal ions.

In 2009, Niamnont and coworkers [11] reported the synthesis and sensing properties of water soluble fluorescent dendritic compound **3**. This dendritic compound composed of phenylene-ethynylene repeating units and anionic carboxylate peripheries. Without a surfactant, compound **3** exhibited a low fluorescent quantum yield, but a good selectivity toward Hg^{2+}. After adding Triton X-100, the quantum yield was drastically increased and the sensitivity for the detection of Hg^{2+} was also improved.

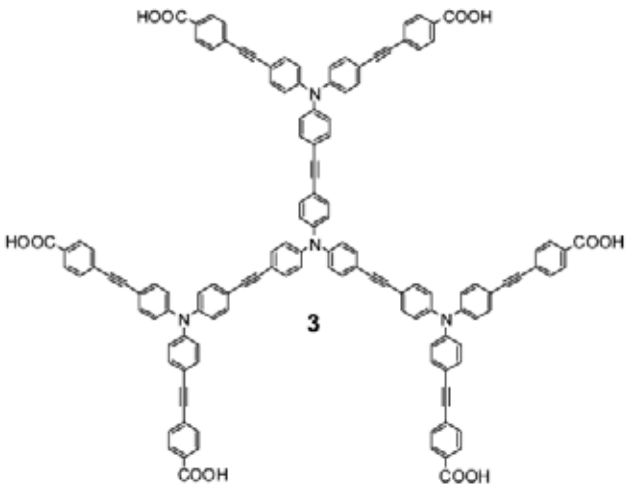

3

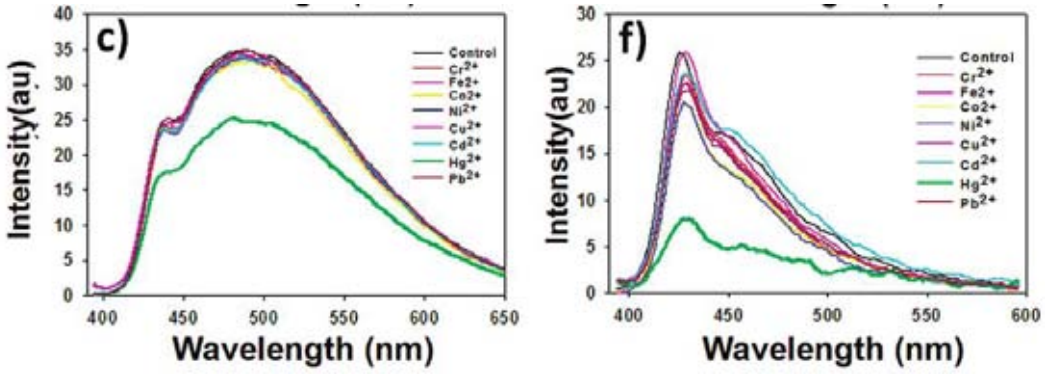

Figure 1.7 Dendritic fluorophore **3** and its selectivity toward Hg^{2+} ion before (c) and after (d) the surfactant added.

In 2010, Goswami and coworkers [12] reported a highly selective and sensitive fluoroionophore for Cu^{2+} based on metal triggered enhanced internal charge transfer (ICT) in six rings annulated structurally rigid perinone dye (receptor 1). The fluoroionophore shows a strong colorimetric change and a dramatic enhancement of fluorescence intensity due to cation-induced excited state ICT during the sensing.

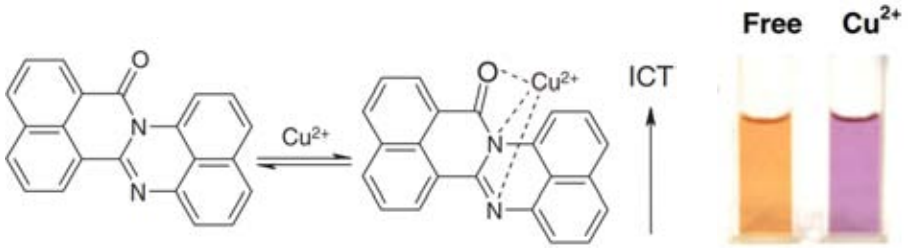

Figure 1.8 Proposed mode of binding with Cu^{2+} and color changes from orange to purple upon Cu^{2+} complexation.

In 2011, a group of Yu and coworkers [13] designed fluorescent chemosensor of naphthalimide modified rhodamine B for high selective and sensitive determination of Cu^{2+} in aqueous media and living cells. The limit of detection (LOD) was obtained as low as 0.18 μM of Cu^{2+}. In addition, the chemosensor was displayed promising for rapid and sensitive determination of Cu^{2+} in biological samples.

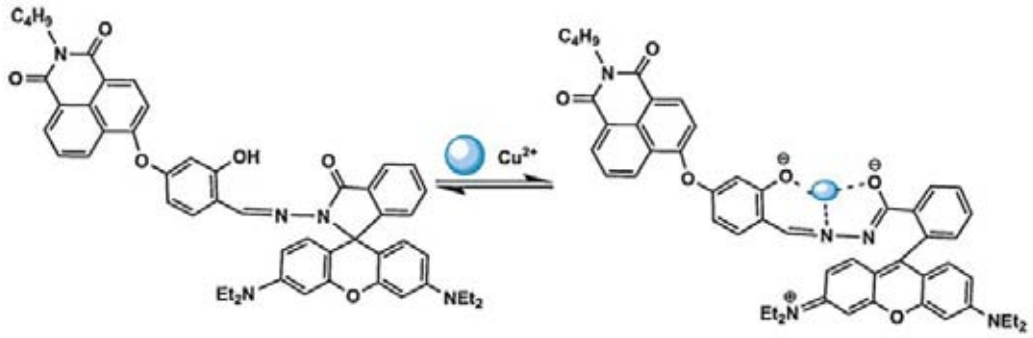

Figure 1.9 Binding mode of fluorescent sensor with Cu^{2+}.

In 2006, Sundari and coworkers [14] immobilized salicylic acid onto styrene-divinylbenzene cross-linked copolymer as a reagent phase for the development of an optical fiber copper (II) sensor. Cu (II) has four coordination numbers that is capable of forming chemical bonds with two molecules of salicylic acid, which acts as a bidentate ligand. The linear dynamic range of Cu (II) was found within the concentration range of 1.0-2.0 mmol/L with its LOD of 0.5 mmol/L.

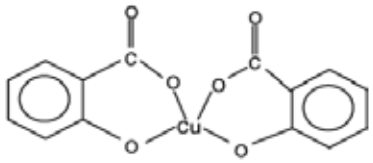

Figure 1.10 Chemical structure of copper (II)-salicylate complex.

In 2011, Sirilaksanapong and coworkers [15] synthesized water-soluble fluorophores from 1,3,5-tris-(4'-iodophenyl)benzene [**Figure 1.11**]. These compound containing three phenylene-ethynylene units and three salicylic acid peripheral groups exhibits a highly selective fluorescence quenching by Cu^{2+} ions. The detection limit for Cu^{2+} improves from 6.49 to 0.19 ppb in aqueous media in the presence of Triton X-100 surfactant as well as the quantum efficiency.

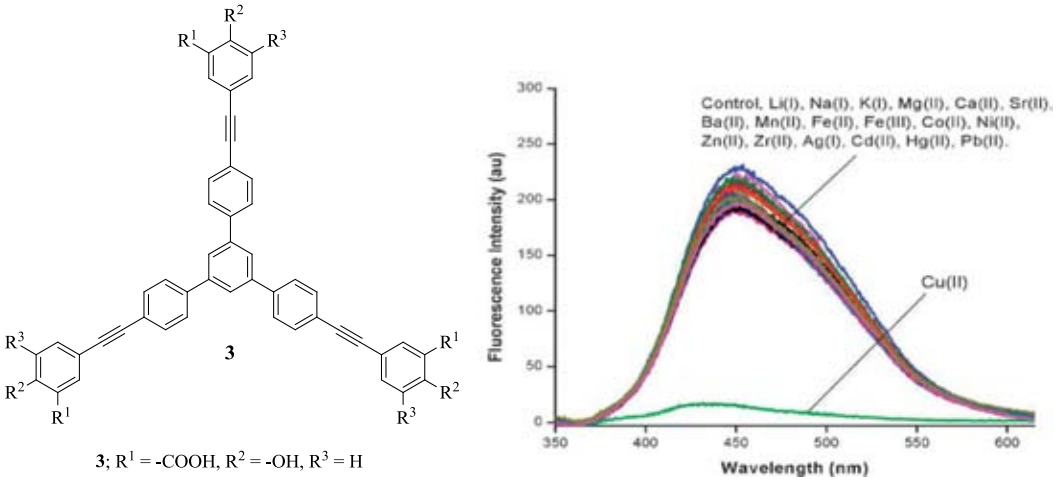

Figure 1.11 Water-soluble fluorophore **3** and its selectivity toward Cu^{2+} ion.

In 2008, Sheng and coworkers [16] were synthesized a coumarin derivative as a colorimetric chemosensor **1** by coupling coumarin aldehyde with diaminomaleonitrile to form Schiff base structure with the enhanced intramolecular charge transfer (ICT). It exhibits good sensitivity and selectivity toward Cu^{2+} ion over other cations in aqueous solution via its optical response. The colorimetric response of **1** to Cu^{2+}, fabrication of **1** test strips exhibits a good sensitivity and selectivity to Cu^{2+} as in solution [**Figure 1.12**].

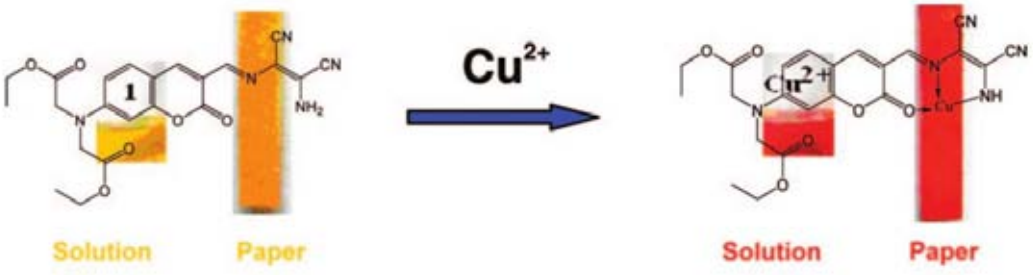

Figure 1.12 Coumarin-based colorimetric chemosensor **1** and its selectivity toward Cu^{2+} ion in aqueous solution and on paper-made test kits.

In 2011, Yang and coworkers [17] were constructed a novel nanoparticle autocatalytic sensor for the Ag^{+} and Cu^{2+} detection, based on the oxidative ability of Ag^{+} and Cu^{2+} toward *o*-phenylenediamine (OPDA). Based on the nanoparticle autocatalytic

sensor, the detection limit for Ag^{+} and Cu^{2+} are 60 nM and 2.5 nM, respectively. In addition, a nanoparticle autocatalytic sensor is applied to test paper for the detection of Ag^{+} and Cu^{2+} with the naked eye. Ag^{+} and Cu^{2+} could be detected at levels as low as 0.06 nmol and 0.3 nmol, respectively.

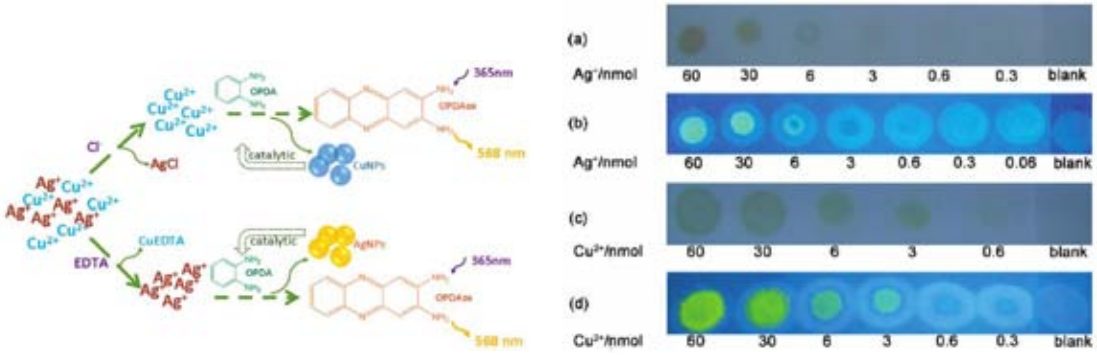

Figure 1.13 The Principle of the nanoparticle autocatalytic sensor for Ag^{+} and Cu^{2+} (left). Test paper for the detection of (a and b) Ag^{+} and (c and d) Cu^{2+}.

1.7 DNA sensor

In 2003, Gaylord and coworkers [18] were used the optical amplification of cationic conjugated polymers (polyfluorene phenylene: **1**) [**Figure 1.14**] to detect single-stranded deoxyribonucleic acid (ssDNA) with specific base sequence which labeled with a dye (fluorescein). The optical propertied of the CP (1) and ssDNA-labeled dye (C^{*}) are optimized so that Förster Resonance Energy Transfer (FRET) from CP (donor) to DNA-C^{*} (acceptor) is favored. The FRET ratio of **1** with hybridized and nonhybridized DNA probe show that CP can be used to monitor the presence of a complementary strand to ssDNA-C^{*}.

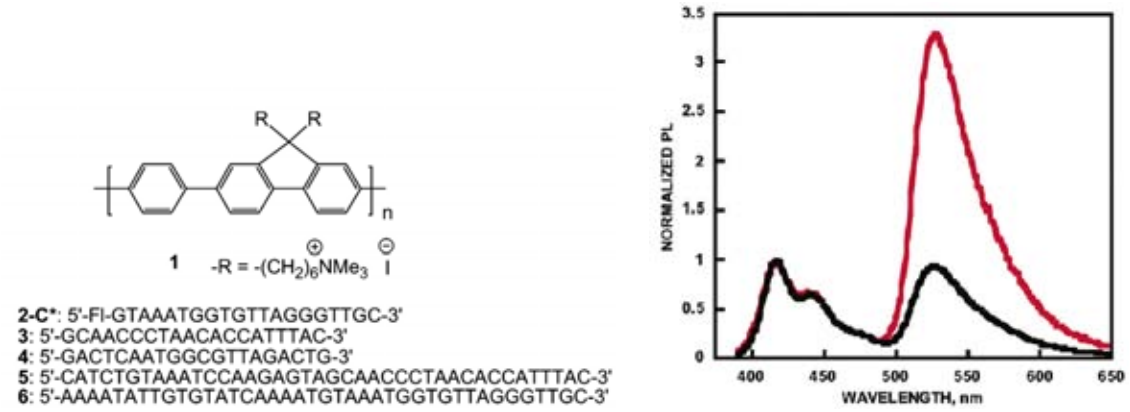

Figure 1.14 Fluorophore **1** and DNA sequence (left). FRET ratio of 1 with hybridized and nonhybridized DNA (right).

In 2008, Lee and coworkers [19] have developed a series of oxadizole-containing conjugated polymers toward chemical degradation and established an on-chip DNA synthesis on thin-layers of conjugated polymers (POX1). The efficient fluorescence resonance energy transfer (FRET) from the polymer layer to dye-labeled DNA shows large signal amplification. These signal have label-free DNA detection capability by combining the signal of POX1-based DNA microarray and the intercalating dye, SYBR green so that without losing good selectivity, sensitive detection of target DNA was achieved.

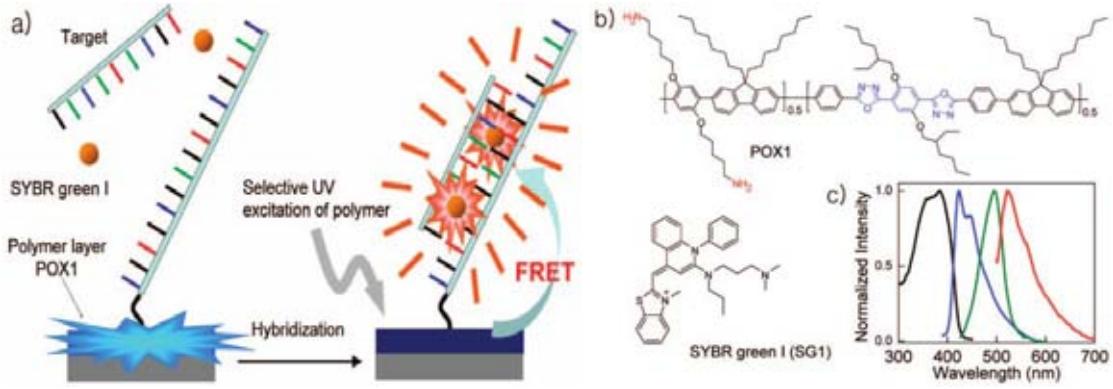

Figure 1.15 (a) Schematic of a label-free conjugated polymer-DNA hybrid microarray, (b) chemical structures of POX1 and SYBR green I and (c) UV-vis/PL spectra (black/blue: POX1 and green/red: SYBR green).

In 2009, Ren and coworkers [20] were develope label-free DNA sensors which PicoGreen used in combination with conjugated polymers. The enhance detection efficiency up to 19-fold through FRET using PFP as a light harvesting complex. The improved selectivity is ascribed to the stronger binding interaction between PicoGreen with dsDNA (complementary) compared to that between PicoGreen and ssDNA (non-complementary), which results in selective repelling of PicoGreen away from the DNA strands.

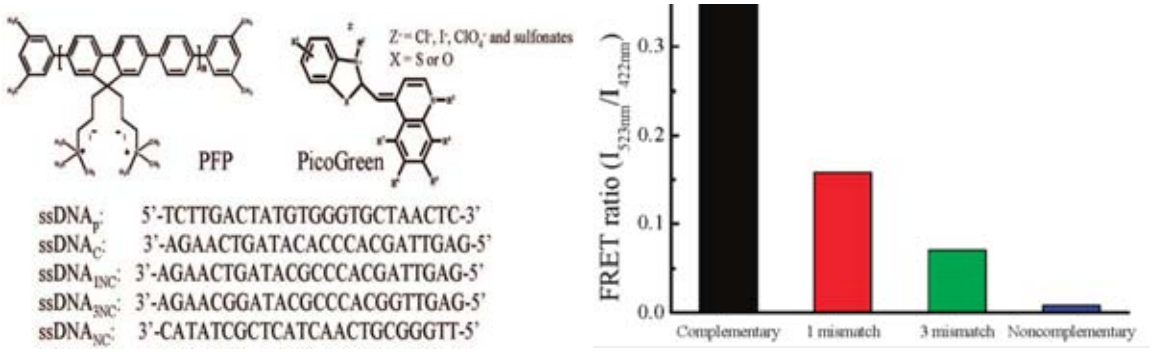

Figure 1.16 Chemical structures of PFP, PicoGreen (PG) and DNA sequences (left). FRET ratio of PFP/PG/DNA with increasing number of mismatched base pairs (right).

In 2010, Tang and coworkers [21] were synthesized water-soluble conjugated polymer containing fluorine moiety and ethylenic moiety in the backbone (PFV) for label-free DNA detection. The structure of PFV provides stronger interactions with double-stranded DNA (dsDNA). The efficient FRET is observed from PFV (donor) to ethidium bromide, EB (acceptor) intercalated in dsDNA. The interaction between PFV and DNA can be measuring the FRET ratio between PFV and EB intercalated in DNA.

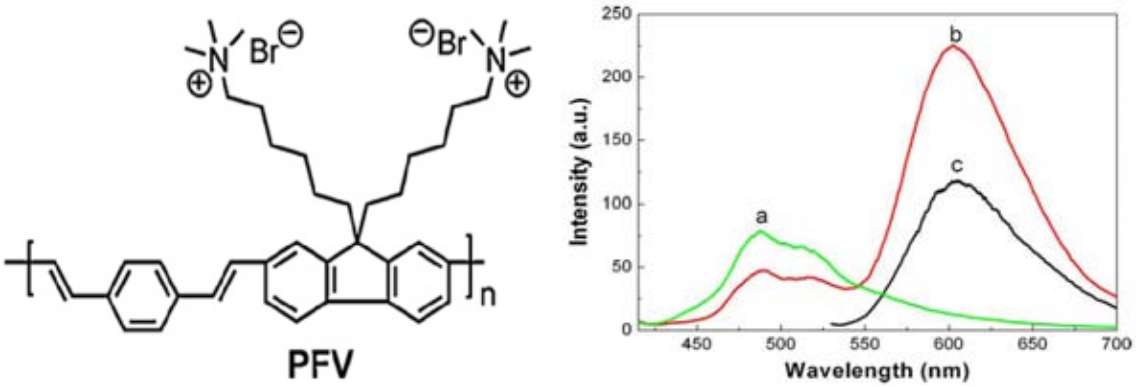

Figure 1.17 (left) Chemical structures of PFV. (right) emission spectra of a) PFV/dsDNA, b) PFV/dsDNA/EB and c) dsDNA/EB.

1.8 Objective of this research

The aim of this work focuses on the synthesis of water soluble dendritic fluorophores composed of phenyleneethynylene repeating units and anionic salicylate or cationic ammonium peripheral groups (**Figure 1.18**) and study of these new fluorophores as metal ion and DNA sensors in a aqueous media.

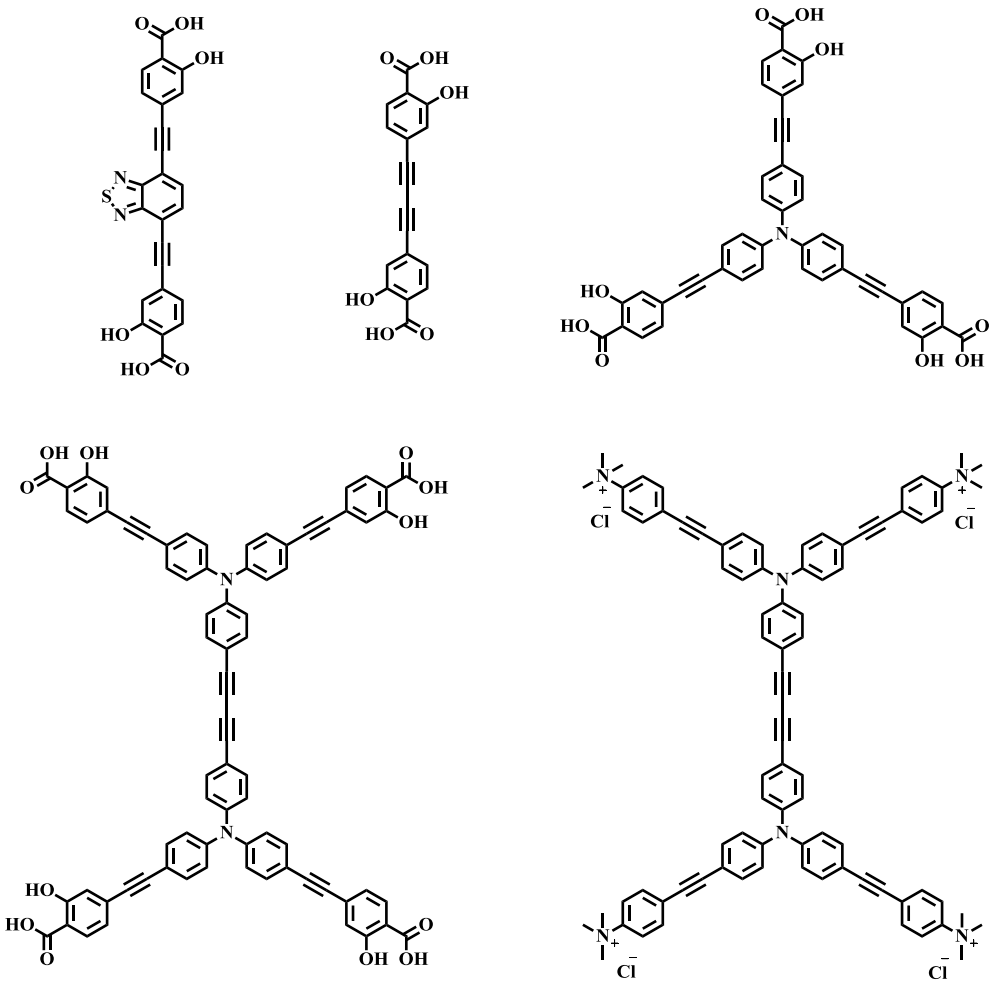

Figure 1.18 The target molecules.

CHAPTER II

EXPERIMENTAL

2.1 Chemicals and materials

Methyl 4-iodosalicylate, 1,8-diabicyclo [5.4.0] undec-7-ene (DBU), copper (I) iodide, sodium chloride were reagent grade which were purchased from Sigma-Aldrich. Bis(triphenylphosphine)palladium(II) dichloride ($PdCl_2(PPh_3)_2$), potassium hydroxide, potassium carbonate, potassium chloride, potassium hydrogen carbonate, dipotassium hydrogen phosphate, nonionic surfactant (Triton X-100) were purchased from Fluka (Switzerland). Trimethylsilylacetylene was purchased from GFS Chemical. Metal ions (Ag^+, Al^{3+}, Ba^{2+}, Ca^{2+}, Cd^{2+}, Co^{2+}, Cu^{2+}, Fe^{2+}, Fe^{3+}, Hg^{2+}, K^+, Li^+, Mg^{2+}, Mn^{2+}, Na^+, Ni^{2+}, Pb^{2+}, Sr^{2+} and Zn^{2+}) were prepared from their commercially available inorganic salts purchased from Sigma-Aldrich and Fluka. Tris base was prepared Tris-HCl buffer purchased from Sigma-Aldrich. The 22-mer oligonucleotides (single-stranded DNA (ssDNA): 5'- ACT ACG ATA CTG GCA GGT GCA T-3', complementary DNA (cDNA): 5'-ATG CAC CTG CCA GTA TCG TAG T-3', non-complementary (ncDNA): 5'-GCG TGA TTT ATC GCG CTA TGA C-3', double mismatched DNA (2mDNA): 5'- ATG CAC TTG CCA GTG TCG TAG T-3') were purchased from Bio Design. Co., Ltd. (Bangkok, Thailand) and used without further purification. SYBR Green II RNA gel stain was purchased from Sigma-Aldrich (Switzerland). For most reactions, solvents such as methylene chloride and acetonitrile were reagent grade stored over molecular sieves. In anhydrous reactions, solvents such as THF and toluene were dried and distilled before use according to the standard procedures. Column chromatography was operated using Merck silica gel 60 (70-230 mesh). Thin layer chromatography (TLC) was performed on silica gel plates (Merck F_{245}). Solvents used for extraction and chromatography such as methylene chloride, hexane, ethyl acetate and methanol were commercial grade and distilled before use while diethyl ether and chloroform were reagent grade. Milli-Q water was used in all experiments unless specified otherwise. The most reactions were carried out under positive pressure of N_2 filled in rubber balloons.

2.2 Analytical instruments

The melting points of all products were acquired from a melting point apparatus (Electrothermal 9100, Fisher Scientific, USA). Elemental (C, H, N) analyses were performed on a PE 2400 series II analyzer (Perkin-Elmer, USA). Mass spectra were recorded on a Microflex MALDI-TOF mass spectrometer (Bruker Daltonics) using doubly recrystallized α-cyano-4-hydroxy cinnamic acid (CCA) as a matrix. The HRMS spectra were measured on an electrospray ionization mass spectrometer (microTOF, Bruker Daltonics). Fourier transform infrared spectra were acquired on Nicolet 6700 FT-IR spectrometer equipped with a mercury-cadmium telluride (MCT) detector (Nicolet, USA). ^{1}H- and ^{13}C-NMR spectra were acquired from sample solution in $CDCl_3$, acetone-*d6*, CD_3CN, CD_3OD and DMSO-*d6* on Varian Mercury NMR spectrometer (Varian, USA) at 400 MHz and100 MHz, respectively. The UV-visible absorption spectra were obtained from a Varian Cary 50 UV-Vis spectrophotometer (Varian, USA) and the fluorescence emission spectra were recorded on a Varian Cary Eclipse spectrofluorometer (Varian, USA).

2.3 Synthesis of fluorophores

2.3.1 Preparation of 4, 4′, 4″-triiodotriphenylamine

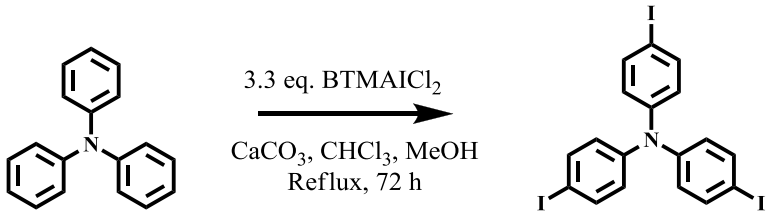

70%

A mixture of triphenylamine (7.4 g, 30 mmol) in chloroform (100 mL) and methanol (50 mL) was added with benzyltrimethylammonium dichloroiodate ($BTMAICl_2$) [22] (34.5 g, 99 mmol) and $CaCO_3$ (18 g, 180 mmol). The reaction mixture was allowed to reflux for 72 h and 20% $Na_2S_2O_3$ solution was then added to the mixture until the mixture became light yellow. The mixture was filtered and the filtrate was extracted with methylene chloride (3 × 50 mL). The combined organic phase was washed with water (2 × 100 mL) and dried over anhydrous $MgSO_4$. The solution was concentrated and the residue was re-precipitated in methanol from

methylene chloride solution. Triiodotriphenylamine (**T3I**) was obtained (13.09 g, 70%) as a white solid: mp; 182-184°C; ^{1}H NMR ($CDCl_3$, 400 MHz): δ (ppm) 7.53 (d, *J* = 8.0 Hz, 6H), 6.81 (d, *J* = 8.0 Hz, 6H); ^{13}C NMR ($CDCl_3$, 100 MHz): δ (ppm) 146.5, 138.4, 126.0, 86.5; MALDI-TOF m/z Calcd. for $C_{18}H_{12}I_3N$, 622.810 Found: 622.561.

2.3.2 Preparation of methyl 2-hydroxy-4-((trimethylsilyl)ethynyl)benzoate

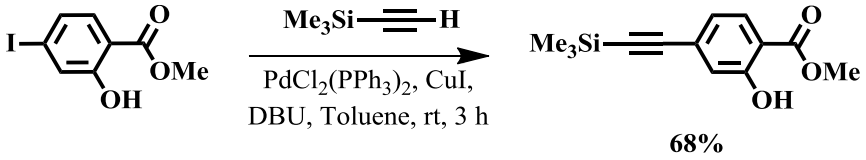

68%

A mixture of methyl 2-hydroxy-4-iodobenzoate (2.00 g, 7.2 mmol), $PdCl_2(PPh_3)_2$ (0.14 g, 0.2 mmol), CuI (0.04 g, 0.2 mmol) and trimethylsilylacetylene (0.85 g, 8.6 mmol) in toluene (10 mL) was added with DBU (1 mL) and the mixture was stirred at room temperature for 3 h. The reaction mixture was then filtered and the solid was washed with toluene (3 × 15 mL). The filtrate was evaporated and the residue was eluted through a silica gel column by gradient solvents starting from hexane to methylene chloride/hexane (1/2 v/v) as an eluent to afford methyl 2-hydroxy-4-((trimethylsilyl)ethynyl)benzoate as a white solid (1.21 g, 68% yield). ^{1}H NMR ($CDCl_3$, 400 MHz): δ (ppm) 10.73 (s, 1H), 7.75 (d, *J* = 8.0 Hz, 1H), 7.06 (d, *J* = 8.0 Hz, 1H) 6.94 (d, *J* = 8.0 Hz, 1H), 3.94 (s, 3H), 0.25 (s, 9H); ^{13}C NMR ($CDCl_3$, 100 MHz): δ (ppm) 170.2, 161.2, 130.4, 129.9, 122.8, 120.9, 112.4, 103.8, 98.1, 52.6, 0.1.

2.3.3 Preparation of methyl 4-ethynyl-2-hydroxybenzoate

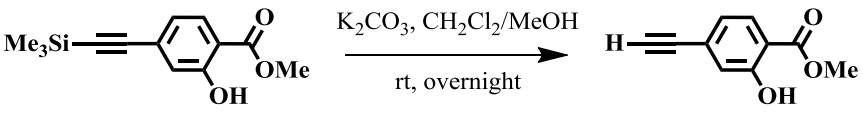

92%

A mixture of methyl 2-hydroxy-4-iodobenzoate (1.00 g, 4.03 mmol) and K_2CO_3 (55 mg, 0.40 mmol) in methylene chloride (15 mL) and methanol (15 mL) was

stirred at room temperature for 24 h. The organic layer was separated and the aqueous phase was extracted with methylene chloride (2 x 50 mL) and was then dried over anhydrous $MgSO_4$. The solvent was evaporated and the residue was eluted through a silica gel column by gradient solvents starting from hexane to methylene chloride/hexane (1/4 v/v) as an eluent to afford methyl 4-ethynyl-2-hydroxybenzoate as a white solid (0.65 g, 92% yield). ^{1}H NMR ($CDCl_3$, 400 MHz): δ (ppm) 10.76 (s, 1H), 7.78 (d, J = 8.0 Hz, 1H), 7.10 (s, 1H), 6.99 (d, J = 8.0 Hz, 1H), 3.95 (s, 3H), 3.21 (s, 1H); ^{13}C NMR ($CDCl_3$, 100 MHz): δ (ppm) 170.2, 161.3, 130.0, 129.4, 122.9, 121.3, 112.8, 82.7, 80.3, 52.6.

2.3.4 Preparation of 2ISA^0, I2SA^0 (4), and 3SA^0 (3).

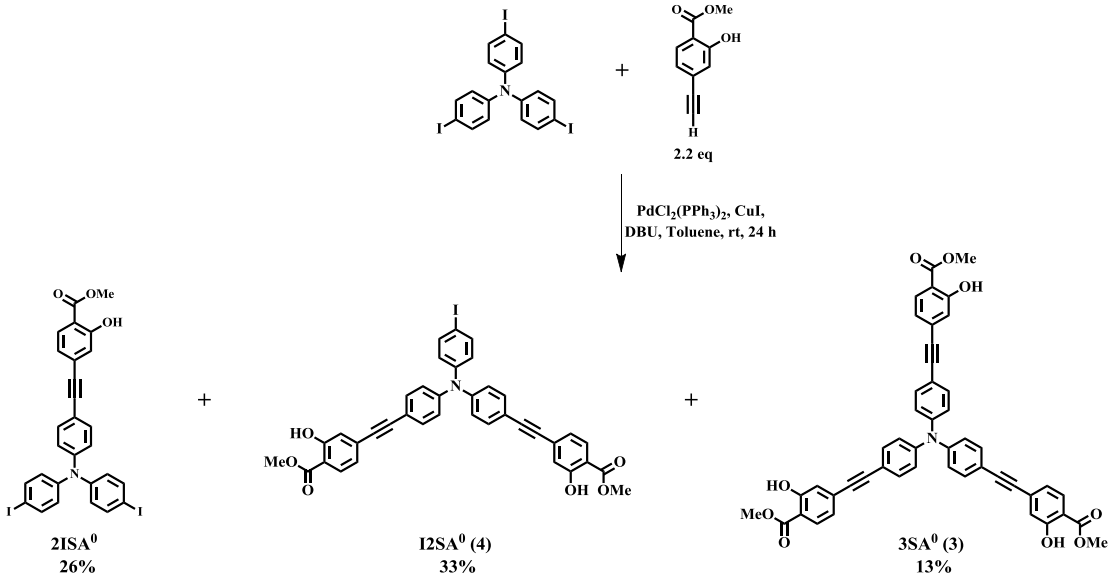

A mixture of **T3I** (2.00 g, 3.21 mmol), $PdCl_2(PPh_3)_2$ (0.11 g, 0.16 mmol), CuI (0.03 g, 0.16 mmol), methyl 4-ethynyl-2-hydroxybenzoate (1.24 g, 7.06 mmol) in toluene (30 mL) was added DBU (2.0 mL) and the mixture was stirred at RT for 24 h. After the combined filtrate was evaporated and the residue was eluted through a silica gel column by gradient solvents from hexane to methylene chloride/hexane (3/1 v/v) as an eluent. **2ISA^0** was obtained as a light yellow solid (0.56 g, 26% yield), ^{1}H NMR ($CDCl_3$, 400 MHz): δ (ppm) 10.78 (s, 1H), 7.79 (d, J = 8.0 Hz, 1H), 7.56 (d, J = 8.0 Hz, 4H), 7.40 (d, J = 8.0 Hz, 2H), 7.11 (d, J = 8.0 Hz, 1H) 7.00 (d, J = 8.0 Hz, 3H), 6.85 (d, J = 8.0 Hz, 4H), 3.96 (s, 3H). ^{13}C NMR ($CDCl_3$, 100 MHz): δ (ppm) 170.3, 161.4, 147.4, 146.6, 138.7, 133.2, 129.9, 126.7, 123.2, 122.4, 120.3, 116.9,

112.1, 92.7, 88.5, 87.2, 52.5. **I2SA^0 (4)** was obtained as a dark yellow solid (0.76 g, 33% yield), ^{1}H NMR ($CDCl_3$, 400 MHz): δ (ppm) 10.78 (s, 2H), 7.80 (d, *J* = 8.0 Hz, 2H), 7.59 (d, *J* = 8.0 Hz, 2H), 7.43 (d, *J* = 8.0 Hz, 4H), 7.11 (d, *J* = 8.0 Hz, 2H), 7.00-7.06 (m, 6H), 6.89 (d, *J* = 8.0 Hz, 2H), 3.96 (s, 6H). ^{13}C NMR ($CDCl_3$, 100 MHz): δ (ppm) 170.2, 161.3, 147.1, 146.4, 138.6, 133.1, 130.7, 129.8, 127.0, 123.6, 122.3, 120.2, 117.2, 111.9, 92.5, 88.5, 87.5, 52.4. **3SA^0 (3)** was obtained as a yellow-orange solid (0.32 g, 13% yield). ^{1}H NMR ($CDCl_3$, 400 MHz): δ (ppm) 10.78 (s, 3H), 7.80 (d, *J* = 8.0 Hz, 3H), 7.45 (d, *J* = 8.0 Hz, 6H), 7.08-7.12 (m, 9H), 7.00-7.03 (m, 3H), 3.96 (s, 9H). ^{13}C NMR ($CDCl_3$, 100 MHz): δ (ppm) 170.3, 161.4, 147.2, 133.3, 130.8, 130.0, 124.2, 122.5, 120.3, 117.6, 112.1, 92.6, 88.7, 52.5. MALDI-TOF m/z Calcd for $C_{48}H_{33}NO_9$, 767.216; Found, 766.807.

2.3.5 Preparation of F4.

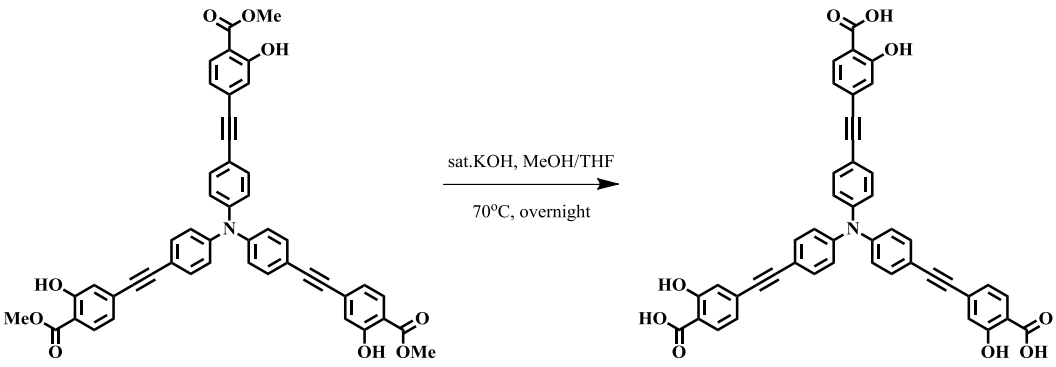

A mixture of **3** (0.50 g, 0.41 mmol) in THF (15 mL) and methanol (15 mL) was added with saturated KOH aqueous solution (0.5 mL) and the mixture was heat to 70^{o}C. After 24 h the solution was evaporated and the residue was dissolved in water (20 mL). Approximately 50 g of ice was then added and the aqueous solution was acidified and stored in the refrigerator for 1 h. The product was filtered to afford **F4** as a yellow solid (0.43 g, 92% yield). mp : > 200^{o}C decompose. ^{1}H NMR (CD_3OD, 400 MHz): δ (ppm) 7.72 (d, *J* = 8.0 Hz, 3H), 7.35 (d, *J* = 8.0 Hz, 6H), 6.84-6.96 (m, 12H). ^{13}C NMR (CD_3OD, 100 MHz): δ (ppm) 173.02, 162.82, 148.38, 134.23, 131.62, 131.55, 125.28, 123.14, 120.58, 118.87, 113.77, 92.94, 89.45. MALDI-TOF m/z Calcd for $C_{45}H_{27}NO_9$, 725.169; Found, 725.210.

2.3.6 Preparation of 5.

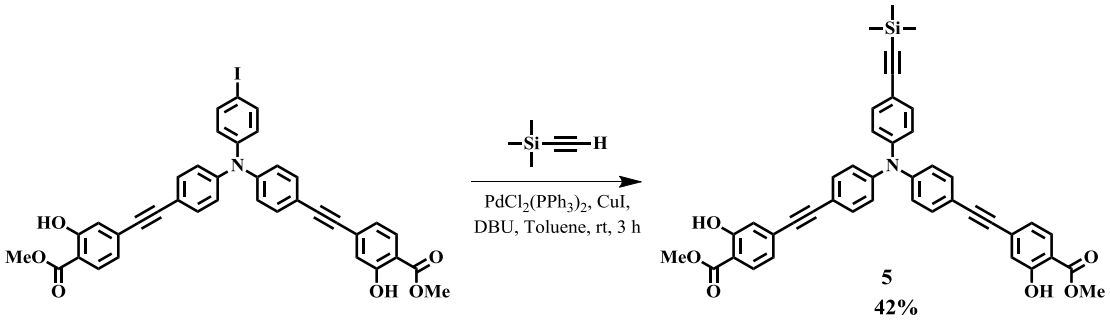

A mixture of **I2SA^0 (4)** (2.00 g, 2.78 mmol), $PdCl_2(PPh_3)_2$ (0.06 g, 0.08 mmol), CuI (0.02g, 0.08 mmol) and trimethylsilylacetylene (0.33 g, 3.3 mmol) in toluene (10 mL) was added with DBU (1 mL) and the mixture was stirred at room temperature for 3 h. The reaction mixture was then filtered and the solid was washed with toluene (3 × 15 ml). The filtrate was evaporated and the residue was eluted through a silica gel column by gradient solvents starting from pure hexane to methylene chloride/hexane (1/4 v/v) as an eluent to afford **5** as a yellow solid (0.81 g, 42% yield). ^{1}H NMR ($CDCl_3$, 400 MHz): δ (ppm) 10.78 (s, 2H), 7.80 (d, J = 8.0 Hz, 2H), 7.41 (d, J = 8.0, 8.0 Hz, 6H), 7.11 (s, 2H) 7.03 (dd, 8H), 3.96 (s, 6H), 0.25 (s, 9H); ^{13}C NMR ($CDCl_3$, 100 MHz): δ (ppm) 170.2, 161.3, 147.1, 133.1, 130.7, 129.8, 123.9, 122.3, 120.2, 117.2, 111.9, 104.8, 94.2, 92.5, 88.5, 52.4, 0.0.

2.3.7 Preparation of 6.

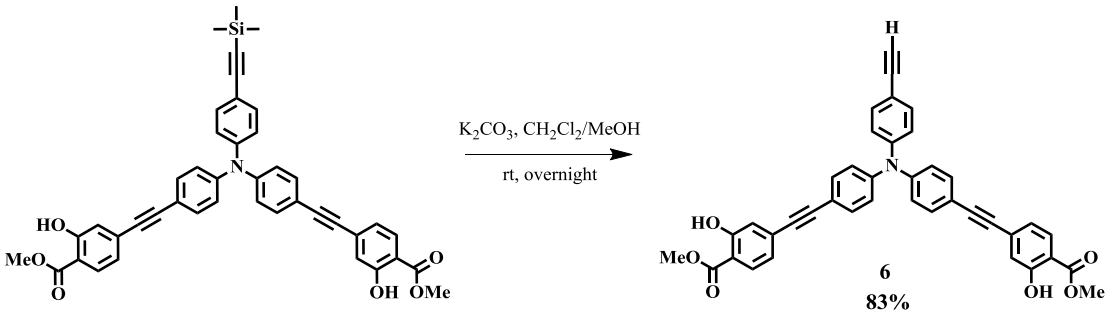

A mixture of **5** (1.00 g, 1.45 mmol) and K_2CO_3 (0.059 g, 0.15 mmol) in methylene chloride (15 mL) and methanol (15 mL) was stirred at room temperature for 24 h. The organic layer was separated and the aqueous phase was extracted with methylene chloride (2 x 50 mL) and was then dried over anhydrous $MgSO_4$. The solvent was evaporated and the residue was eluted through a silica gel column by

gradient solvents starting from pure hexane to methylene chloride/hexane (1/4 v/v) as an eluent to afford **6** as a brown solid (0.74 g, 83% yield). ^{1}H NMR ($CDCl_3$, 400 MHz): δ (ppm) 10.79 (s, 2H), 7.80 (d, *J* = 8.0 Hz, 2H), 7.59 (d, *J* = 8.0 Hz, 1.5H) 7.43 (d, *J* = 8.0 Hz, 4.5H), 7.00-7.12 (m, 8.5H), 6.89 (d, *J* = 8.0 Hz, 1.5H), 3.96 (s, 6H), 3.08 (s, 1H); ^{13}C NMR ($CDCl_3$, 100 MHz): δ (ppm) 170.3, 161.4, 147.2, 133.6, 133.3, 130.0, 124.4, 124.1, 122.5, 120.3, 117.5, 112.1, 92.6, 88.7, 83.5, 52.5.

2.3.8 Preparation of 7.

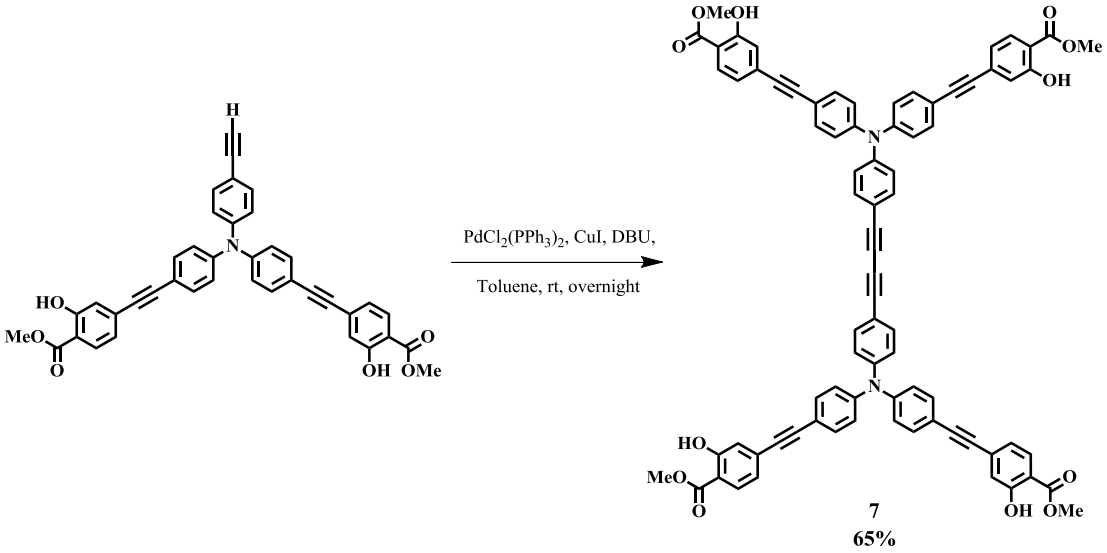

A mixture of **6** (0.50 g, 0.41 mmol), $PdCl_2(PPh_3)_2$ (20 mg, 0.02 mmol), CuI (40 mg, 0.02 mmol) in toluene (15 mL) was added DBU (1.0 mL) and the mixture was stirred at rt for 24 h. After the combined filtrate was evaporated and the residue was eluted through a silica gel column by gradient solvents from pure hexane to methylene chloride/hexane (3/1 v/v) as an eluent. **7** was obtained as a dark yellow solid (0.33 g, 65% yield). ^{1}H NMR ($CDCl_3$, 400 MHz): δ (ppm) 10.79 (s, 4H), 7.80 (d, *J* = 8.0 Hz, 4H), 7.45 (d, *J* = 8.0 Hz, 12H), 7.01-7.12 (m, 20H), 3.96 (s, 12H). ^{13}C NMR ($CDCl_3$, 100 MHz): δ (ppm) 170.3, 161.4, 147.0, 133.3, 130.8, 130.0, 124.4, 122.5, 120.4, 117.8, 116.6, 112.1, 92.5, 88.8, 81.9, 74.3, 52.5. MALDI-TOF m/z Calcd for $C_{80}H_{52}N_2O_{12}$, 1232.352; Found, 1232.357.

2.3.9 Preparation of F5.

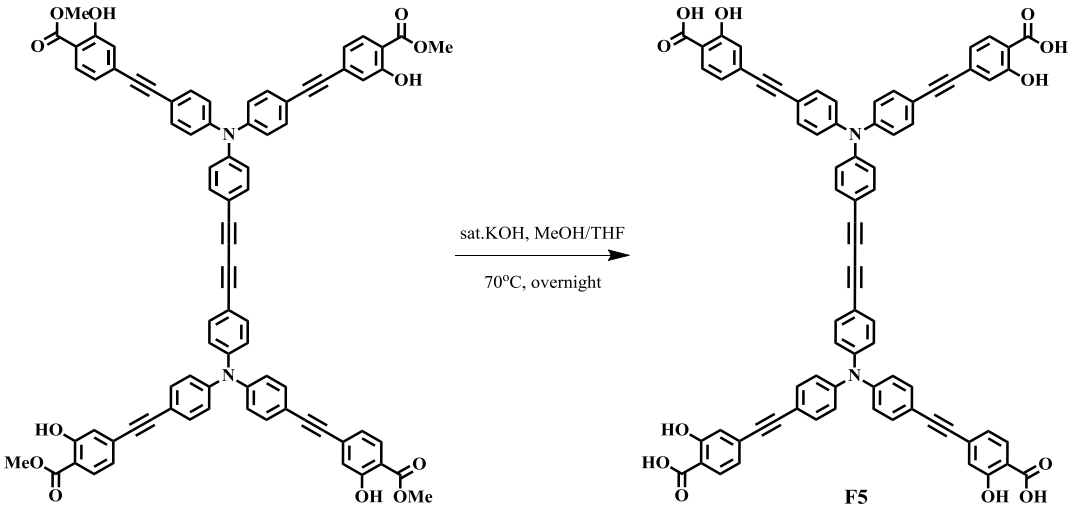

82%

A mixture of **7** (0.50 g, 0.41 mmol) in THF (15 mL) and methanol (15 mL) was added with saturated KOH aqueous solution (0.5 mL) and the mixture was heat to 70°C. After 24 h the solution was evaporated and the residue was dissolved in water (20 mL). Approximately 50 g of ice was then added to the aqueous solution, acidified and kept in a refrigerator for 1 h. The product was filtered to afford **F5** as a yellow solid (0.39 g, 82% yield). mp : > 200°C decompose. ^{1}H NMR (CD_3OD, 400 MHz): δ (ppm) 7.91 (d, 4H), 7.57 (m, 12H), 7.14 (m, 20H); ^{13}C NMR (CD_3OD, 100 MHz): δ (ppm) 173.0, 162.7, 148.0, 143.5, 135.2, 134.4, 131.6, 125.4, 123.4, 120.7, 119.0, 113.5, 93.3, 89.9; MS-ES$^-$ m/z Calcd for $C_{76}H_{44}N_2O_{12}$, 1176.2894, 293.07 $[M]^{4-}$ Found : 292.83 $[M]^{4-}$.

2.3.10 Preparation of 1.

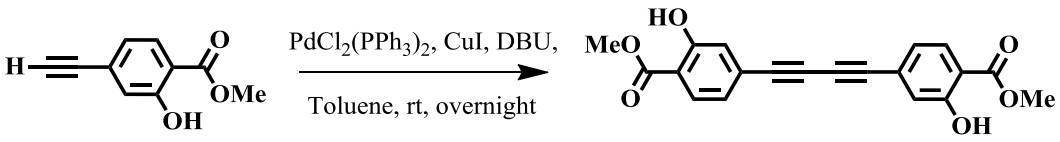

1

88%

A mixture of methyl 4-ethynyl-2-hydroxybenzoate (0.50 g, 2.84 mmol), $PdCl_2(PPh_3)_2$ (0.11 g, 0.16 mmol), CuI (0.03 g, 0.16 mmol) in toluene (15 mL) was added DBU (1.0 mL) and the mixture was stirred at RT for 24 h. After the combined filtrate was evaporated, the residue was eluted through a silica gel column by gradient

solvents from pure hexane to methylene chloride/hexane (3/1 v/v) as an eluent. **1** was obtained as a light-yellow solid (0.44 g, 88% yield), ^{1}H NMR ($CDCl_3$, 400 MHz): δ (ppm) 10.79 (s, 2H), 7.82 (d, *J* = 8.0 Hz, 2H), 7.14 (s, 2H), 7.03 (d, *J* = 8.0 Hz, 2H), 3.96 (s, 6H). ^{13}C NMR ($CDCl_3$, 100 MHz): δ (ppm) 170.2, 161.4, 130.1, 129.9, 122.8, 122.7, 120.8, 112.7, 91.3, 52.6; MALDI-TOF m/z Calcd for $C_{20}H_{14}O_6$, 350.079; Found, 350.367.

2.3.11 Preparation of F3.

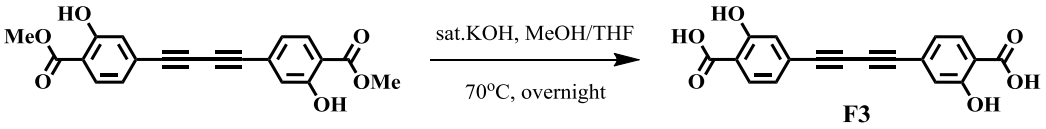

F3

91%

A mixture of dimethyl **1** (0.50 g, 1.43 mmol) in THF (15 mL) and methanol (15 mL) was added with saturated KOH aqueous solution (0.5 mL) and the mixture was heat to 70°C. After 24 h the solution was evaporated and the residue was dissolved in water (20 mL). Approximately 50 g of ice was then added to the aqueous solution. The mixture was acidified and stored in the refrigerator for 1 h. The product was filtered to afford **F3** as a light-yellow solid (0.42 g, 91% yield). ^{1}H NMR (CD_3OD, 400 MHz): δ (ppm) 7.82 (d, J = 8.0 Hz, 2H), 7.00-7.03 (m, 8H), 7.64; ^{13}C NMR ($CDCl_3$, 100 MHz): δ (ppm) 131.9, 131.8, 130.4, 123.7, 123.2, 120.9, 91.5.

2.3.12 Preparation of 2.

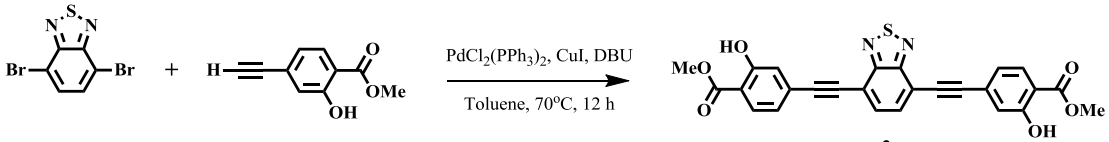

2

64%

A mixture of 2BrDZ (133.5 mg, 0.45 mmol), $PdCl_2(PPh_3)_2$ (28 mg, 0.04 mmol), CuI (8.0 mg, 0.04 mmol) and methyl 4-ethynyl-2-hydroxybenzoate (179.6 mg, 1.02 mmol) in toluene (15 mL) was added with DBU (0.5 mL) and the mixture was stirred at 70°C for 12 h. After the combined filtrate was evaporated, the residue was eluted through a silica gel column by gradient solvents from pure hexane to methylene chloride/hexane (1/1 v/v) as an eluent.to afford **2** was obtained as a yellow green solid (139.5 mg, 64% yield). ^{1}H NMR ($CDCl_3$, 400 MHz) : δ (ppm) 10.81 (s,

2H), 7.86 (d, *J* = 8.0 Hz, 2H), 7.83 (s, 2H), 7.28 (s, 2H), 7.18 (d, *J* = 12.0 Hz, 2H), 3.98 (s, 6H); ^{13}C NMR ($CDCl_3$, 100 MHz) : δ (ppm) 170.2, 161.4, 154.4, 133.0, 130.1, 130.0, 122.8, 121.0, 117.3, 113.0, 96.6, 88.0, 52.6.

2.3.13 Preparation of F2.

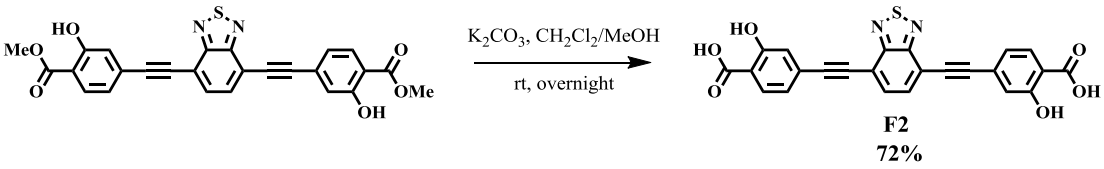

F2
72%

A mixture of **2** (0.50 g, 1.03 mmol) in THF (15 mL) and methanol (15 mL) was added with saturated KOH aqueous solution (0.5 mL) and the mixture was heat to 70^{o}C. After 24 h the solution was evaporated and the residue was dissolved in water (20 mL). Approximately 50 g of ice was then added to the aqueous solution. The mixture was acidified and stored in the refrigerator for 1 h. The product was filtered to afford **F2** as a green solid (0.34 g, 72% yield). ^{1}H NMR (DMSO-d6, 400 MHz) : δ (ppm) 8.00 (s, 2H), 7.85 (d, *J* = 8.0 Hz, 2H), 7.16-7.18 (m, 4H); ^{13}C NMR ($CDCl_3$, 100 MHz) : δ (ppm) 171.1, 160.7, 153.5, 133.3, 130.9, 128.1, 122.3, 119.6, 116.0, 114.1, 95.7, 87.8.

2.3.14 Preparation of 4-iodo-*N*, *N*-dimethylaniline

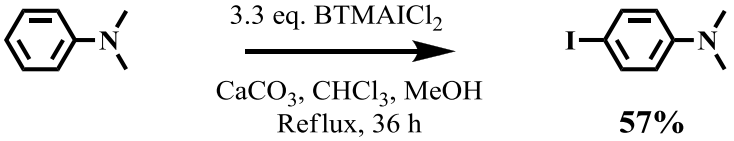

57%

A mixture of *N, N*-dimethylaniline (6.0 g, 50 mmol) in chloroform (100 mL) and methanol (50 mL) was added with $BTMAICl_2$(18.08 g, 52 mmol) and $CaCO_3$ (16.45 g, 0.15 mmol). After the reaction mixture was refluxed for 36 h, 20% $Na_2S_2O_3$ solution was added to the mixture until the mixture became light yellow. The mixture was filtered and the filtrate was extracted with methylene chloride (3 × 50 mL). The combined organic phase was washed with water (2 × 100 mL) and dried over anhydrous $MgSO_4$. The solution was concentrated and the residue was re-precipitated in methanol from methylene chloride solution. Compound 4-iodo-*N*,*N*-dimethylaniline was obtained as a purple solid (6.97 g, 57%): mp ; 91-93^{o}C; ^{1}H NMR

($CDCl_3$, 400 MHz): δ (ppm) 7.46 (d, *J* = 5.6 Hz, 2H), 6.49 (d, *J* = 5.6 Hz, 2H), 2.92 (s, 6 H); ^{13}C NMR ($CDCl_3$, 100 MHz): δ (ppm) 150.0, 137.5, 114.7, 77.4, 40.3.

2.3.15 Preparation of *N*,*N*-dimethyl-4-((trimethylsilyl)ethynyl)aniline

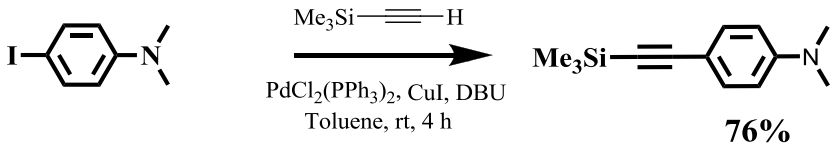

76%

A mixture of 4-iodo-*N*,*N*-dimethylaniline (2.51 g, 10 mmol), $PdCl_2(PPh_3)_2$ (0.35 g, 0.5 mmol), CuI (0.08 g, 0.5 mmol) and trimethylsilylacetylene (1.08 g, 11 mmol) in toluene (10 ml) was added with DBU (1 mL) and the mixture was stirred at room temperature for 4 h. The reaction mixture was then filtered and the solid was washed with toluene (3 × 15 ml). The filtrate was evaporated and the residue was eluted through a silica gel column by gradient solvents starting from pure hexane to methylene chloride/hexane (1/3 v/v) as an eluent to afford *N*,*N*-dimethyl-4-((trimethyl-silyl)ethynyl)aniline as a yellow solid (1.68 g, 76% yield). mp: 88-89°C; ^1H NMR ($CDCl_3$, 400 MHz): δ (ppm) 7.34(d, *J* = 8.0 Hz, 2H), 6.59 (d, *J* = 8.0 Hz, 2H), 2.97 (s, 6H), 0.23 (s, 9H); ^{13}C NMR ($CDCl_3$, 100 MHz): δ (ppm) 150.2, 133.1, 111.6, 109.9, 106.5, 91.1, 40.1, 0.21.

2.3.16 Preparation of 4-ethynyl-*N*,*N*-dimethylaniline

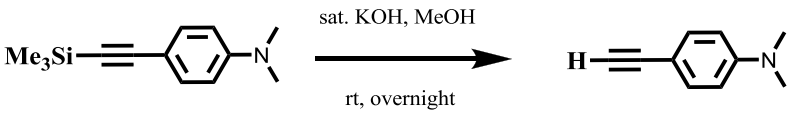

84%

A mixture of *N*,*N*-dimethyl-4-((trimethylsilyl)ethynyl)aniline (1.00 g, 4.6 mmol) and K_2CO_3 (0.059 g, 0.43 mmol) in methylene chloride (15 mL) and methanol (15 mL) was stirred at room temperature for 12 h. Next addition of water, the organic layer was separated and the aqueous phase was extracted with methylene chloride (2 × 50 mL) and was then dried over anhydrous $MgSO_4$. The filtrate was evaporated and the residue was eluted through a silica gel column by gradient solvents starting from pure hexane to methylene chloride/hexane (1/3 v/v) as an eluent to afford 4-ethynyl-*N*, *N*-dimethylaniline as a brown-yellow solid (0.56 g, 84 % yield). mp: 67-69°C. ^1H NMR ($CDCl_3$, 400 MHz): δ (ppm) 7.37 (d, *J* = 8.8 Hz, 2H), 6.62 (d, *J* = 8.8 Hz, 2H),

2.97 (s, 7H); ^{13}C NMR ($CDCl_3$, 100 MHz): δ (ppm) 150.3, 133.1, 111.6, 108.7, 84.8, 74.7, 40.1.

2.3.17 Preparation of $2IN^0$, $I2N^0$, and $3N^0$.

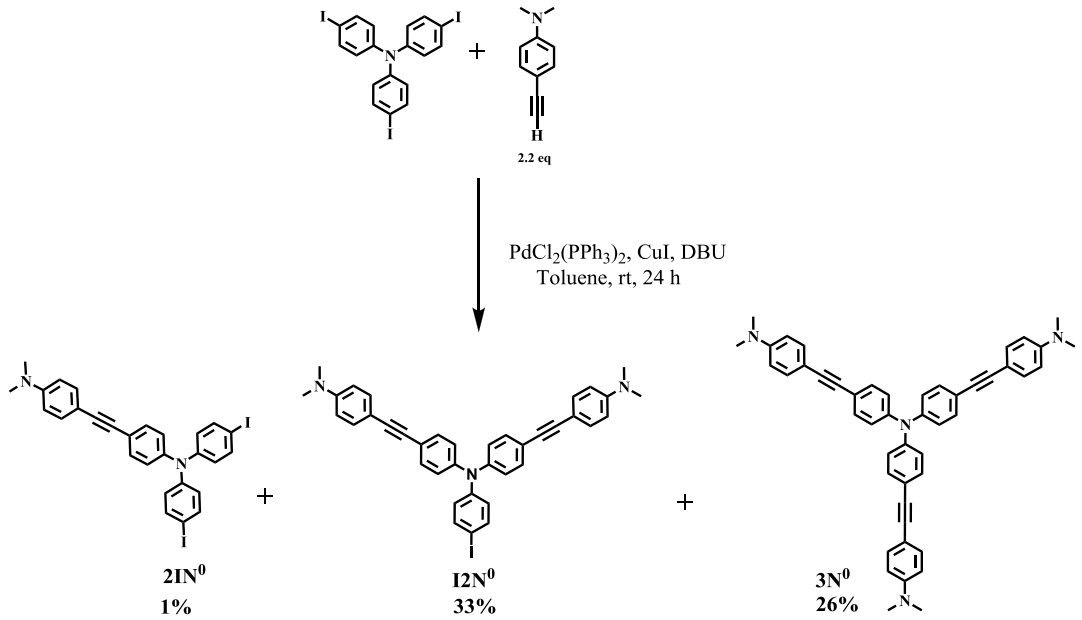

To a mixture of **T3I** (5.0 g, 8.03 mmol), $PdCl_2(PPh_3)_2$ (0.17 g, 0.24 mmol), CuI (0.05 g, 0.24 mmol) and 4-ethynyl-*N*, *N*-dimethylaniline (2.57 g, 17.67 mmol) in toluene (40 mL) was added with DBU (2 mL) and the reaction mixture was stirred at room temperature for 24 h. The reaction mixture was filtered and the solvent was evaporated under reduced pressure. The residue was purified by flash chromatography on silica gel using gradient eluents varied from pure hexane to CH_2Cl_2/hexane (2/1 v/v). **$2IN^0$** was obtained as a yellow solid (0.05 g, 1% yield) mp: 166-169°C. ^{1}H NMR ($CDCl_3$, 400 MHz): δ (ppm) 7.54 (d, *J* = 8.0 Hz, 4H), 7.36-7.40 (m, 4H), 6.98 (d, *J* = 8.0 Hz, 2H), 6.83 (d, *J* = 8.0 Hz, 4H), 6.66 (d, *J* = 8.0 Hz, 4H), 2.99 (s, 6H). ^{13}C NMR ($CDCl_3$, 100 MHz): δ (ppm) 150.1, 146.7, 145.9, 138.4, 132.5, 126.2, 123.7, 119.0, 111.9, 90.5, 87.0, 86.4, 40.3. **$I2N^0$** was obtained as a yellow solid (1.74 g, 33% yield), mp: > 200°C. ^{1}H NMR ($CDCl_3$, 400 MHz): δ (ppm) 7.54 (d, *J* = 8.0 Hz, 2H), 7.38 (dd, 8H), 7.01 (d, *J* = 8.0 Hz, 4H), 6.86 (d, *J* = 8.0 Hz, 2H), 6.66 (d, *J* = 8.0 Hz, 4H), 2.99 (s, 12H). ^{13}C NMR ($CDCl_3$, 100 MHz): δ (ppm) 150.0, 146.8, 146.0, 138.3, 132.6, 126.3, 123.8, 118.7, 111.8, 110.1, 90.4, 87.1, 40.2. **$3N^0$** was obtained as a yellow-brown solid (1.41 g, 26% yield). mp: > 200°C; ^{1}H NMR ($CDCl_3$, 400 MHz): δ

(ppm) 7.39 (dd, 12H), 7.04 (d, J = 8.0 Hz, 6H), 6.66 (d, J = 8.0 Hz, 6H), 2.99 (s, 18H); ^{13}C NMR ($CDCl_3$, 100 MHz): δ (ppm) 149.9, 146.2, 132.6, 123.9, 118.6, 111.9, 90.3, 87.2, 40.2.

2.3.18 Preparation of $4N^0$.

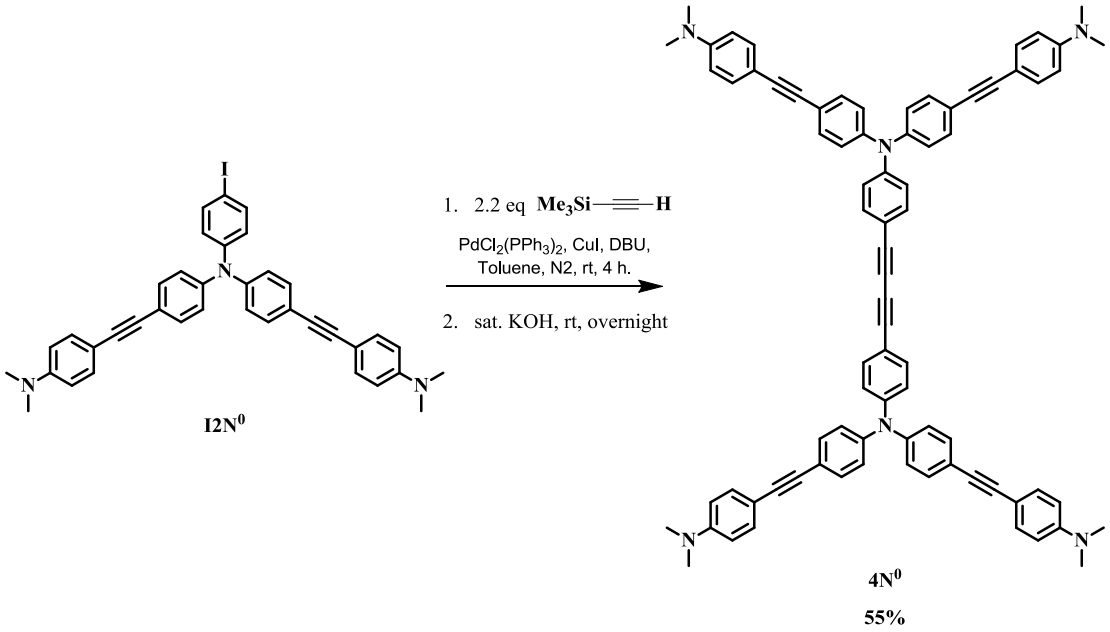

A mixture of **$I2N^0$** (200 mg, 0.30 mmol), $PdCl_2(PPh_3)_2$ (55 mg 0.080 mmol), CuI (15 mg 0.08 mmol) and trimethylsilylacetylene (0.5 mL) in toluene (10 mL) was added with DBU (1 mL) and the mixture was stirred at room temperature for 4 h. Then saturated potassium hydroxide (0.1 mL) was added to the mixture and stirred at room temperature for 24 h. The mixture was filtered and the filtrate was evaporated. The residue was eluted through a silica gel column by gradient solvents starting from pure hexane to hexane/methylene chloride (1/4 v/v) as an eluent to afford **$4N^0$** as a yellow solid (55% yield). mp : > 200°C decompose. ^{1}H NMR ($CDCl_3$, 400 MHz) : δ (ppm) 7.39 (m, 20H), 7.03 (d, J = 8.0 Hz, 12H), 6.66 (d, J = 8.0 Hz, 8H), 2.99 (s); ^{13}C NMR ($CDCl_3$, 100 MHz) : δ (ppm) 150.1, 147.7, 145.8, 133.6, 132.7, 132.5, 124.5, 122.9, 119.4, 115.4, 111.9, 110.2, 90.6, 87.1, 81.8, 73.9, 40.2; MS-ES$^+$ m/z Calcd : for $C_{80}H_{64}N_6$, 1108.5192 Found : 1109.281. Anal. Calcd for $C_{80}H_{64}N_6$: C, 86.61; H, 5.81; N, 7.58. Found : C, 86.60; H, 5.47; N, 7.58.

2.3.19 Preparation of $4N^+I^-$.

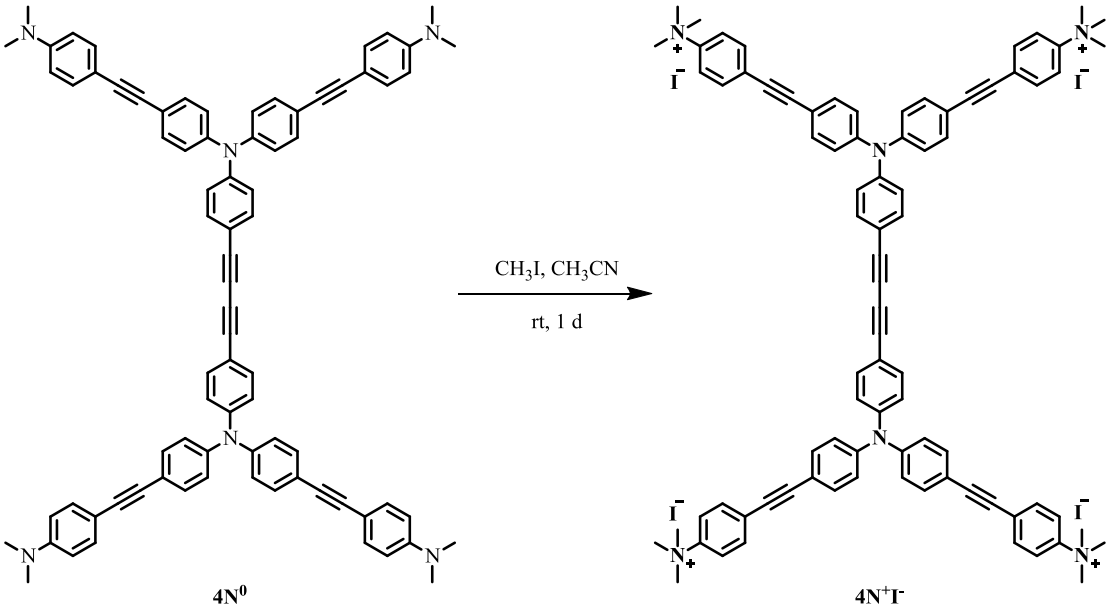

Compound **4N^0** (0.0550 g, 0.05 mmol) was charged into a sealed-tube then CH_3CN (5 mL) and CH_3I (0.5 mL) were added. The mixture was stirred at room temperature for 1 d then precipitated with ether to give **4N$^+$I$^-$** as yellow solid (59% yield). mp: >200^{o}C decompose. ^{1}H NMR ($CDCl_3$, 400 MHz) : δ (ppm) 7.93(d, *J* = 8.0 Hz, 8H), 7.74(d, *J* = 8.0 Hz, 8H), 7.48 (d, *J* = 8.0, 8.0 Hz, 12H), 7.09 (d, *J* = 12.0, 8.0 Hz, 12H), 3.67 (s); ^{13}C NMR ($CDCl_3$, 100 MHz) : δ (ppm) 148.9, 148.6 147.7, 134.9, 134.3, 134.2, 127.4, 125.6, 125.2, 121.6, 118.8, 117.8, 93.0, 87.9, 82.3, 74.7, 57.8; MS-ES$^+$ m/z Calcd : 1168.6110 Found : 292.00 $[M]^{4+}$.

2.3.20 Preparation of $4N^+Cl^-$.

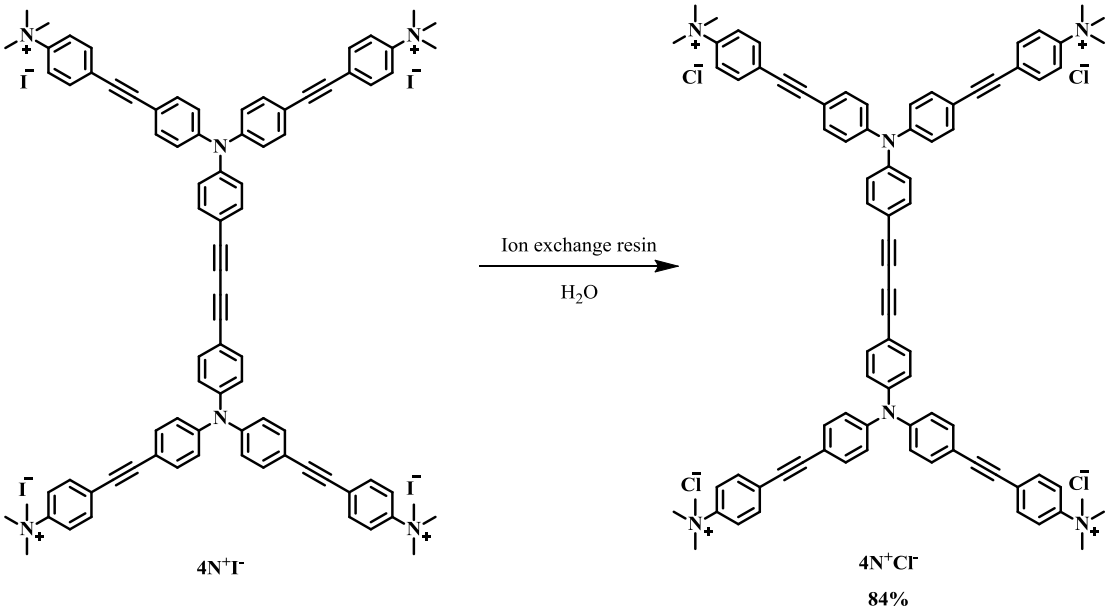

Compound $\mathbf{4N^+I^-}$ (100 mg, 0.06 mmol) was passed through Amberlite IRA-410 anionic ion exchange resin column using DI-water as a mobile phase. The counter anion was exchanged from a strongly nucleophilic iodide ion to a less nuleophilic chloride ion. The fluorophore with chloride anion was obtained as a yellow-orange solid compound $\mathbf{4N^+Cl^-}$ (84 %yield). mp : >200^{o}C decompose. ^{1}H NMR ($CDCl_3$, 400 MHz) : δ (ppm) 7.93 (d, J = 8.0 Hz, 8H), 7.72 (d, J = 8.0 Hz, 8H), 7.46 (d, J = 8.0, 8.0 Hz, 12H), 7.07 (m, 12H), 3.67 (s); ^{13}C NMR ($CDCl_3$, 100 MHz) : δ (ppm) 148.8, 148.5, 147.8, 135.0, 134.4, 134.3, 127.2, 125.6, 125.1, 121.8, 118.8, 117.7, 93.0, 88.1, 82.6, 74.9, 57.9; MS-ES$^+$ m/z Calcd : 1168.6110 Found: 292.00 $[M]^{4+}$.

2.4 Photophysical property study

The stock solutions of fluorophores at 1.0 mM were diluted to 100 μM using phosphate buffer saline (PBS, 10 mM, pH 7.4) and Tris-HCl buffer (10 mM, pH 7.4).

2.4.1 UV-Visible spectroscopy

The UV-Visible absorption spectra of the stock solutions of fluorophores were recorded from 200 nm to 700 nm at ambient temperature.

2.4.2 Fluorescence spectroscopy

The stock solutions of fluorophores were diluted to 1 μM, respectively, with their respective solvents. The emission spectra of fluorophores were recorded from 390 nm to 700 nm at ambient temperature using an excitation wavelength at 320 to 400 nm, respectively.

2.4.3 Fluorescence quantum yields

The fluorescence quantum yield of fluorophores were performed in phosphate buffer saline (PBS, 10 mM) pH 7.4 and Tris-HCl buffer pH 7.4 using quinine sulphate (Φ_F = 0.54) in 0.1 M H_2SO_4 as a reference [23]. The UV-Visible absorption spectra of five analytical samples and five reference samples at varied concentrations were recorded. The maximum absorbance of all samples should not exceed 0.1. The fluorescence emission spectra of the same solutions using appropriate excitation wavelengths selected were recorded based on the absorption maximum wavelength (λ_{max}) of each compound. Graphs of integrated fluorescence intensities were plotted against the absorbance at the respective excitation wavelengths. Each plot should be linear with a y-interception at 1 and gradient *m* [24].

In addition, the fluorescence quantum yield (Φ_F) was obtained from a plot between integrated fluorescence intensity and absorbance as represented in the following equation:

$$\Phi_X = \Phi_{ST}\left(\frac{Grad_X}{Grad_{ST}}\right)\left(\frac{\eta_X^2}{\eta_{ST}^2}\right)$$

The subscripts Φ_{ST} denotes the fluorescence quantum yield of a standard reference which used quinine sulphate in 0.1 M H_2SO_4 (Φ_F = 0.54) and Φ_X is the fluorescence quantum yield of sample and η is the refractive index of the solvent.

2.5 Fluorescent sensor study

2.5.1 Metal ion sensor

The stock solutions of **F2-F5** with a concentration of 10 mM in phosphate buffer saline pH 7.4 were prepared. The emission spectrum of compound was recorded from 390 nm to 700 nm at ambient temperature using an excitation

wavelength in the range of 316-395 nm. The fluorescent responses were monitored in the presence of 19 metal ions, with and without surfactants. Metal acetate, sulphate, nitrate and chloride solutions were prepared in Milli-Q water. Concentrations of all stock metal ion solutions were adjusted to 1 mM and were added with the desired volumes (0-500 μL) to the fluorophore solutions. The final volumes of the samples were adjusted to 1.0 mL.

2.5.2 Surfactant enhancement

The stock solution of compound **F4** and **F5** with a concentration of 100 μM in phosphate buffer saline pH 7.4 was prepared. The emission spectrum of **F4** and **F5** were recorded from 390 nm to 700 nm at ambient temperature using an excitation wavelength at 373 and 379 nm, respectively. The photophysical properties were studied in the presence of three surfactants (anionic, cationic and non-ionic surfactants). The stock surfactants were prepared in Milli-Q water. Concentrations of all stock surfactants were adjusted to 1 mM and were added with the desired volumes (0-300 μL) to the fluorophore solutions. The final volumes of the samples were adjusted to 1.0 mL.

2.5.3 DNA sensor

The excitation wavelength of compound **4N$^+$Cl$^-$** was 378 nm and the emission was recorded from 390 to 600 nm. Solutions of all fluorophores were prepared in 10 mM Tris-HCl buffer pH 7.4 using a sonication bath. Tris-HCl buffer was added fluorophore solution at room temperature, and then DNA was added to the solution. The fluorescent spectra were measured after mixing for 3 min. The final volume of the mixture was adjusted to 1.0 mL by Tris-HCl buffer to afford the final concentration of 1 μM for fluorophore and 0.25 μM for DNA. After the solution was mixed and incubated for 3 min, SYBR Green II 10,000x diluted was added. The fluorescent spectra were acquired after the mixture was incubated for 1 min at room temperature (25^{o}C). The FRET ratios were observed as the intensity of the acceptor (SYBR Green II) signal from the normalized spectrum of the fluorophore signal.

CHAPTER III

RESULTS AND DISCUSSION

3.1 Synthesis and characterization of fluorophores

To enhance the water solubility of the fluorophores, salicylic acid group was used for the peripheral group of the target molecules. The peripheral group, methyl-4-ethynyl-2-hydroxybenzoate was synthesized by the Sonogashira coupling of trimethylsilylacetylene with methyl 2-hydroxy-4-iodobenzoate followed by a base-catalyzed desilylation (**Scheme 3.1**).

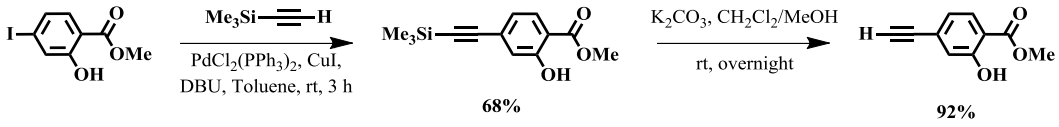

Scheme 3.1 Synthesis of peripheral group.

The reactive core, 4, 4′, 4″-triiodotriphenylamine (**T3I**), was prepared from triple iodination of triphenylamine using benzyltrimethyl-ammonium iododichloride ($BTMAICl_2$) **(Scheme 3.2**). With the necessary 35 building blocks in hands, we proceeded with the Sonogashira coupling between **T3I** and methyl 4-ethynyl-2-hydroxybenzoate to form di-substitution compound and followed by another Sonogashira coupling with trimethylsilylacetylene and desilylation with potassium carbonate to afford compound **4** (**Scheme 3.3**).

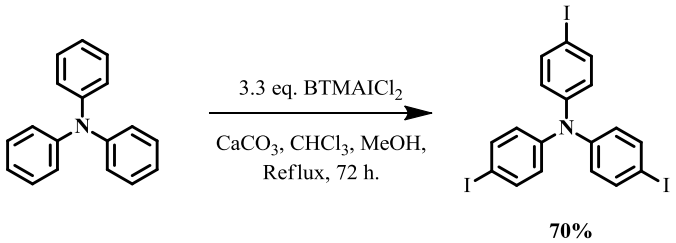

Scheme 3.2 Synthesis of reactive core.

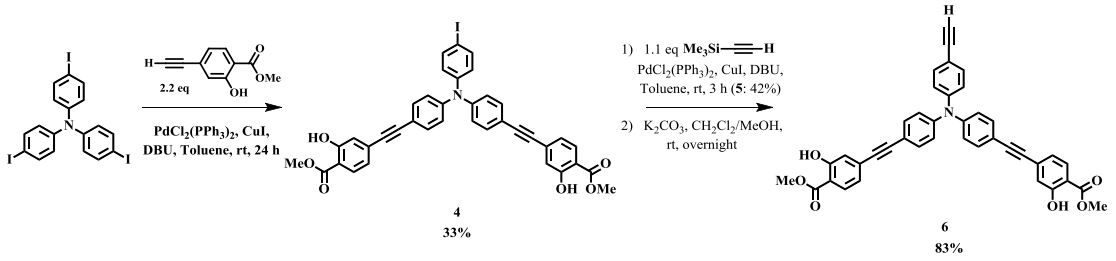

Scheme 3.3 Synthesis of **6**.

The synthesis of the dendritic fluorophore starting from the Sonogashira coupling of the core **T3I** with 2.2 eq of methyl-4-ethynyl-2-hydroxybenzoate gave to the **3** and **4**, which **3** was treated with KOH to provide the trisalicylic acid (**F4**) (**Scheme 3.4**). The homocoupling of methyl-4-ethynyl-2-hydroxybenzoate and **4** were prepared under Sonogashira coupling condition to afford dimethyl-salicylate (**1**) and tetramethyl-salicylate (**7**), respectively. The base-catalyzed hydrolysis of both of methyl-salicylate were given anionic dendritic fluorophore **F3** and **F5** in satisfactory yield (**Scheme 3.5**). The fluorophore **F2** was obtained from a base hydrolysis of compound **2** which was prepared from the coupling between two equivalents of methyl 4-ethynyl-2-hydroxybenzoate and 4,7-dibromo-2,1,3-benzothidiazole (**Scheme 3.6**).

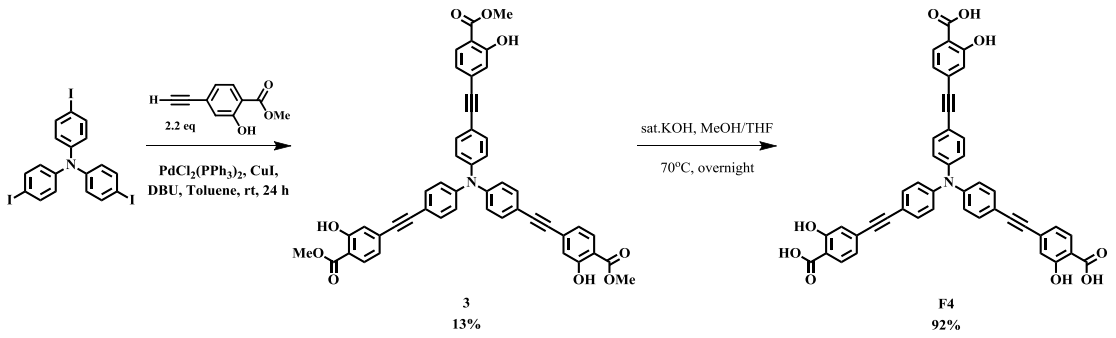

Scheme 3.4 Synthesis of **F4**.

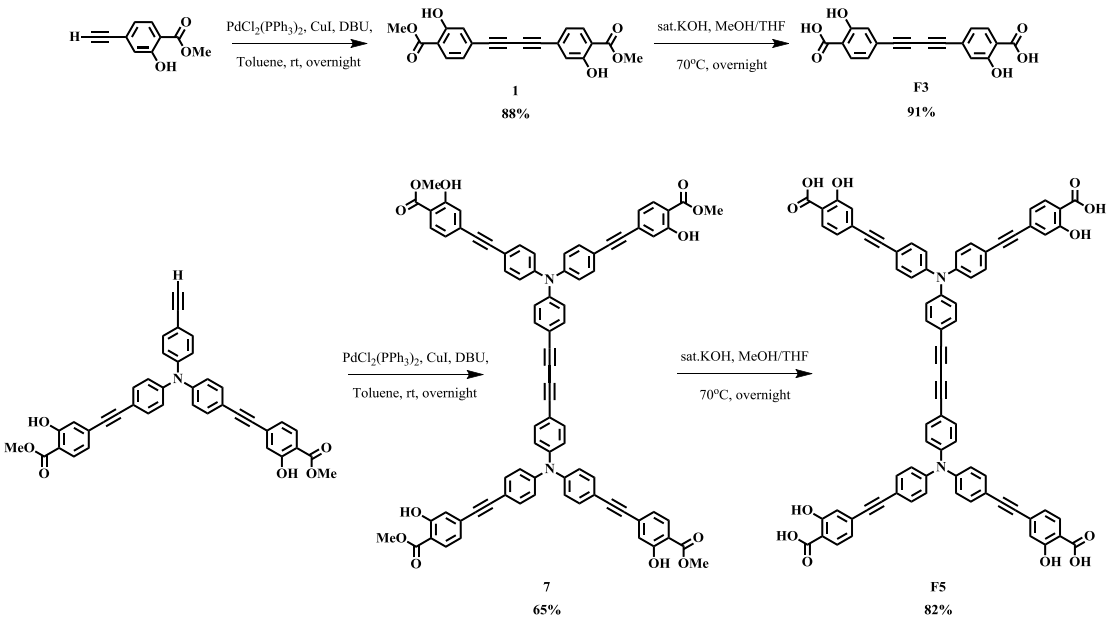

Scheme 3.5 Synthesis of **F3** and **F5**.

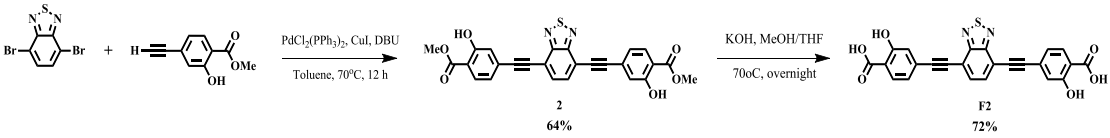

Scheme 3.6 Synthesis of **2** and **F2**.

The ^{1}H NMR spectra of compound **F2**, **F3**, **F4**, **6**, and **F5** are shown in **Figure 3.1-3.5**. All signals can be assigned to all protons in each corresponding structure. Initially, methyl 4-ethynyl-2-hydroxybenzoate peripheral group showed signals of ethynyl, methyl ester and hydroxyl protons at 3.21, 3.95 and 10.76, respectively. The aromatic signals appeared as singlet and two doublet at 7.10, 6.99 and 7.78 ppm. Then, homocoupling of methyl-4-ethynyl-2-hydroxybenzoate by using Sonogashira reaction, the product **1** showed signals of the methyl ester and hydroxyl protons as a singlet at 3.98 and 10.81 ppm, singlet and two doublet signals at 7.14, 7.03 and 7.82 ppm correspondingto the aromatic protons. The hydrolysis of **1** gave **F3**, which is soluble in Methanol-d4 solution. The spectrum showed that the singlet signal of the methylester proton at 3.98 ppm disappeared upon the hydrolysis (**Figure 3.1**).

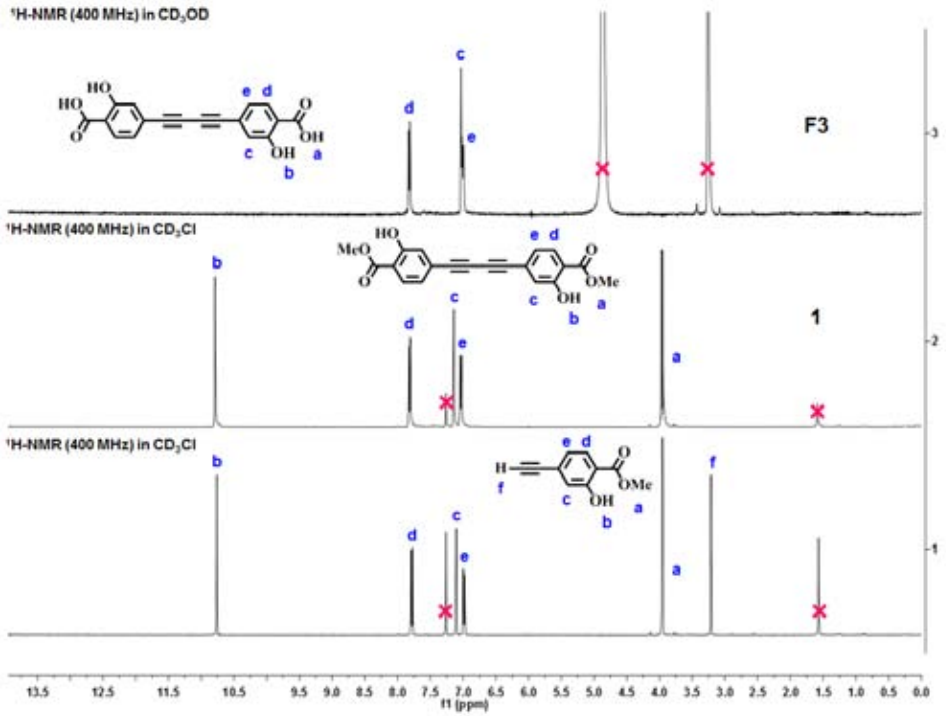

Figure 3.1 ^{1}H-NMR (400 MHz) of methyl-4-ethynyl-2-hydroxybenzoate**, 1** and **F3**.

The 4,4',4"-triiodotriphenylamine core (**T3I**) showed two doublet signals at 6.81 and 7.53 ppm corresponding to its aromatic protons. Then, **T3I** coupling with methyl-4-ethynyl-2-hydroxybenzoate by using Sonogashira coupling reaction, the tri-substitution product (**3**) showed singlet signals of the methyl ester protons at 3.96 ppm and aromatic proton signals at 7.01, 7.10, 7.45 and 7.80 ppm The signal of hydroxyl proton on phenyl ring at 10.78 ppm. For **F4**, a signal of methyl ester protons and hydroxyl proton disappeared upon the hydrolysis (**Figure 3.2**).

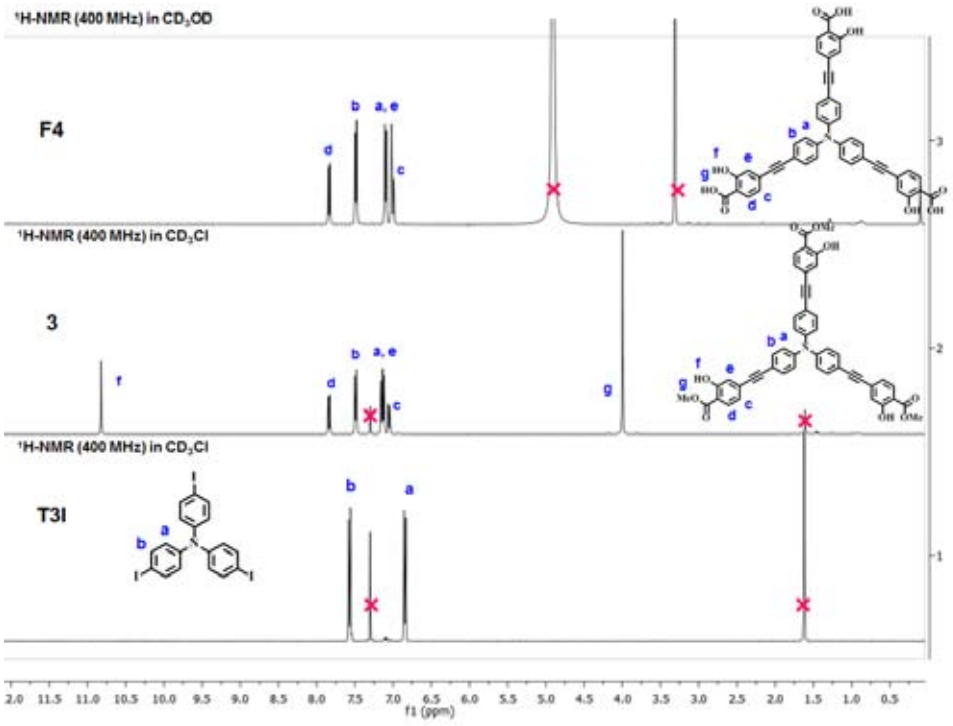

Figure 3.2 ^{1}H-NMR (400 MHz) of **T3I, 3** and **F4**.

The coupling of **4** with trimethylsilylacetylene by Sonogashira coupling reaction. Compound **5** showed signals of the trimethylsilylacetylene protons at 0.25 ppm. The desilylation of **5** gave **6**, the signal of ethyne proton at 3.96 ppm appeared (**Figure 3.3**). For the homocoupling reaction of **6**, the ethyne proton signal was disappeared and showed new doublet and multiplet signals of aromatic protons of **7** at 7.02, 7.45, 7.80 and 7.10 ppm. Upon the hydrolysis, the signal of methylester protons at 3.96 ppm disappeared (**Figure 3.4**).

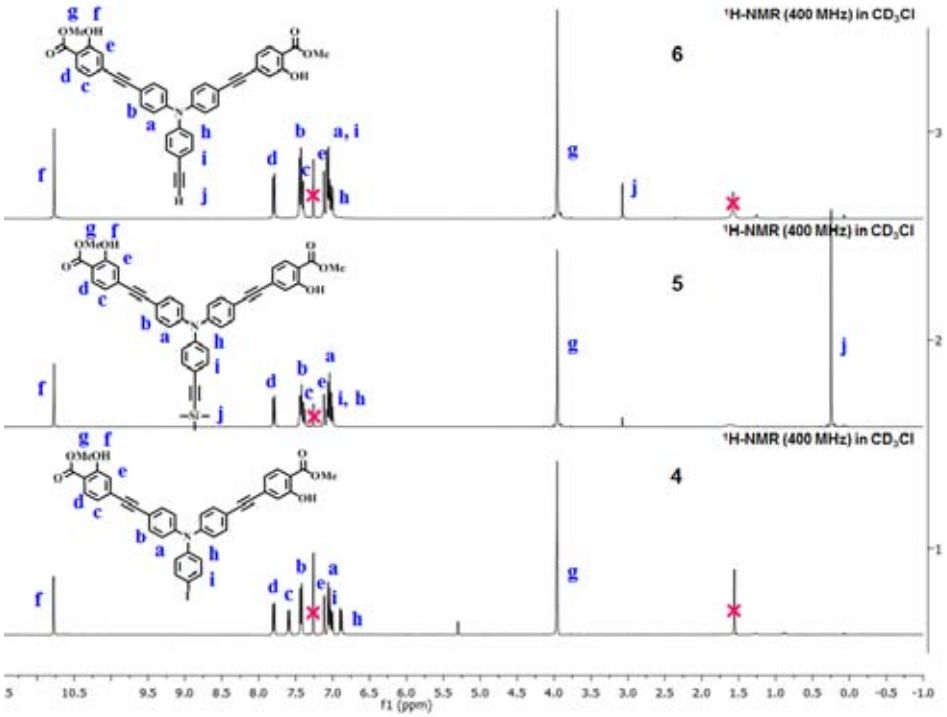

Figure 3.3 ^{1}H-NMR (400 MHz) of **4, 5** and **6**.

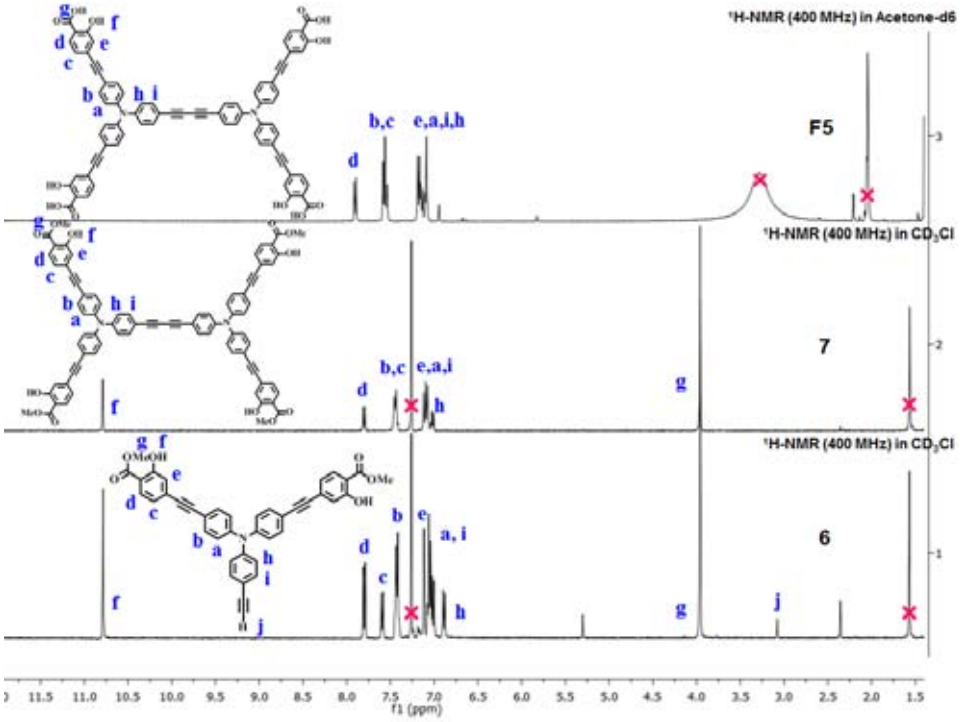

Figure 3.4 ^{1}H-NMR (400 MHz) of **6, 7** and **F5**.

The methyl 4-ethynyl-2-hydroxybenzoate coupling with 4,7-dibromo-2,1,3-benzothidiazole to provide the fluorophore **2**, which showed signals of the methyl ester protons as a singlet at 3.98 ppm and hydroxyl protons at 10.79 ppm. The aromatic protons showed two singlet at 7.28 and 7.83 ppm, two doublet signals at 7.18 and 7.86 ppm (**Figure 3.5**). For hydrolysis of **2** to afford **F2**, the signals of the aromatic protons appeared at 7.18 and 8.00 ppm of singlet signal, 7.16 and 7.85 ppm of doublet signal.

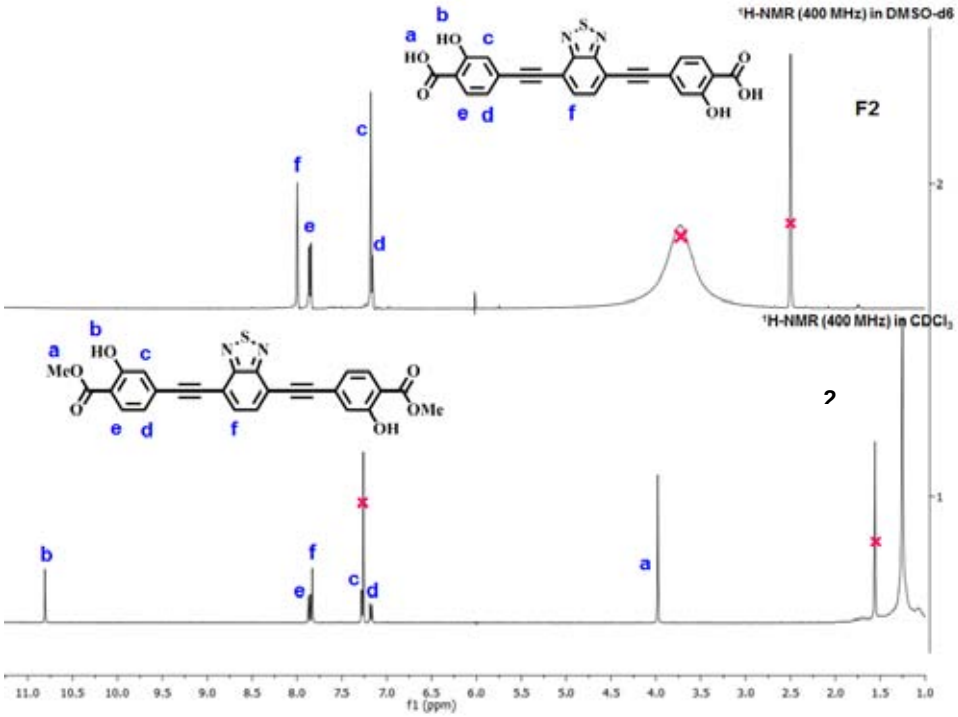

Figure 3.5 ^{1}H-NMR (400 MHz) of **2** and **F2**.

3.2 Photophysical property study

The photophysical properties of the four new fluorophores (**F2-F5**) in phosphate buffer saline (PBS) pH 7.4 are compiled in **Table 1** and for spectra see **Figure 3.6** along with those of **F1**. The fluorophores showed the maximum absorption wavelength (λ_{ab}) in the range of 316-395 nm. The order of λ_{ab}, **F2** > **F5** > **F4** > **F3** > **F1**, indicated the sizes of the HOMO-LUMO gaps associated with the delocalization of π-conjugated system. The observed molar extinction coefficients of all fluorophores were well above 1×10^{4} excepted for that of **F2** which was probably underestimated due to its poor solubility in water at physiological pH. All

fluorophores showed maximum emission wavelengths (λ_{em}) in the range of 434-532 nm with the fluorescence quantum yield of 0.2-3.2%. Among the four new fluorophores, only **F4** showed higher quantum yield than **F1** that probably due to its least planar conformation allowing the least self-quenching via intermolecular π-π interaction [25-29].

Table 3.1 Photophysical properties of **F2-F5** in PBS (10 mM, pH 7.4).

Compound	Absorption		Emission	
	λ_{ab} (nm)	log ε	λ_{em} (nm)	Φ (%)[a]
F1[b]	316	4.28	465	0.7
F2	395	3.61	532	0.2
F3	322	4.44	434	0.3
F4	373	4.84	506	3.2
F5	379	4.80	480	0.4

[a]Quinine sulfate in 0.1 M H_2SO_4 (Φ = 54%) was used as the standard.

[b]The data are taken from ref. 15.

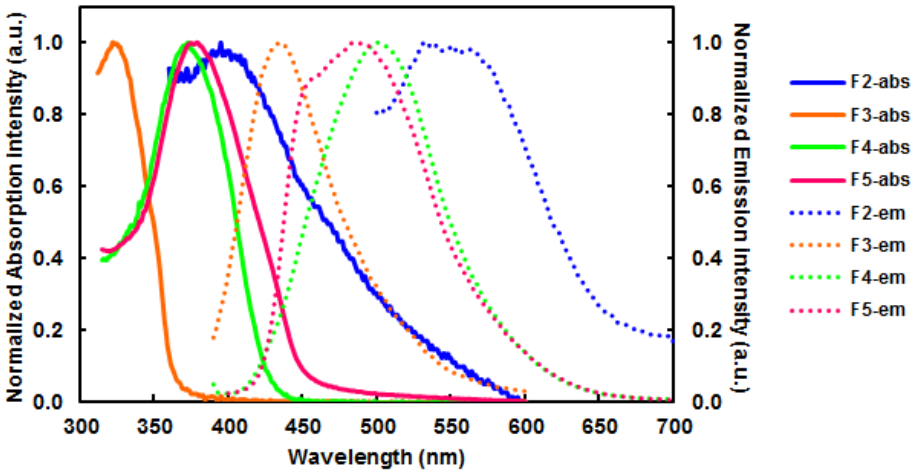

Figure 3.6 Normalized absorption and emission spectra of **F2-F5** in 10 mM phosphate buffer saline pH 7.4.

3.3 Metal ion sensor

To evaluate the Cu^{2+} sensing ability of the four new salicylic fluorophores, the fluorescence signal of **F2-F5** solution in PBS pH 7.4 were recorded in the absence and presence of Cu^{2+}. **Figure 3.7** clearly shows that only the fluorescence signal of **F4** and **F5** are quenched by Cu^{2+} ions while **F2** and **F3** do not show any responses. The results indicated that not only the salicylic acid binding sites but also the π-conjugated systems are important for Cu^{2+} quenching ability. Since the fluorescence quenching mechanism of Cu^{2+} is widely accepted as the photo-induced electron transfer (PET) process, the differences in the quenching ability should be the result of energy level mismatch between the electron donor and acceptor due to the variation of the π-conjugated systems. In this case, the most stable excited state level of **F2** is probably too low and that of **F3** is too high to allow efficient PET from the fluorophores to the Cu-salicylate complex.

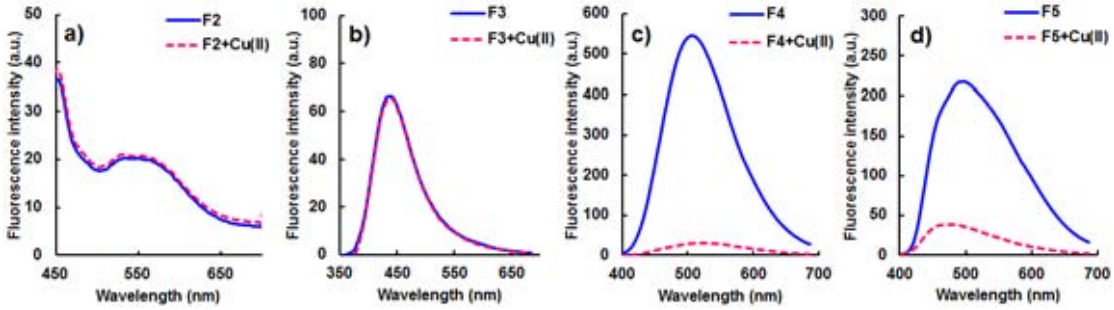

Figure 3.7 Emission spectra of (a) **F2**, (b) **F3**, (c) **F4** and (d) **F5** (1 μM) in the absence and presence of Cu^{2+} (10 μM) in PBS pH 7.4.

To study the selectivity of **F4** and **F5** toward metal ions, the fluorescence responses upon the addition of various metal ions (Ag^{+}, Al^{3+}, Ba^{2+}, Ca^{2+}, Cd^{2+}, Co^{2+}, Fe^{2+}, Fe^{3+}, Hg^{2+}, K^{+}, Li^{+}, Mg^{2+}, Mn^{2+}, Na^{+}, Ni^{2+}, Pb^{2+}, Sr^{2+} and Zn^{2+}) were monitored. We found that the fluorescence signal of **F4** was distinctively quenched by Cu^{2+} (over 20 times) and slightly quenched by Fe^{2+} (**Figure 3.8a**). However, **F5** showed less quenching sensitivity toward Cu^{2+} as well as less selectivity between Cu^{2+} and Fe^{2+} (**Figure 3.8b**). The interference test, performed by using the interfering metal ions at 10 times of concentration of Cu^{2+}, showed low interference levels of all ions tested on

F4 (**Figure 3.9a**) but high interference levels of Fe^{2+} tested on **F5** (**Figure 3.9b**). **F4** gave ratio of the fluorescence intensity in the absence (I_0-I) and presence (I_0-I_M) of interfering ions very close to 1.

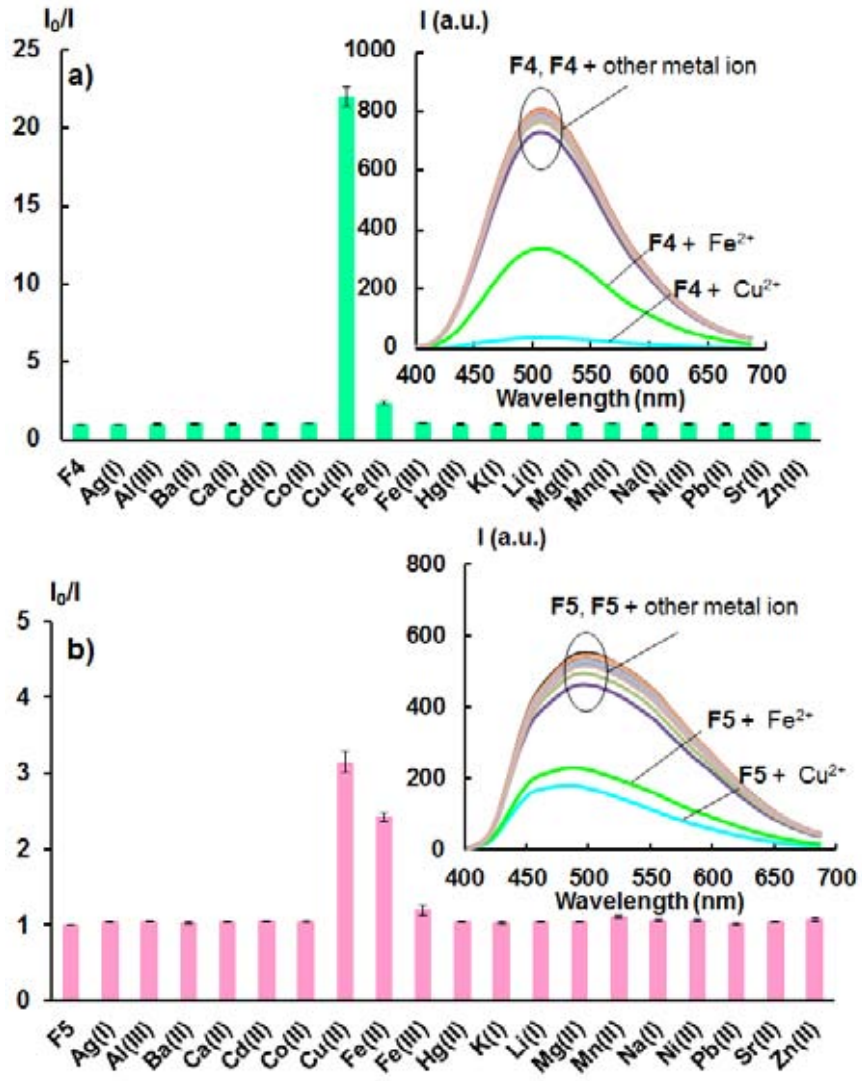

Figure 3.8 Fluorescence quenching of (a) **F4** and (b) **F5** (5 μM) by various metal ions (5 μM) in PBS (10 mM, pH 7.4) showing along with the corresponding fluorescence spectra in the insets.

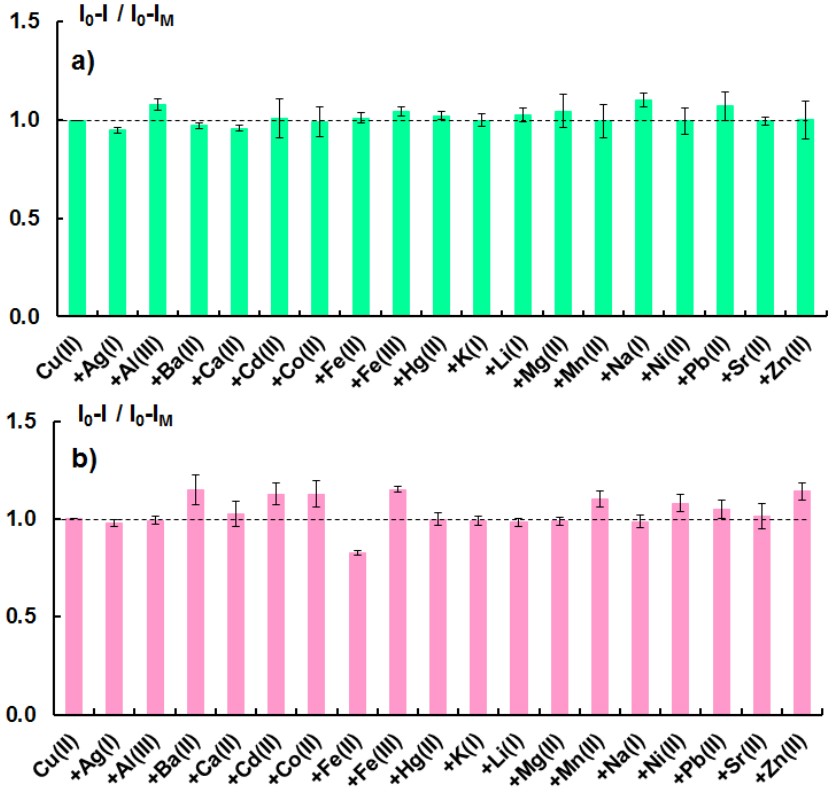

Figure 3.9 Bar chart displays fluorescence intensity ratio (I_0-I/I_0-I_M) of (a) **F4** and (b) **F5** in the presence of Cu^{2+} (5 μM) and another interfering metal ion (50 μM).

The Stern-Volmer plots of the fluorescence quenching against the Cu^{2+} concentration gave linear lines with the slopes corresponding to the quenching efficiency (K_{sv}) of 5.79 × 10^6 M^{-1} and 1.31 × 10^6 M^{-1} for **F4** and **F5**, respectively (**Figure 3.10**). Clearly, Cu^{2+} quenched **F4** more efficiently than **F5** that is mainly contributed by the higher initial fluorescence quantum yield of **F4**. The results confirmed that **F4** is a better Cu^{2+} sensor. It is also important to mention here that **F4** gave quenching efficiency about 3 times of what was reported for our previous fluorophore **F1** [15]. In PBS pH 7.4, **F4** and **F5** gave the detection limits (at 3×noises) of 0.5 ppb and 6.9 ppb, respectively, well below the WHO recommendation for the concentration limit of 2 mg/L in drinking water [30].

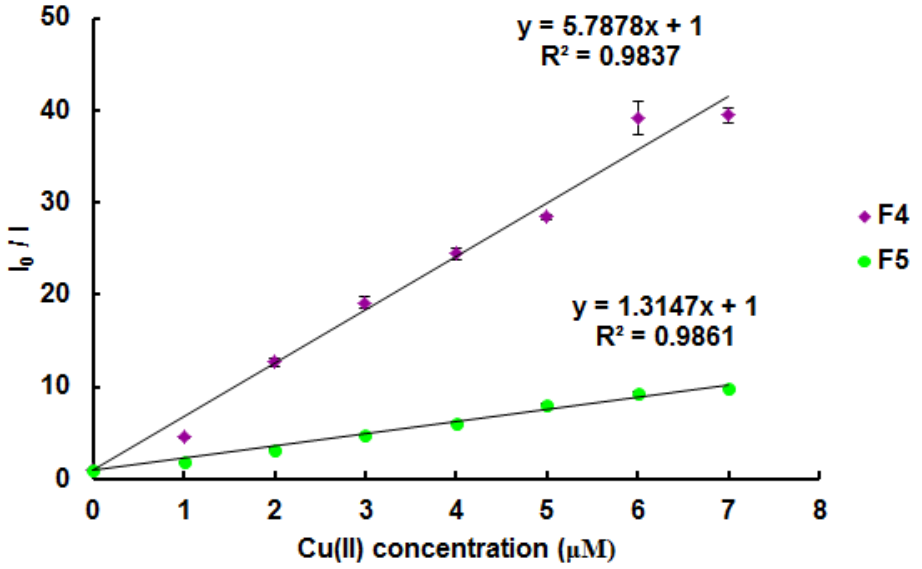

Figure 3.10 Stern-Volmer plots for fluorescence quenching of **F4** and **F5** (1 μM) by Cu^{2+} in PBS (10 mM, pH 7.4).

Several fluorescent molecules in the literature report have demonstrated fluorescence enhancements by addition of surfactants [31, 32 and 33]. In this study, the anionic, cationic and non-ionic surfactant (SDBS, HTAB and Triton X-100, respectively) were selected to test. The fluorescent signals of fluorophore **F4** and **F5** in the presence of each surfactant (0.1 mM), both before and after the addition of Cu^{2+}, are shown in **Figure 3.11** and **Figure 3.12**, respectively. It is showed that the Triton X-100 could provide a clear differentiation for the systems with and without Cu^{2+}. Therefore, Triton X-100 was chosen for further studies.

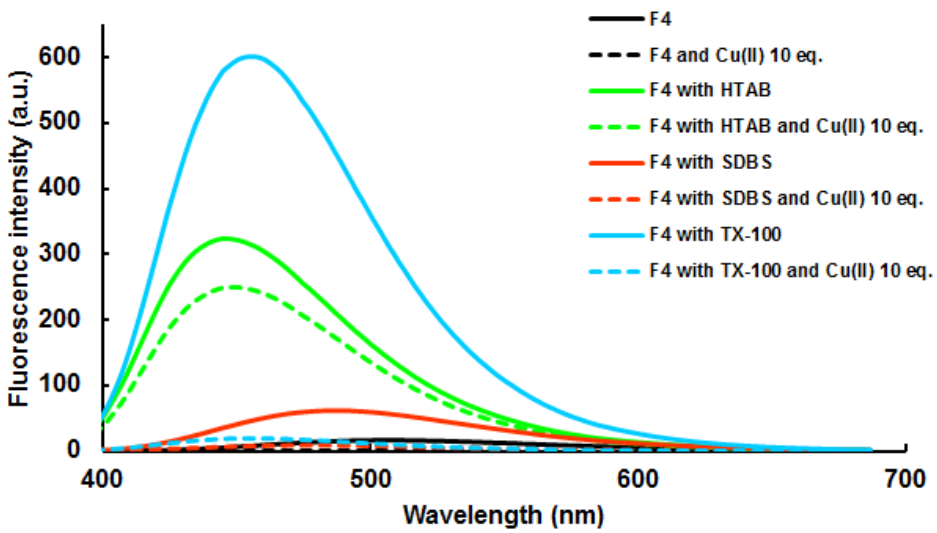

Figure 3.11 Effects of surfactants on fluorescent intensity of **F4** and its responses to Cu^{2+}.

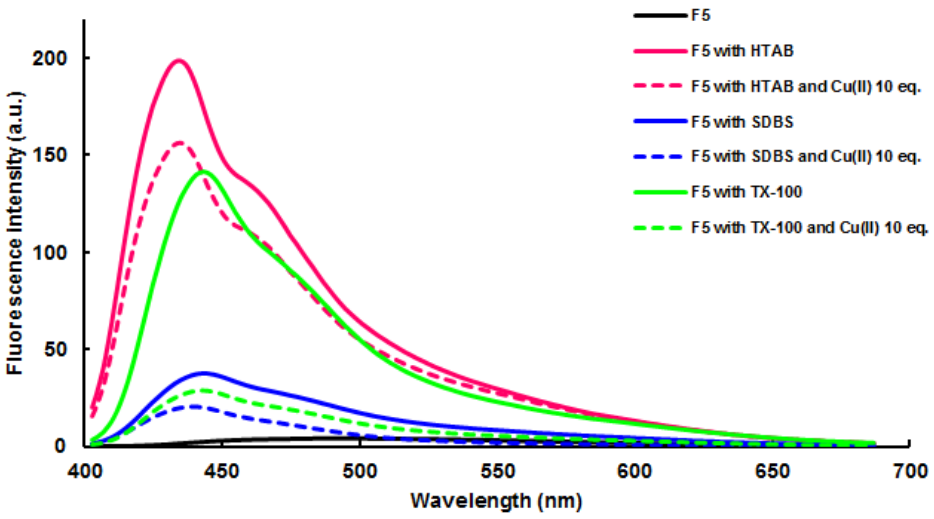

Figure 3.12 Effects of surfactants on fluorescent intensity of **F5** and its responses to Cu^{2+}.

By comparing the fluorescence intensity of **F4** and **F5** in various concentrations of Triton X-100, found that the concentration of 10 μM (0.01 mM) could provide the best quenching efficiency upon addition of Cu^{2+}. While the concentration more than 10 μM, the fluorescence signals were slightly quenched by Cu^{2+}. Since the concentration of Triton X-100 was used lower than the Critical

Micelle Concentration (CMC) of the Triton X-100 (0.2 mM). This result suggested that the fluorescence enhancement was not due to the micellar effect. The addition of non-ionic surfactant could change the polarity of the medium or interact with the fluorophore bring about hydrophobic environment. The hydrophobic environment reduces the ICT process of the fluorophore that increase the sensitivity of the sensing system (**Figure 3.13** and **Figure 3.14**).

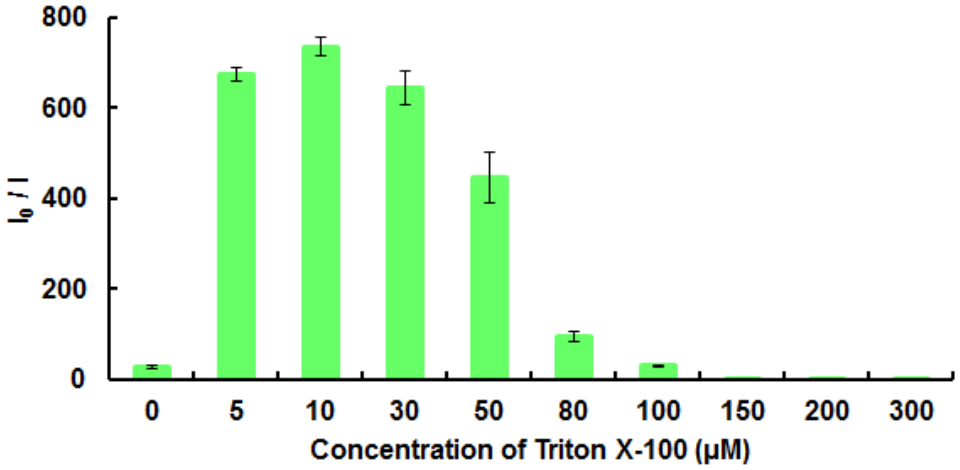

Figure 3.13 Quenching efficiencies of **F4** (1 μM) with Cu^{2+} (10 μM) under various concentrations of Triton X-100.

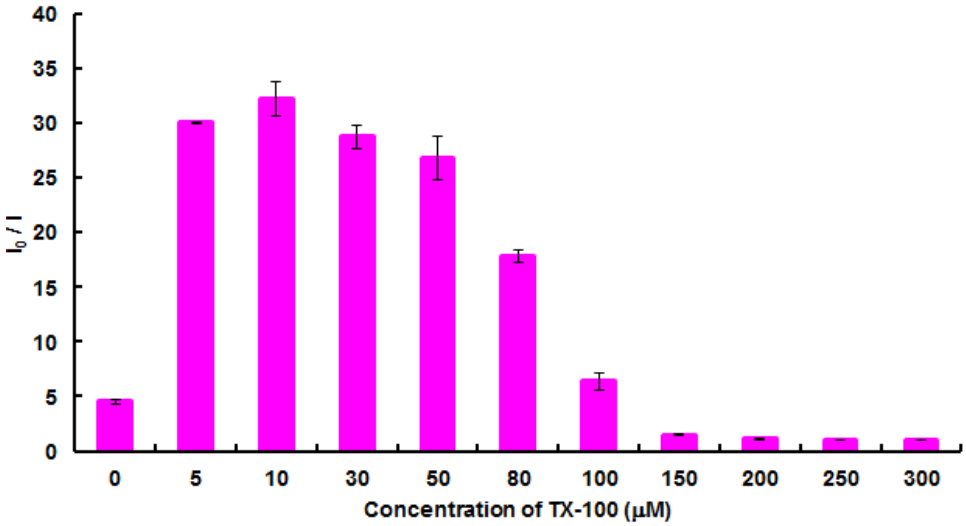

Figure 3.14 Quenching efficiencies of **F5** (1 μM) with Cu^{2+} (10 μM) under various concentrations of Triton X-100.

A Stern-Volmer plots of the fluorescence quenching of **F4** and **F5** in the presence of Triton X-100 were obtained by a series of experiments using various concentration of Cu^{2+}. The slope of the plot provided quenching efficiency (K_{sv}) for the **F4** and **F5** sensing systems (**Figure 3.15** and **Figure 3.16**). Noticeably, the system of **F4** with Triton X-100 gave the K_{sv} of 2.72×10^6 M^{-1} which is about two times higher than that of the surfactant free system (1.16×10^6 M^{-1}). The plots also gave the detection limit of Cu^{2+} as 5.19×10^{-8} M (3.29 ppb) and 1.23×10^{-7} M (7.82 ppb) for the system with and without Triton X-100, respectively. While **F5**, the K_{sv} of 4.97×10^6 M^{-1} in the without TX-100 system. The K_{sv} of **F5** in the presence of TX-100 could not be calculated because a Stern-Volmer plots was obtained in S-curve plot. The quenching efficiency increased slightly at 1-3 μM of Cu^{2+} concentration, when the concentration of Cu^{2+} 4-10 μM, observed a fluorescence switching-off effect because occurred a superquenching behavior.

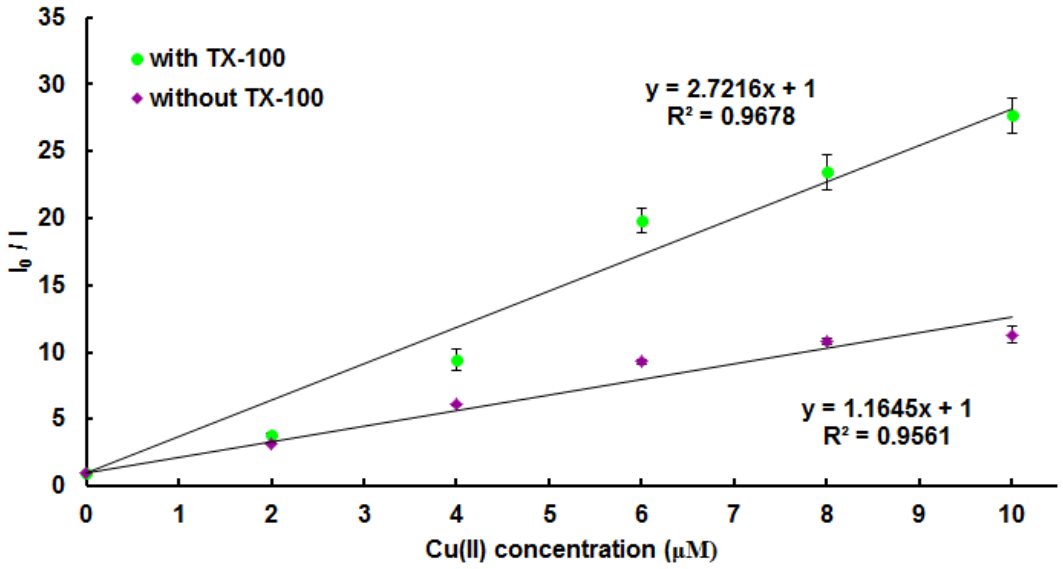

Figure 3.15 The Stern-Volmer plots of fluorescence quenching of **F4** by Cu^{2+} in the presence and absence of Triton X-100.

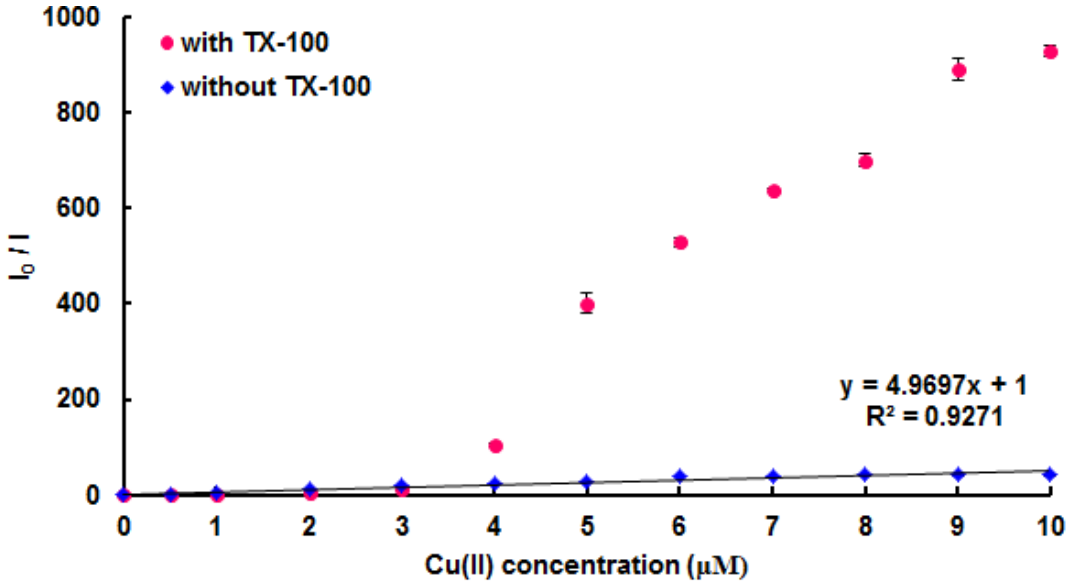

Figure 3.16 The Stern-Volmer plots of fluorescence quenching of **F5** by Cu^{2+} in the presence and absence of Triton X-100.

The fluorescence quenching of **F4** by Cu^{2+} is probably due to the good selectivity of the chelation of salicylate groups with Cu^{2+} to form **F4**·Cu^{2+} complex. Interestingly, the fluorescence quenching signal of could be completely restored by addition of cysteine (Cys). Transition metal ions are known to have high affinity towards the thiols containing compounds, for instance, fluorescence turn-on assay for GSH can be established since the free thiols can form the complex with Cu^{2+} [34,35]. The fluorescence ratio of **F4** with Cu^{2+} are increase rapidly with the increase of the cysteine (Cys) concentration (**Figure 3.17**). The release of **F4** due to competitive binding of Cys with Cu^{2+} is clear by the fluorescence turn-on.

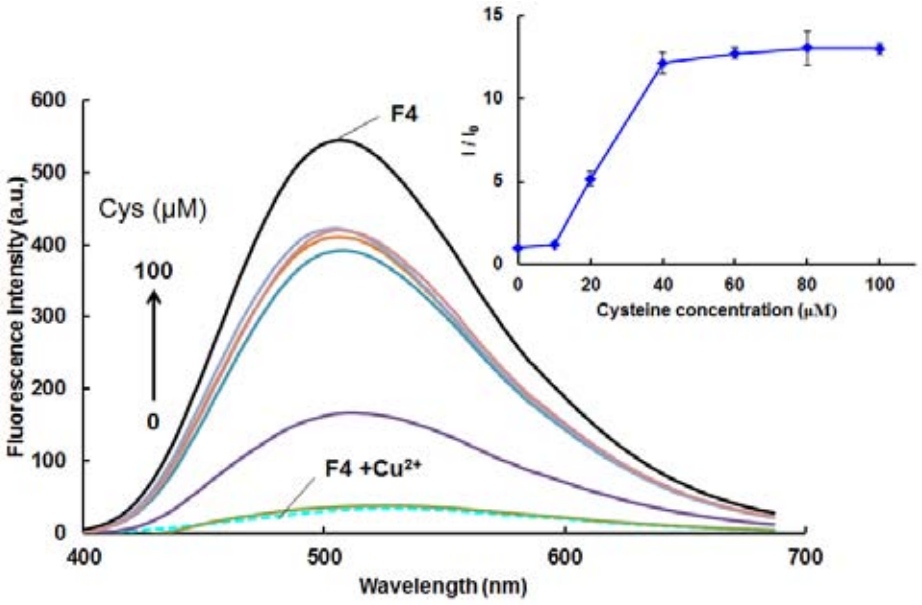

Figure 3.17 Changes in the fluorescence quenching of **F4** (1 μM) with Cu^{2+} under various concentration of Cys. Inset: fluorescence restoration (I/I_0) versus the concentration of Cys.

It is interested to examine the fluorescence response of **F4**·Cu^{2+} complex to other amino acids, because highly selective response to cysteine over other amino acids is an essential, so that the selectivity was extended to various amino acids. The experimental results indicated that other amino acids could be recovered the fluorescence quenching of **F4**·Cu^{2+} complex (**Figure 3.18**). This result described low cysteine concentration could slightly recover the fluorescence quenching signal of the complex. The signal could be fully recovered when the cysteine concentration of 40 μM (**Figure 3.17 inset**).

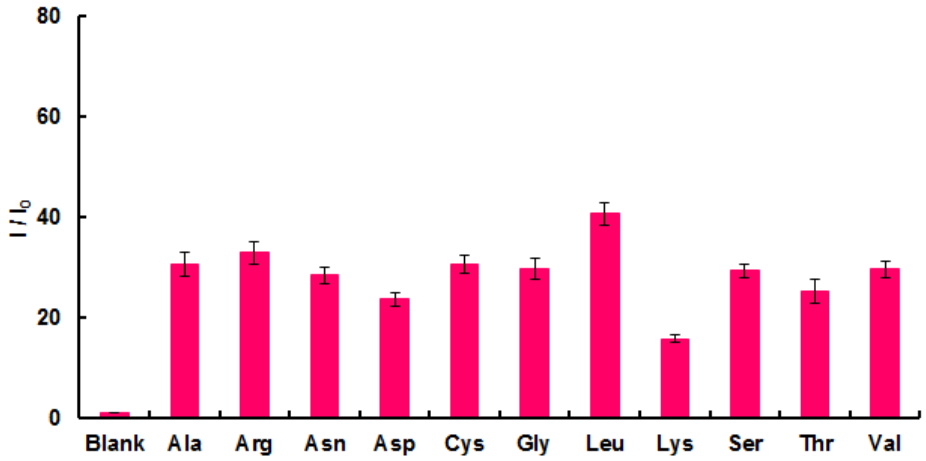

Figure 3.18 Fluorogenic responses of **F4** (1 μM in 10 PBS pH 7.4) with Cu^{2+} (10 μM) in the presence of 11 amino acids (10 μM).

To fabricate solid state sensor for convenient detection of Cu^{2+}, we applied a series of 1.0 μL drops of **F4** solutions in EtOH (0.01-1.0 mM) on to a piece of filter paper and allowed for air dry to generate spots each containing 0.01-1.0 nmol of **F4**. The prepared filter paper was dropped with a series of 1.0 μL $CuSO_4$ solutions (10-500 μM) to the same positions of the fluorophore blots. After drying, the filter paper was visualized under an ordinary 20W black light lamp. The photographic images of the filter paper showed bright blue emission spots which contained at least 0.1 nmol of **F4** (**Figure 3.19**). The quenching of the blue emission was clearly observed where at least 40 pmol of Cu^{2+} was applied on both 0.1 and 1.0 nmol of **F4**. The detection limit for naked eye observation from this paper-based sensor is thus a mere 40 pmol of Cu^{2+}. This naked eye detection limit is well below the warning level, of 0.6 μmol in urine collected for 24 hours for Wilson's disease [36, 37 and 38]. To our knowledge, this microliter-dropped paper-based sensor constructed from **F4** is one of the most sensitive and convenient platform for Cu^{2+} detection ever been reported to date [39-51].

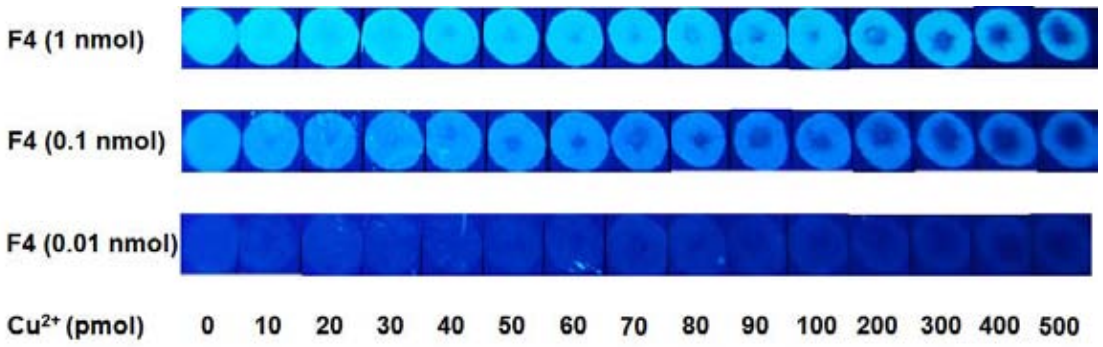

Figure 3.19 Photographic images for paper-based detection of Cu^{2+} under 20W black light (365 nm).

3.4 DNA sensor

The synthesis of the cationic fluorophore **4N^{+}Cl^{-}**. The Sonogashira coupling of 4,4',4"-triiodotriphenylamine with *N*,*N*-dimethyl-4-ethynylaniline using Pd-Cu catalysts in the presence of DBU base provided the di-substituted compound **I2N^{0}** in 33% yield (**Scheme 3.7**). The homocoupling of **I2N^{0}** gave **4N^{0}** which quaterization of all four dimethylamino groups of **4N^{0}** by methyl iodide in acetonitrile at room temperature yielding the desired compound **4N^{+}I^{-}** in 84%. Compound **4N^{+}Cl^{-}** was obtained by a Cl^{-} - I^{-} ion exchange of **4N^{+}I^{-}** through an Amberlite IRA-410 anionic ion exchange resin column.

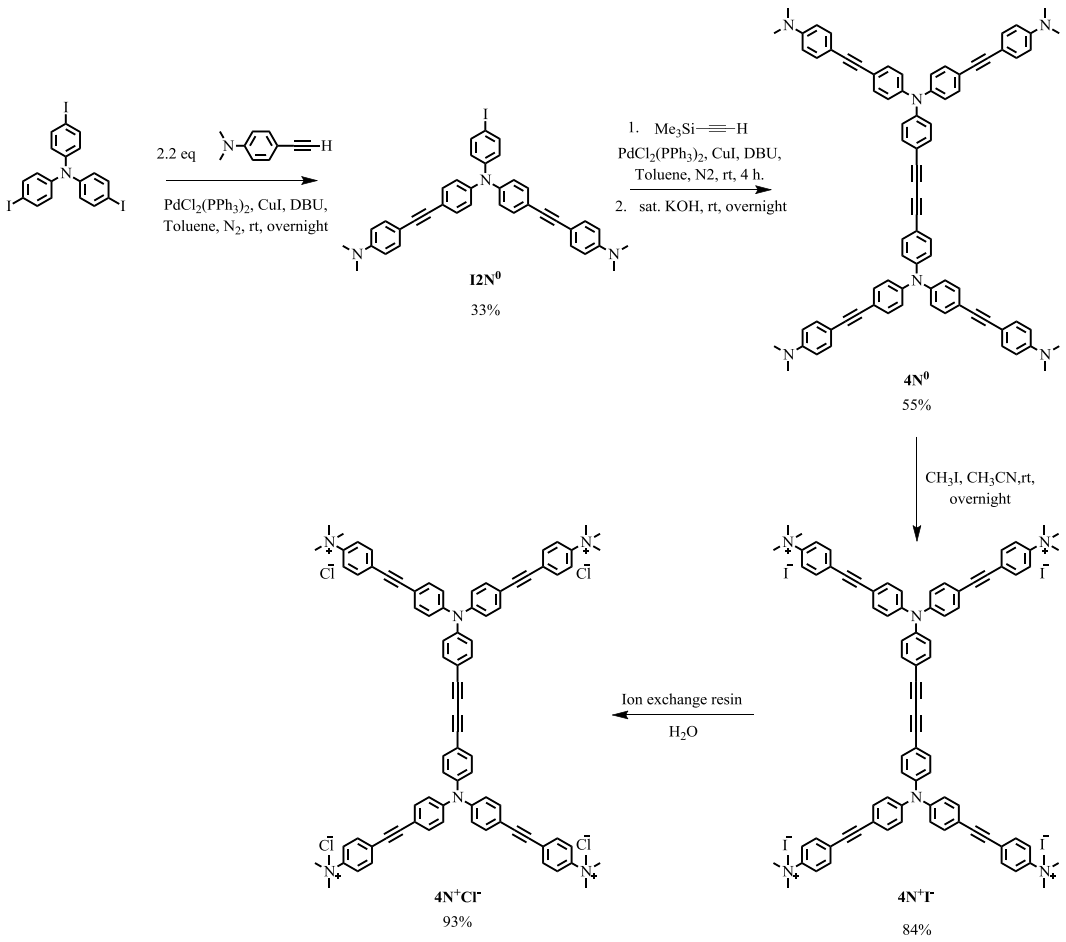

Scheme 3.7 Synthesis of **4N$^+$Cl$^-$**.

The coupling of **T3I** with *N*,*N*-dimethyl-4-ethynylaniline by Sonogashira reaction, the di-substitute dimethylaniline product (**I2N^0**) showed signals of the methyl protons as a singlet at 3.0 ppm and six doublet signals at 6.7, 6.9, 7.0, 7.4, 7.39, and 7.54 ppm corresponding to the aromatic protons. For **4N^0**, the aromatic signals appeared as multiplets at 7.4 ppm and three doublets at 6.7, 7.0, and 7.1. The methylation of **4N^0** to **4N$^+$I$^-$** show signals of the aromatic proton at 7.1, 7.5, 7.7 and 7.9 ppm. The conversion of **4N$^+$I$^-$** to **4N$^+$Cl$^-$** by ion exchange was evidenced by a doublet signal for aromatic protons at around 7.1-7.9 ppm (**Figure 3.20**).

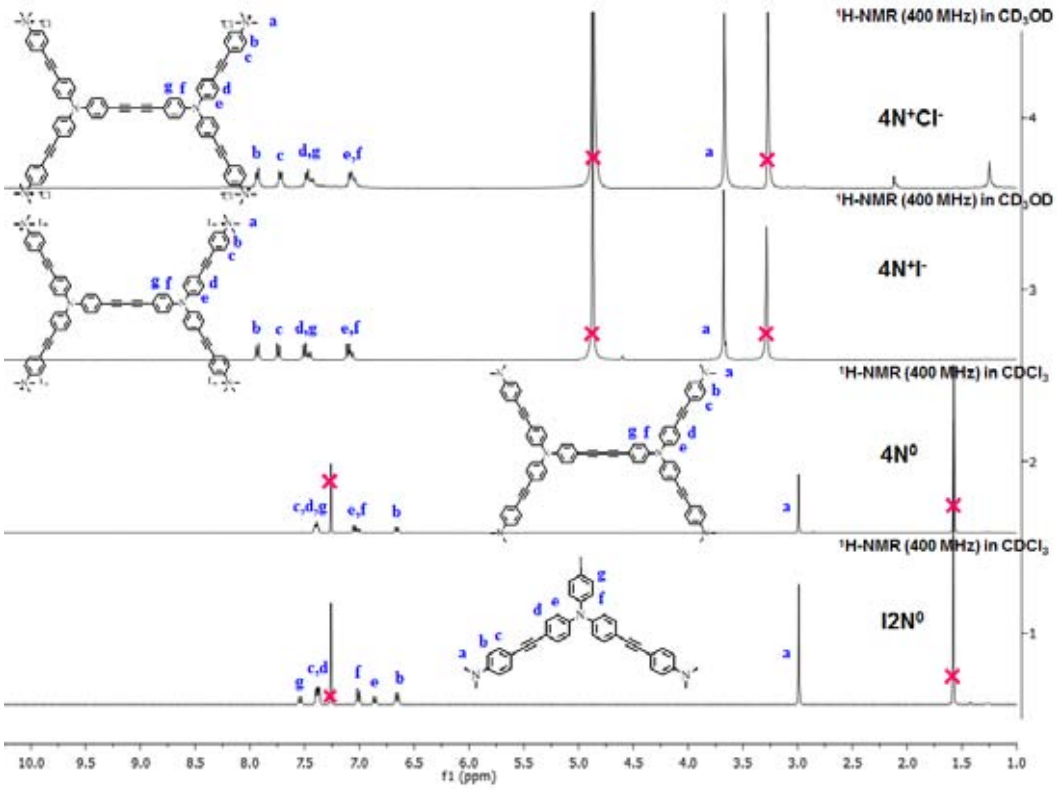

Figure 3.20 ^{1}H-NMR (400 MHz) of **I2N^{0}**, **4N^{0}**, **4N^{+}I^{-}**, and **4N^{+}Cl^{-}**.

The photophysical properties of **4N^{+}Cl** was shown in **Table 3.2**. The structure of **4N^{+}Cl^{-}** and the DNA sequences for this study as shown in **Figure 3.22**. The fluorophore in Tris-HCl buffer displayed absorption peaks at 378 nm with molar absorptivity of 4.56. The emission maxima of the fluorophore appeared at 450 nm with quantum yield of 6.2% measured relative to quinine sulfate standard. The normalized electronic absorption and emission spectra of **4N^{+}Cl^{-}** was presented in **Figure 3.21**.

Table 3.2 Photophysical properties of **4N^{+}Cl^{-}** in Tris-HCl buffer (10 mM, pH 7.4).

Compound	Absorption		Emission	
	λ_{ab} (nm)	log ε	λ_{em} (nm)	Φ (%)[a]
4N^{+}Cl^{-}	378	4.56	450	6.2

[a] Quinine sulfate in 0.1 M H_2SO_4 (Φ = 54%) was used as the standard.

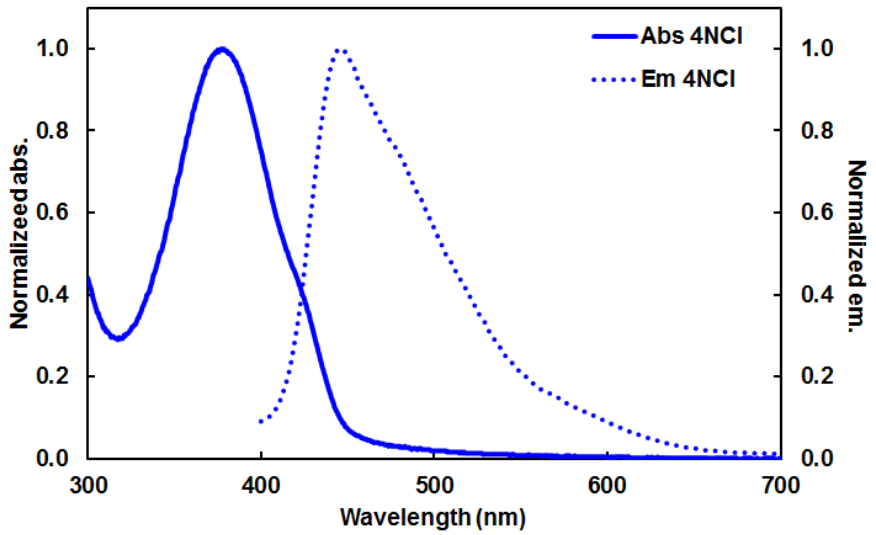

Figure 3.21 Schematic representation of DNA sequence detection and structure of **4N$^+$Cl$^-$**.

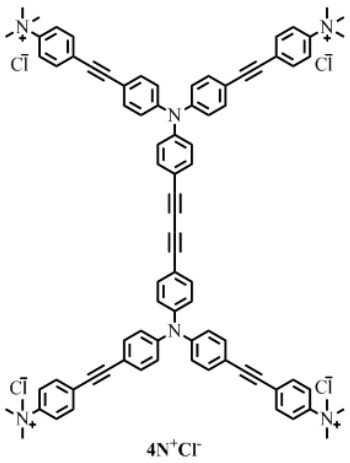

ssDNA	: 5' AAT-TAC-GAC-ATC-ATA 3'	probe target
cDNA	: 5' TAT-GAT-GTC-GTA-ATT 3'	complementary
ncDNA	: 5' AAG-CCA-TGA-TGT-CTT 3'	non-complementary
1mDNA	: 5' TAT-GAT-GTT-GTA-ATT 3'	one base mismatch
2mDNA	: 5' TAT-GCT-GTC-GCA-ATT 3'	two based mismatch

*Double-stranded DNA (**dsDNA**) = ssDNA/cDNA duplex

Figure 3.22 Schematic representation of DNA sequence detection and structure of **4N$^+$Cl$^-$**.

To begin our study, we must first demonstrate the relative fluorescence intensity of **4N$^+$Cl$^-$** upon the addition of the ssDNA. We found that the ssDNA enhanced the fluorescent intensity signal of **4N$^+$Cl$^-$**. The phenomena is presumably deaggregation because ssDNA (negative charge) can reduce π-π stacking of fluorophore (positive charge) at the periphery group through charge interaction. For double-stranded DNA (dsDNA : ssDNA + cDNA), the emission intensity of **4N$^+$Cl$^-$** is slightly decreased because of the flexibility conformation of the dsDNA less than the ssDNA (**Figure 3.23**). The fluorescence intensity change of **4N$^+$Cl$^-$** in the presence of DNA sequence is explained *via* the electrostatic interaction between cationic fluorophore and negative charged phosphate group of DNA, and geometry lock to deaggregate fluorophore in aqueous media.

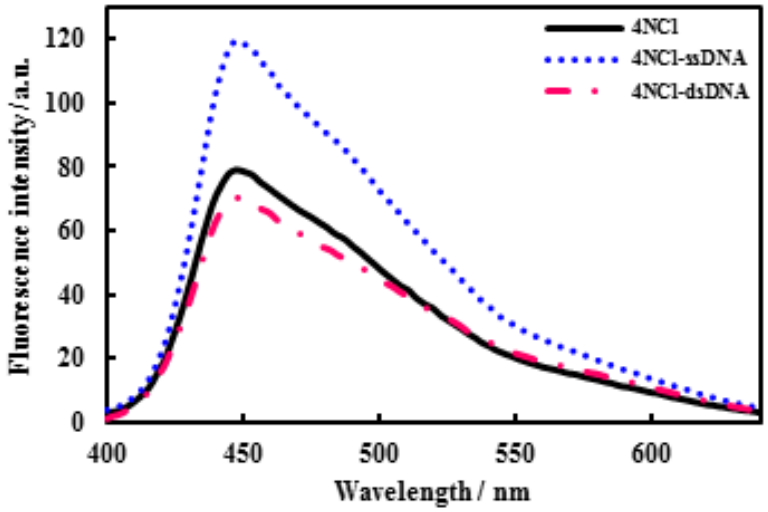

Figure 3.23 Emission spectra of **4N$^+$Cl$^-$** 1.0 μM (—), **4N$^+$Cl$^-$** + ssDNA$_4$ (0.25 μM) (···), **4N$^+$Cl$^-$** + dsDNA (0.25 μM) (—·—) in 10 mM Tris-HCl buffer pH 7.4.

Althought, the **4N$^+$Cl$^-$** discriminated between the fluorescence signal of ssDNA and dsDNA but the result is not the best efficient separation of ssDNA and dsDNA. So, we tried to investigate the other fluorescence method that can distinguish the ssDNA and the dsDNA as well as the commercial technique. Förster Resonance Energy Transfer (FRET) was the best suitable performance to use for our method. The experiment was studied by using **4N$^+$Cl$^-$** as a FRET donor and SyBrGreen II dye (SG II: the most sensitive dye used for DNA, RNA detection) [52] as a FRET acceptor.

The SG II provide high fluorescent enhancement upon binding to dsDNA over ssDNA [53]. The absorption-emission spectra of **4N$^+$Cl$^-$** and SG II are shown in **Figure 3.24**.

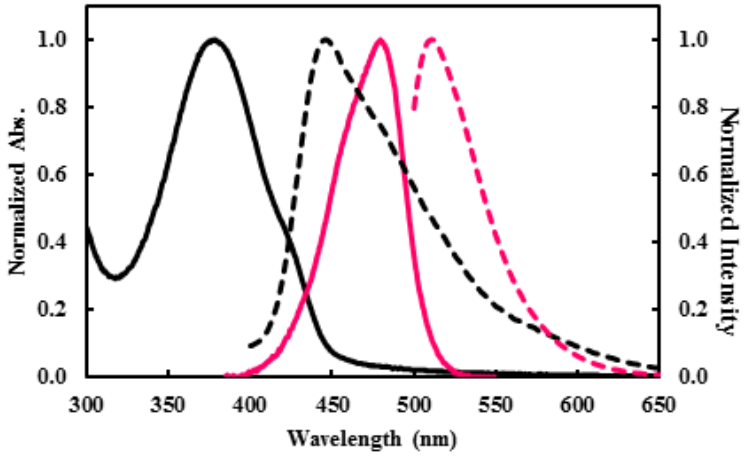

Figure 3.24 Normalized absorption [solid line] and fluorescent spectra [dash line] of **4N$^+$Cl$^-$** (black) and SyBrGreen II (pink) in 10 mM Tris-HCl buffer, pH 7.4.

The **4N$^+$Cl$^-$** can be taken advantage of achieving goal to discriminate single, and double-stranded DNA based on FRET ratios. **Figure 3.24** shows the normalized fluorescent intensity (FRET ratio) of **4N$^+$Cl$^-$**/SG II/dsDNA show energy transfer higher than **4N$^+$Cl$^-$**/SG II/ssDNA (5-fold) because of emission peak of fluorophore can be complete overlapped with absorption peak of SG II (**Figure 3.25**). The phenomenon is from the double-stranded DNA (ssDNA+cDNA) provided good efficient energy transfer because the SG II can intercalate to double helix DNA (dsDNA). Moreover, this intercalation can reduce positive charge repulsion between **4N$^+$Cl$^-$** and SG II, which produce the close distance with **4N$^+$Cl$^-$** and SG II shorter than 10 nm. This distance is suitable to occur FRET.

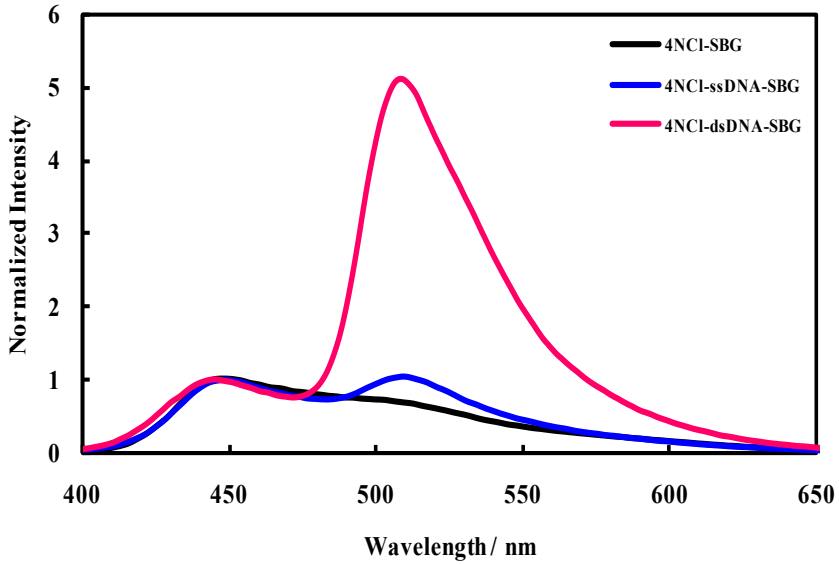

Figure 3.25 FRET ratio of **4N$^+$Cl$^-$**/SG II/DNA (I_{508nm}/I_{450nm}). ([**4N$^+$Cl$^-$**] = 1.0 μM, [ssDNA] = [dsDNA] = 0.25 μM, SG II 10,000x diluted).

The **4N$^+$Cl$^-$** could be advantaged of achieving goal to discriminate single, and double DNA based on FRET ratios. **Figure 3.26** shows the normalized fluorescent intensity of **4N$^+$Cl$^-$**/SG II/DNA with an increasing base pairs number of mismatch and complementary DNA. The FRET ratio decreased with an increasing base pairs number of mismatched in DNA strands. The emission intensity of **4N$^+$Cl$^-$** is slightly changed in the presence of single-mismatched base pairs with SG II. However the emission intensity is distinctly different from the complementary strand in case of upon the addition of the single-mismatched base pairs (1mDNA), double-mismatched base pairs (2mDNA), noncomplementary DNA (ncDNA) and single-stranded DNA (ssDNA), respectively. Nevertheless, the **4N$^+$Cl$^-$** with double-stranded DNA show good efficient energy transfer (~ 5-fold), whereas 1-, 2-mismatched DNA strands are gradually decreasing in its FRET ratio. The FRET ratio of **4N$^+$Cl$^-$**/SG II/dsDNA complex is higher than other DNA strands due to SG II mixed dsDNA duplex. Cationic fluorophore, **4N$^+$Cl$^-$** and SG II are induced to close distance and enough to preferably energy transfer from fluorophore as energy donor to dye as energy acceptor. The **4N$^+$Cl$^-$**/SG II/ssDNA and **4N$^+$Cl$^-$**/SG II/ncDNA complexes have low FRET ratio because SG II is unable to bind ssDNA strand or ncDNA. The distance between **4N$^+$Cl$^-$** and SG II are longer than 10 nm. Accordingly, the FRET ratios

between **4N$^+$Cl$^-$** and SG II occur less efficiency. For **4N$^+$Cl$^-$**/SG II/single- or double-mismatched DNA, the complexes have FRET ratio less than **4N$^+$Cl$^-$**/SG II/dsDNA complex because the binding between SG II and single- or double-mismatched DNA is poorer than that of **4N$^+$Cl$^-$**/SG II/dsDNA complex.

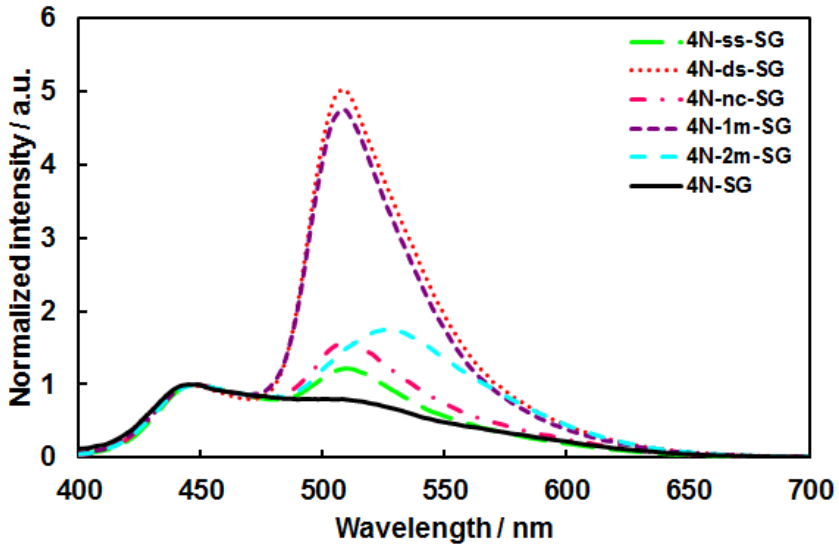

Figure 3.26 Normalized intensity of fluorophore **4N$^+$Cl$^-$** with SG II and ssDNA (−), dsDNA (---), smDNA (····) and dmDNA (−··), respectively, in 10 mM Tris-HCl buffer pH 7.4. The spectra are normalized with respect to the **4N$^+$Cl$^-$** emission. ([**4N$^+$Cl$^-$**/SG II/ssDNA] = 1.0 μM, [ssDNA] = [dsDNA] = [ncDNA] = [smDNA] = [dmDNA] = 0.25 μM, SG II 10,000x diluted).

CHAPTER IV

CONCLUSION

Five new fluorophores containing phenylene-ethynylene branches with salicylic acid (**F2**-**F5**) and trimethylammonium (**4N$^+$Cl$^-$**) termini are successfully synthesized via Sonogashira coupling reaction as a key step. The tribranched and tetrabranched fluorophores (**F4** and **F5**) with salicylic acid termini exhibits Cu^{2+} fluorescence quenching in aqueous solution with K_{sv} of 5.79×10^6 and 1.31×10^6 M^{-1}. Due to its greater selectivity and sensitivity, the paper-based sensors were fabricated from **F4** by a microliter dropping technique. The paper-based sensors were capable of detecting picomole level of Cu^{2+} by naked eye under conventional black light. The tetrabranched fluorophore (**4N$^+$Cl$^-$**) with trimethylammonium termini was found to interact with DNA in aqueous buffered solution pH 7.4. Upon DNA binding, the fluorescent signal of the fluorophore increases presumably due to the reduction of geometrical relaxation and collisional self-quenching processes. The interaction between the fluorophore and DNA was used in combination with SyBrGreen commercial fluorescence dye for the FRET detection of DNA sequences via DNA/DNA hybridization.

Suggestion for future work:

1. To focus the Cu^{2+} detection in real sample such as sewage or drinking water and utilize for Cu^{2+} sensor in living cell.
2. To focus on the study of detection of DNA sequence to use for medical diagnostics.

REFERENCES

[1] Lakowicz, J. R. *Principles of fluorescence spectroscopy*. 3rd ed. Kluwer : John Wiley & Sons, 2006.

[2] Keck, W.M. Center for Cellular Imaging. *Fluorescence Resonance Energy Transfer spectroscopy* [Online]. 2010. Available from : http://www.kcci virginia.edu/FRET/index.php [2010, November]

[3] Thomas, S. W., Joly, G. D., and Swager, T. M. Chemical sensors based on amplifying fluorescent conjugated polymers. *Chem. Rev.* 107 (2007) : 1339-1386.

[4] Hertzberg, R. P., and Pope, A. J. High-throughput screening: new technology for the 21st century. *Curr. Opin. Chem. Biol.* 4 (2000) : 445-451.

[5] Achyuthan, K. E., et al. Fluorescence superquen-ching of conjugated polyelectrolytes: applications for biosensing and drug discovery. *J. Mater. Chem.* 15 (2005) : 2648-2656.

[6] Dore, K., et al. Fluorescent polymeric transducer for the rapid, simple, and specific detection of nucleic acids at the zeptomole level. *J. Am. Chem. Soc.* 126 (2004) : 4240-4244.

[7] Tan, C. Y., et al. Amplified quenching of a conjugated polyelectrolyte by cyanine dyes. *J. Am. Chem. Soc.* 126 (2004) : 13685-13694.

[8] Kim, I.-B., Dunkhorst, A., Gilbert, J., and Bunz, U. H. F. Sensing of lead ions by a carboxylate-substituted PPE: multivalency effects. *Macromolecules* 38 (2005) : 4560-4562.

[9] Kim, I.-B., and Bunz, U. H. F. Modulating the sensory response of a conjugated polymer by proteins: an agglutination assay for mercury ions in water. *J. Am. Chem. Soc.* 128 (2006) : 2818-2819.

[10] Tolosa, J., and Bunz, U. H. F. Water soluble cruciforms: effect of surfactants on fluorescence. *Chem. Asian J.* 4 (2009) : 270–276.

[11] Niamnont, N. Siripornnoppakhun, W. Rashatasakhon, P. and Sukwattanasinitt, M. A Polyanionic Dendritic Fluorophore for Selective Detection of Hg^{2+} in Triton X-100 Aqueous Media. *Organic Letters*. 11 (2009) : 2768-2771.

[12] Goswami, s., Sen, D., Das, N. K., and Hazsa, G. Highly selective colorimetric fluorescence sensor for Cu^{2+}: cation-induced '*switching on*' of fluorescence due to excited state internal charge transfer in the red/near-infrared region of emission spectra. *Tetrahedron Lett*. 51 (2010) : 5563-5566.

[13] Yu, C., et al. "Off-On" based fluorescent chemosensor for Cu^{2+} in aqueous media and living cells. *Talanta* 85 (2011) : 1627-1633.

[14] Sundari, R., Ahmad, M., and Heng, L. Y. Development of an optical fibre reflectance sensor for copper (II) detection based on immobilized salicylic acid. *Sensor actuat B-Chem*. 113 (2006) : 201-206.

[15] Sirilaksanapong, S., Sukwattanasinitt, M., and Rashatasakhon, P. 1,3,5-Triphenylbenzene fluorophore as a selective Cu^{2+} sensor in aqueous media. *Chem. Commun*. 48 (2012) : 293-295.

[16] Sheng, R., et al. Colorimetric Test Kit for Cu^{2+} Detection. *Organic Letters*. 10 (2008) : 5015-5018.

[17] Yang, X. and Wang, E. A. Nanoparticle Autocatalytic Sensor for Ag^{+} and Cu^{2+} Ions in Aqueous Solution with High Sensitivity and Selectivity and Its Application in Test Paper. *Anal. Chem.* 83 (2011) : 5005-5011.

[18] Gaylord, B. S., Heeger, A. J. and Bazan, G. C. DNA Hybridization detection with water-soluble conjugated polymers and chromophore-labeled single-stranded DNA. *J. Am.Chem. Soc.* 125 (2003) : 896-900.

[19] Lee, K., Maisel, K., Rouillard, J.-M., Gulari, E., and Kim, J. Sensitive and selective label-free DNA detection by conjugated polymer-based microarrays and intercalating dye. *Chem. Mater*. 20 (2008) : 2848-2850.

[20] Ren, X., and Xu, Q.-H. Label-free DNA sequence detection with enhanced sensitivity and selectivity using cationic conjugated polymers and PicoGreen. *Langmuir* 25 (2009) : 43-47.

[21] Tang, Y., Achyuthan, K. E., and Whitten, D. G. Label-free and real-time sequence specific DNA detection based on supramolecular self-assembly. *Langmuir* 26 (2010) : 6832-6837.

[22] Kajigaeshi, S., Kakinami, T., Moriwaki, M., Fujisaki, S., Maeno, K., and Okamoto, T. α-Chlorination of aromatic acetyl derivatives with benzyltrimethylammonium dichloroiodate. *Synthesis* (1988) : 545-546.

[23] Fery-Forques, S., and Lavabe, D. Are fluorescence quantum yields so tricky to measure? A demonstration using familiar stationery products. *J. Chem. Educ.* 76 (1999) : 1260-1264.

[24] Du, H., Fuh, R. A., Li, J., Corkan, A., and Lindsey, J. S. Photochem CAD: A computer-aided design and research tool in photochemistry. *Photochem. Photobiol*. 68 (1999) : 141-142.

[25] Burrows, H. D., et al. Fluorescence enhancement of the water-soluble poly{1.4-phenylene-[9,9-bis-(4-phenoxybutylsulfonate)]fluorine-2,7-diyl} copolymer in n-Dodecylpentaoxyethylene glycol ether micelles. *Macromolecules* 37 (2004) : 7425-7427.

[26] Kaur, P., Yue, H., Wu, M., Liu, M., Treece, J., and Waldeck, D. H. Solvation and aggregation of polyphenylethynylene based anionic polyelectrolytes in dilute solutions. *J. Phy. Chem. B*. 111 (2007) : 8589-8596.

[27] Pang, Y. and Chu, Q. Molecular Aggregation of Poly[(1,3-phenyleneethynylene)-alt-oligo(2,5-dialkoxy-1,4-phenyleneethynylene)]: Effects of Solvent, Temperature, and Polymer Conformation. *Macromolecules* 36 (2003) : 4614-4618.

[28] Masuo, S., Yoshikawa, H., Asahi, T. and Masuhara, H. Fluorescence Spectroscopic Properties and Single Aggregate Structures of π-Conjugated Wire-Type Dendrimers. *J. Phy. Chem. B*. 107 (2003) : 2471-2479.

[29] Pang, Y. and Chu, Q. Aggregation and Self-Assembly of Oligo (2,5-dialkoxy-1,4-phenyleneethynylene)]s: An Improved probe to Study Inter- and Intramolecular Interaction. *Macromolecules* 38 (2005) : 517-520.

[30] World Health Organization (WHO). Copper in Drinking-water: WHO Guidelines for Drinking-water Quality, pp.1-23. Geneva : WHO publications, 2004.

[31] Plater, J. M., McKay, M. and Jackson, T. Synthesis of 1,3,5-tris[4(diarylamino)phenyl]benzene and 1,3,5-tris(diarylamino)benzene derivatives. *J. Chem. Soc*. *Perkin Trans. 1*. (2000) : 2695-2701.

[32] Zeng, D., et al. A new sensor for copper (II) ion based on carboxyl acid groups substituted polyfluoreneethynylene. *React. Funct. Polym*. 68 (2008) : 1715-1721.

[33] Pu, K.-Y., Pan, S. Y.-H. and Liu, B. Optimization of Interactions between a cationic conjugated polymer and chromophore-labeled DNA for optical amplification of fluorescent sensors. *J Phys Chem B*. 112 (2008) : 9295–9300.

[34] Fan, H., Zhang, T., Lv, S. and Jin, Q. Fluorescence turn-on assay for glutathione reductase activity based on a conjugated polyelectrolyte with multiple carboxylate groups. *J. Mater. Chem*. 20 (2010) : 10901-10907.

[35] Pu, F., Huang, Z., Ren, J. and Qu, X. DNA/Ligand/Ion-Based Ensemble for Fluorescence Turn on Detection of Cysteine and Histidine with Tunable Dynamic Range. *Anal. Chem*. 82 (2010) : 8211-8216.

[36] Ala, A., Walker, A. P., Ashkan, K., Dooley, J. S. and Schilsky, M. L. Wilson's disease. *Lancet* 369 (2007) : 397-408.

[37] Macreadie, I. G. Copper transport and Alzheimer's disease. *Eur Biophys J*. 37 (2008) : 295-300.

[38] Gaggelli, E., Kozlowski, H., Valensin, D. and Valensin, G. Copper Homeostasis and Neurodegenerative Disorders (Alzheimer's, Prion,and Parkinson's Diseases and Amyotrophic Lateral Sclerosis). *Chem. Rev.* 106 (2006) : 1995-2044.

[39] Yang, X. and Wang, E. A nanoparticle autocatalytic sensor for Ag^{+} and Cu^{2+} ions in aqueous solution with high sensitivity and its application in test paper. *Anal. Chem*. 83 (2011) : 5005-5011.

[40] Chereddy, N. R. and Thennarasu, S. Synthesis of a highly selective bis-rhodamine chemosensor for naked-eye detection of Cu^{2+} ions and its application in bio-imagin. *Dyes and Pigments* 91 (2011) : 378-382.

[41] Dalapati, S., Jana, S., Alam, M. A. and Guchhait, N. Multifunctional fluorescent probe selective for Cu(II) and Fe(III) with dual-mode of binding approach. *Sensor. Actuat. B-Chem*. 160 (2011) : 1106-1111.

[42] Sheng, R., et al. Colorimetric test kit for Cu^{2+} detection. *Org. Lett*. 10 (2008) : 5015-5018.

[43] Yang, Y., et al. Rhodamine-based Derivatives for Cu^{2+} sensing: Spectroscopic studies, structure recognition relationships and its test strips. *Spectrochimica Acta Part A*. 81 (2011) : 14-20.

[44] Basurto, S., Riant, O., Moreno, D., Rojo, J. and Torroba, T. Colorimetric Detection of Cu[II] Cation and Acetate, Benzoate, and Cyanide Anions by Cooperative Receptor Binding in New α,α′-Bis-substituted Donor-Acceptor Ferrocene Sensors. *J. Org. Chem*. 72 (2007) : 4673-4688.

[45] Lu, C.-H., Wang, Y.-W., Ye, S.-L., Chen, G.-N. and Yang, H.-H. Ultrasensitive detection of Cu^{2+} with the naked eye and application in immunoassays. *NPG Asia Materials*. 4 (2012) : 1-7.

[46] Ma, Y.-R., Niu, H.-Y., Zhang, X.-L. and Cai, Y.-Q. Colorimetric detection of copper ions in tap water during the synthesis of silver/dopamine nanoparticles. *Chem. Commun*. 47 (2011) : 12643-12645.

[47] Martinez, A. W., Phillips, S. T., Butte, M. J. and Whitesides, G. M. Patterned Paper as a Platform for Inexpensive, Low-Volume, Portable Bioassays. *Angew. Chem. Int. Ed*. 46 (2007) : 1318-1320.

[48] Martinez, A. W., Phillips, S. T. and Whitesides, G. M. Diagnostics for the Developing World: Microfluidic Paper-Based Analytical Devices. *Anal. Chem*. 82 (2010) : 3-10.

[49] Thongmalai, W., et al. Polydiacetylenes carrying amino groups for colorimetric detection and identification of anionic surfactants. *J. Mater. Chem*. 21 (2011) : 16391-16397.

[50] Pumtang, S., Siripornnoppakhun, W., Sukwattanasinitt, M. and Ajavakom, A. Solvent colorimetric paper-based polydiacetylene sensors from diacetylene lipids. *J. Colloid. Interf. Sci*., 364 (2011) : 366-372.

[51] Eaidkong, T., Mungkarndee, R., Phollookin, C., Tumcharern, G., Sukwattanasinitt, M. and Wacharasindhu, S. Polydiacetylenes carrying amino groups for colorimetric detection and identification of anionic surfactants. *J. Mater. Chem*. 22 (2012) : 5970-5977.

[52] McCarthy, L., Egeler, T. J., Bickerstaff, L. E., Cunha, M. P. and Millard, P. J. Detection and identification of IHN and ISA viruses by isothermal DNA amplification in microcapillary tubes. *Anal Bioanal Chem*. 386 (2006) : 1975-1984.

[53] Yatsushiro, S., Yamaguchi, Y., Yamamura, S., Shinohara, Y., Baba, Y. and Kataoka, M. Highly sensitive DNA detection with a combination of 2 DNA-intercalating dyes for microchip electrophoresis. *J. Pharmaceut. Biomed. Anal.* 55 (2011) : 202-205.

APPENDIX

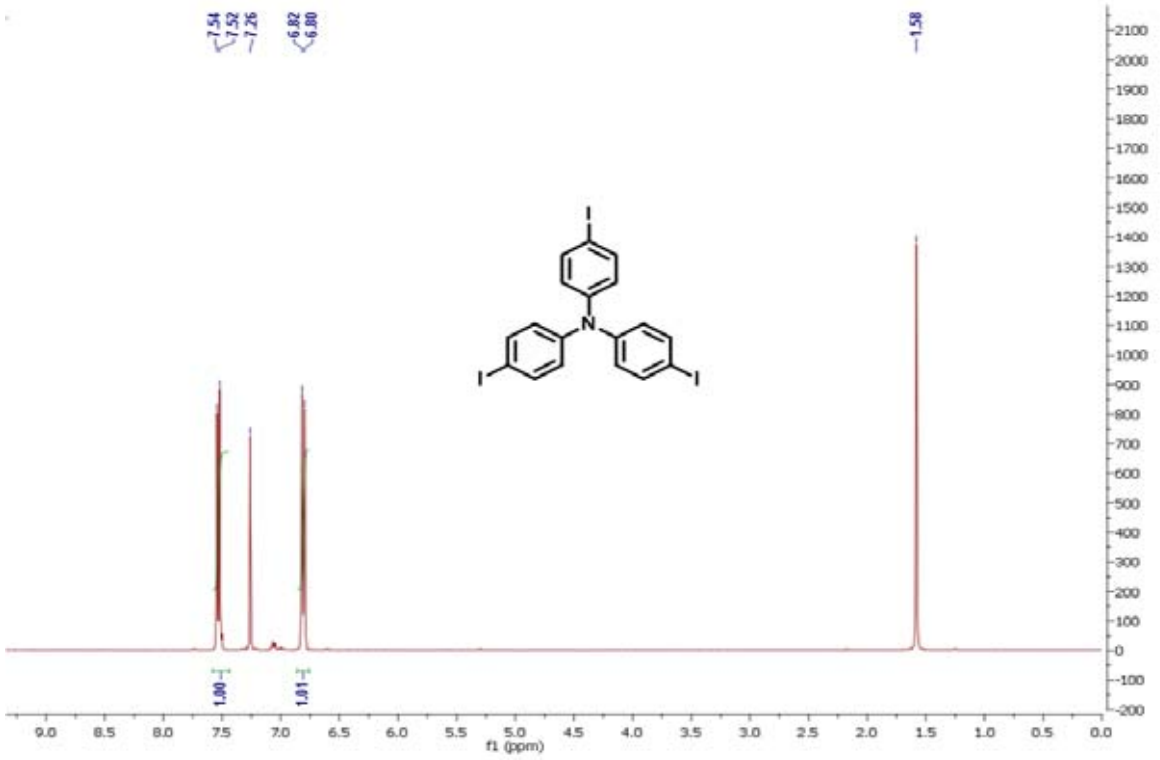

Figure A.1 ^{1}H NMR of **T3I** in $CDCl_3$.

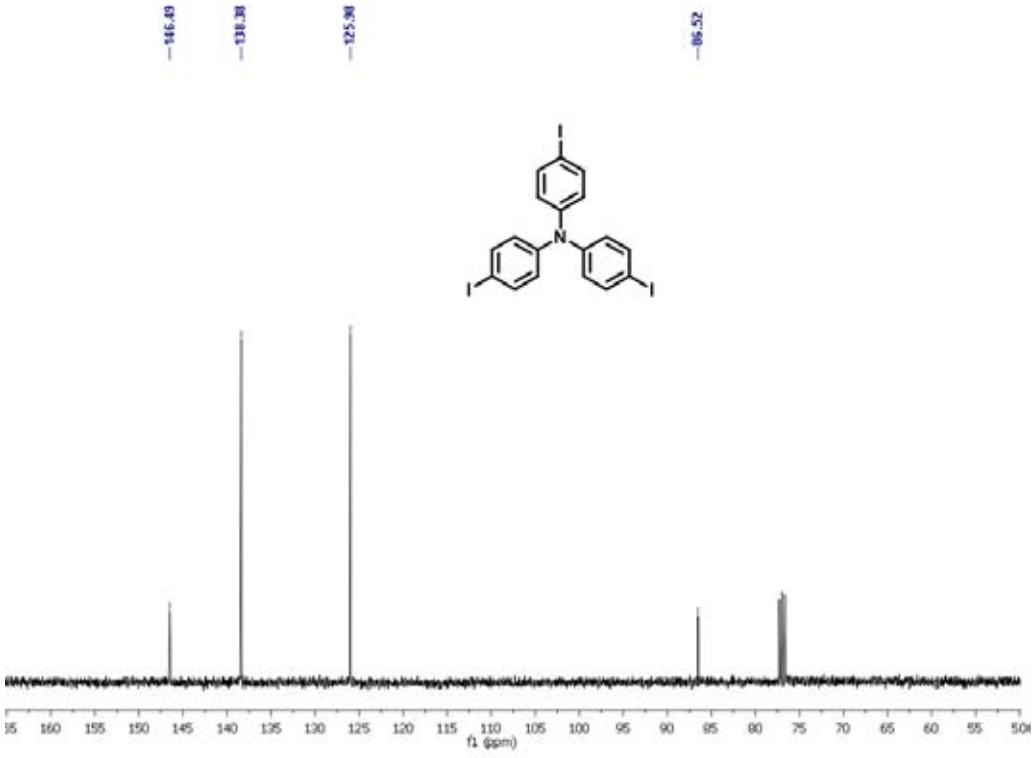

Figure A.2 ^{13}C NMR of **T3I** in $CDCl_3$.

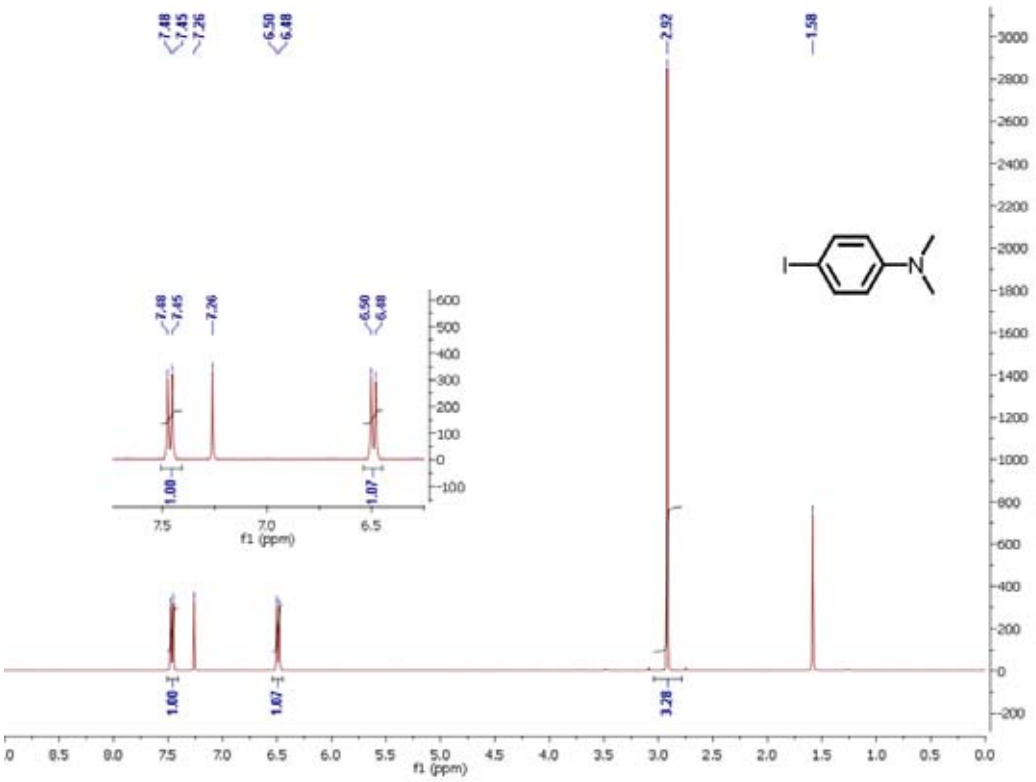

Figure A.3 ^{1}H NMR of 4-iodo-*N*, *N*-dimethylaniline in $CDCl_3$.

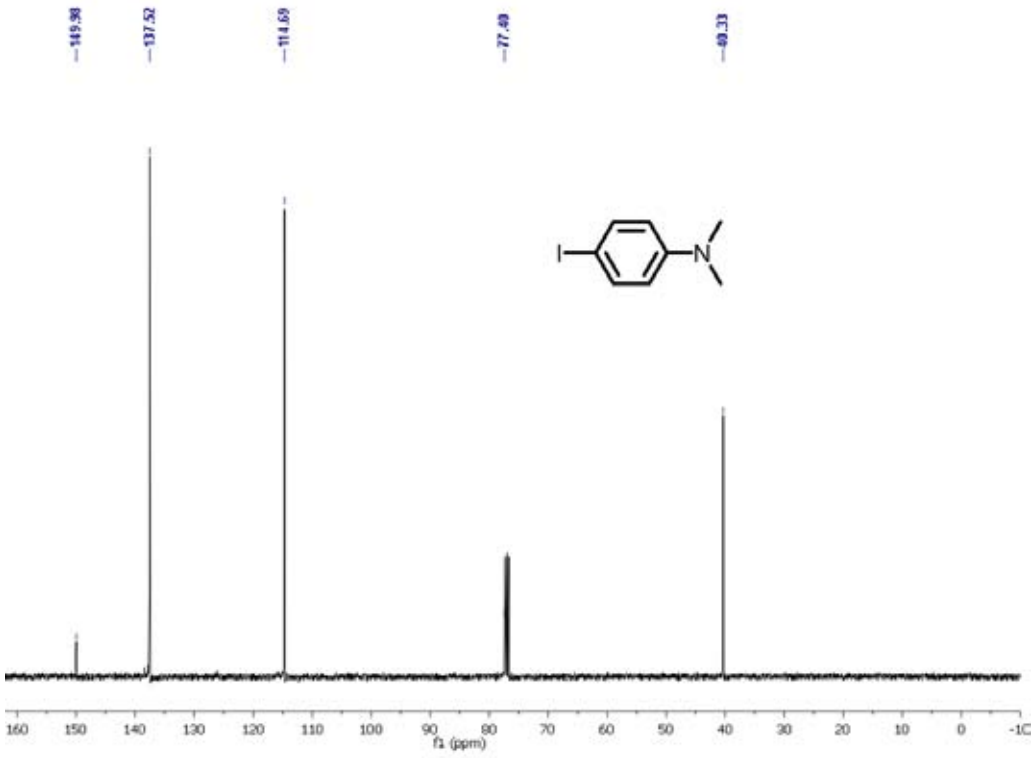

Figure A.4 ^{13}C NMR of 4-iodo-*N*, *N*-dimethylaniline in $CDCl_3$.

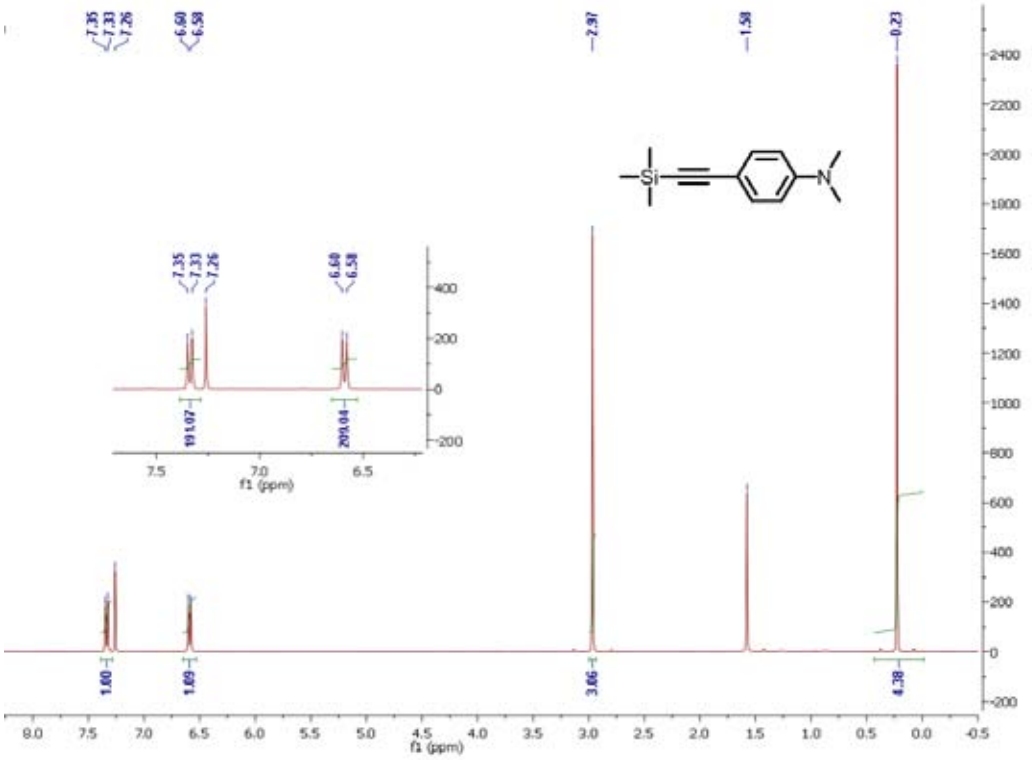

Figure A.5 ^{1}H NMR of *N*, *N*-dimethyl-4-((trimethylsilyl)ethynyl)aniline in $CDCl_3$.

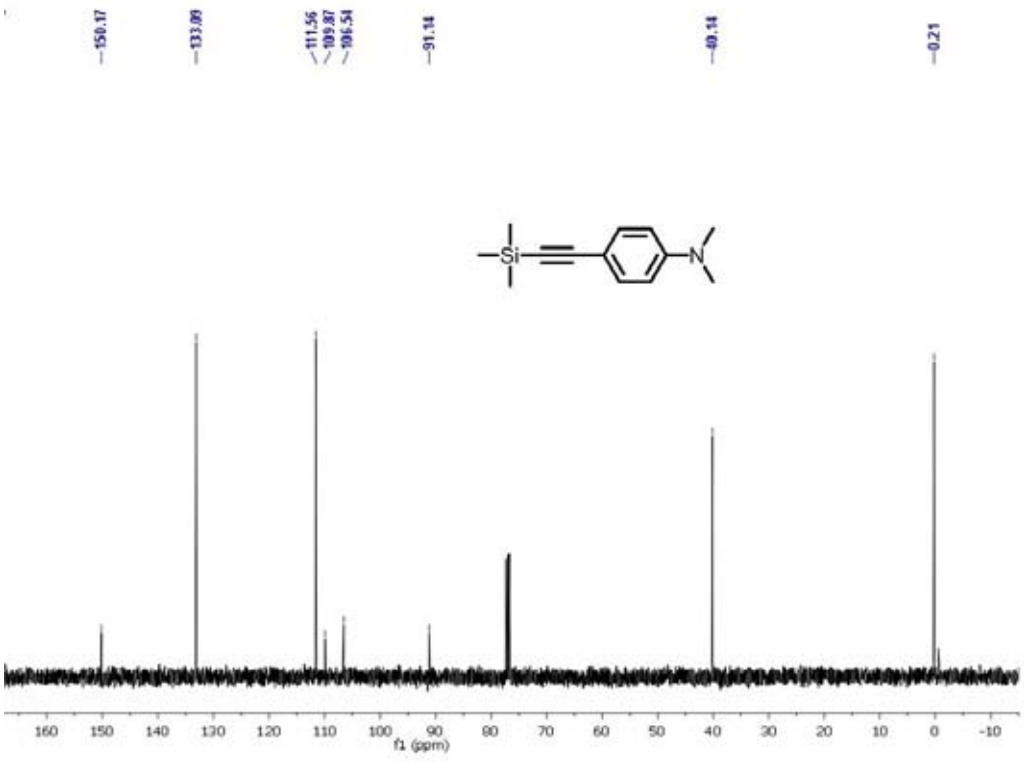

Figure A.6 ^{13}C NMR of *N*, *N*-dimethyl-4-((trimethylsilyl)ethynyl)aniline in $CDCl_3$.

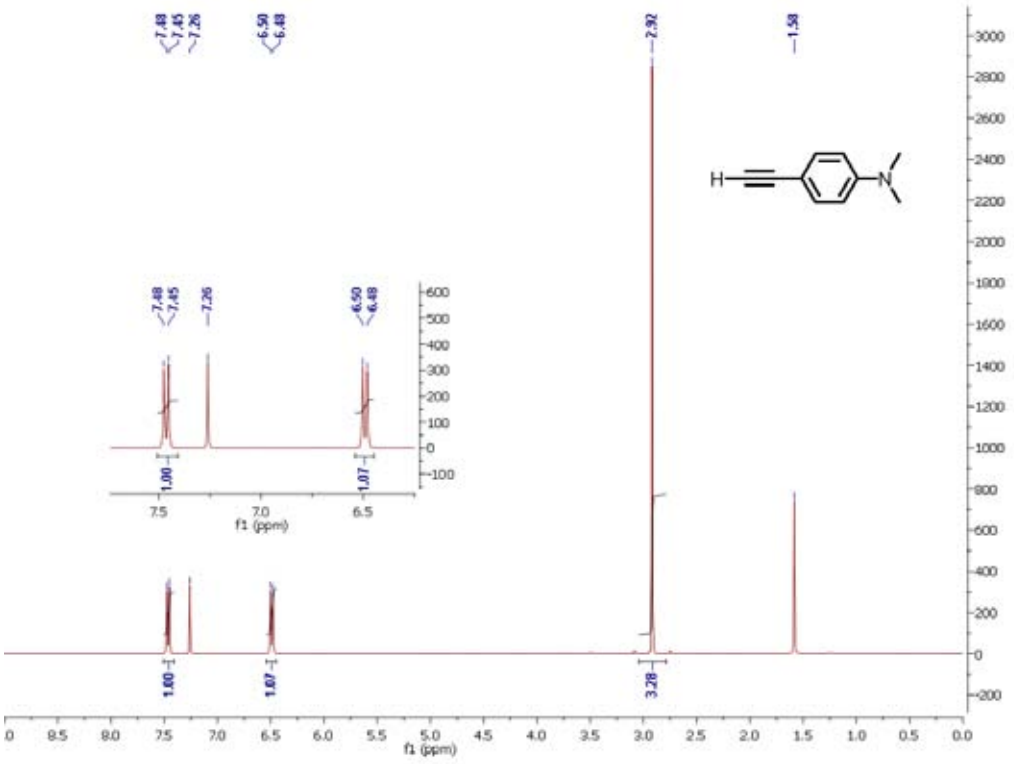

Figure A.7 ^{1}H NMR of 4-ethynyl-*N*, *N*-dimethylaniline in $CDCl_3$.

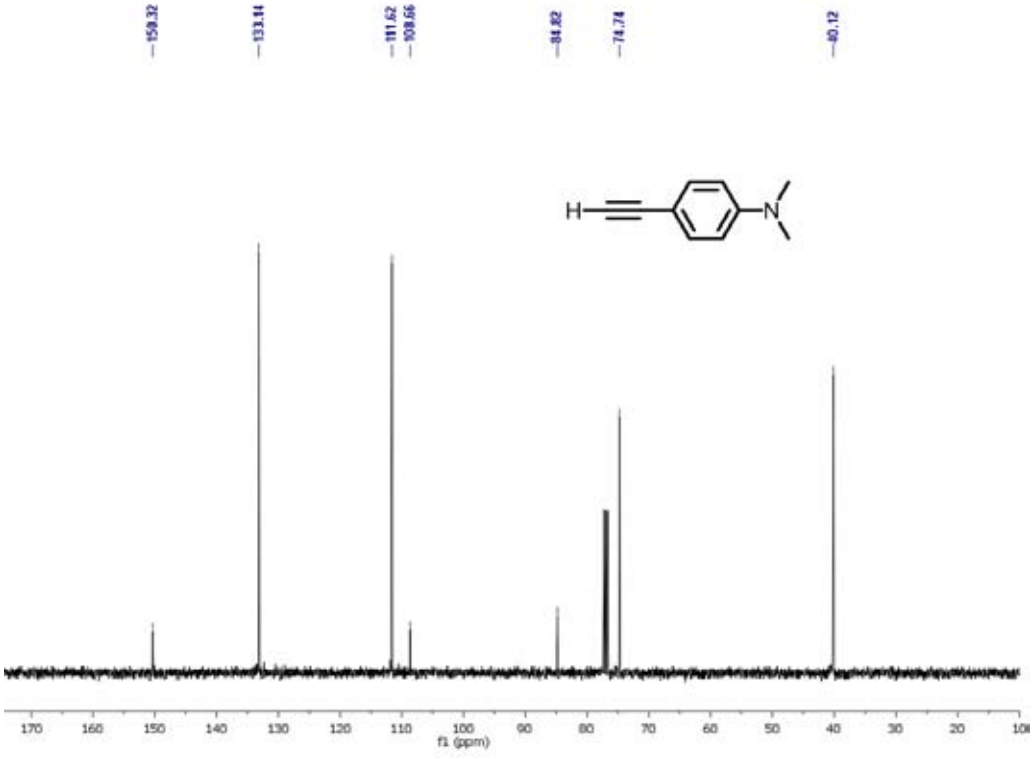

Figure A.8 ^{13}C NMR of 4-ethynyl-*N*, *N*-dimethylaniline in $CDCl_3$.

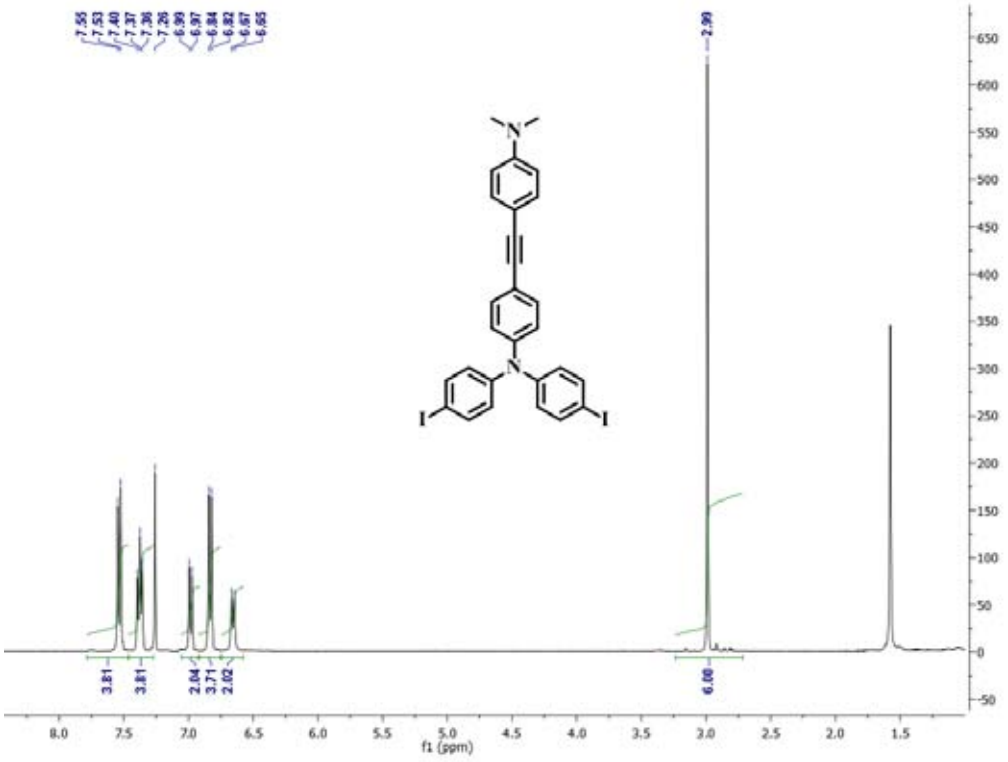

Figure A.9 ^{1}H NMR of **2IN^{0}** in $CDCl_3$.

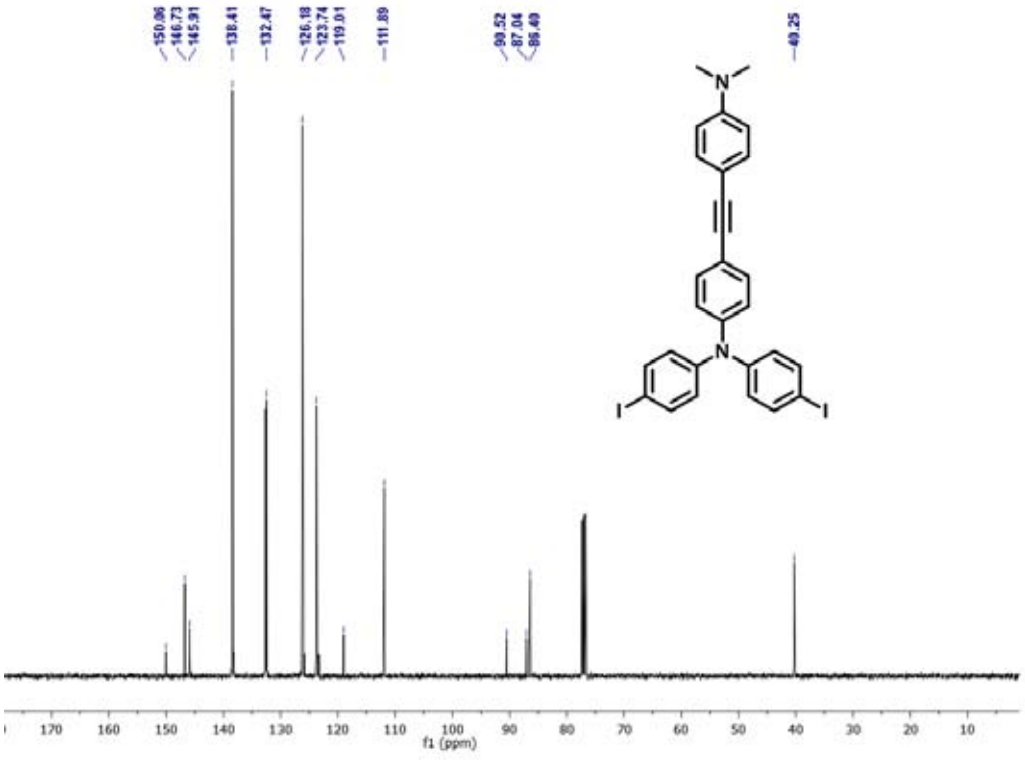

Figure A.10 ^{13}C NMR of **2IN^{0}** in $CDCl_3$.

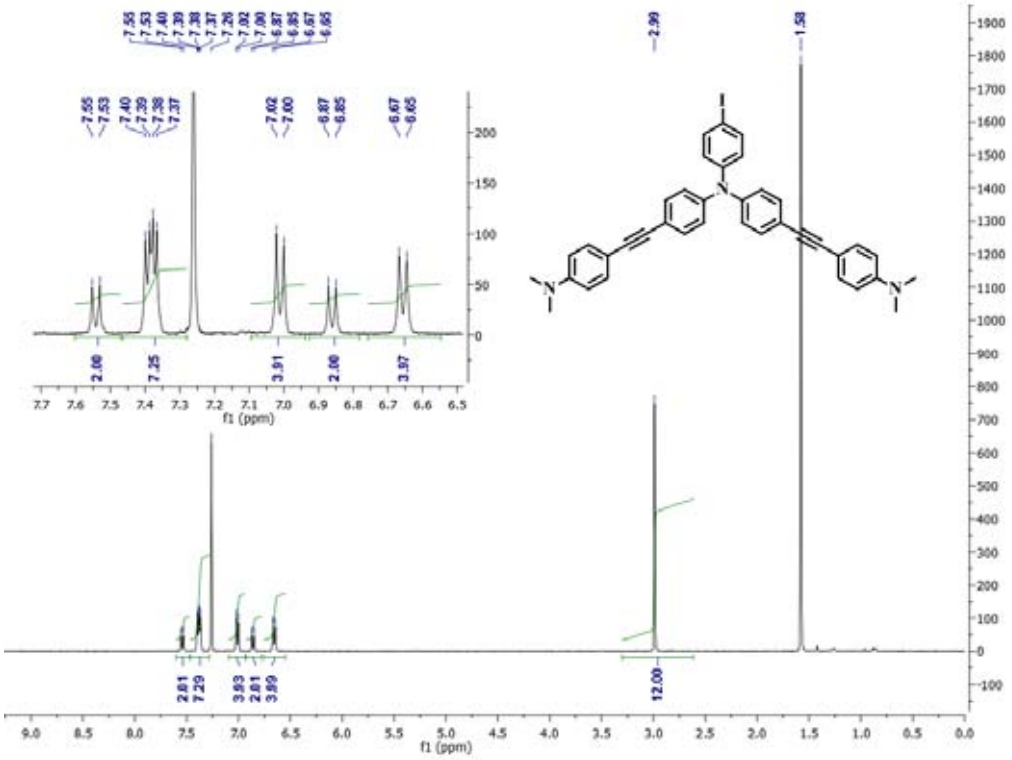

Figure A.11 ^{1}H NMR of **I2N^{0}** in $CDCl_3$.

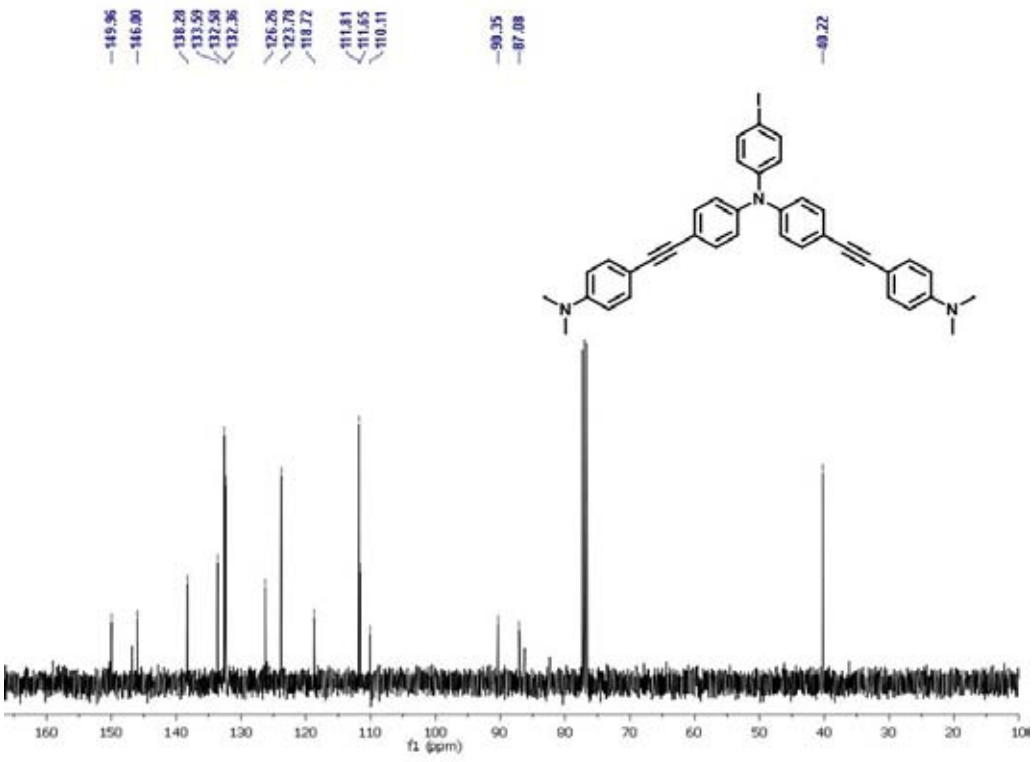

Figure A.12 ^{13}C NMR of **I2N^{0}** in $CDCl_3$.

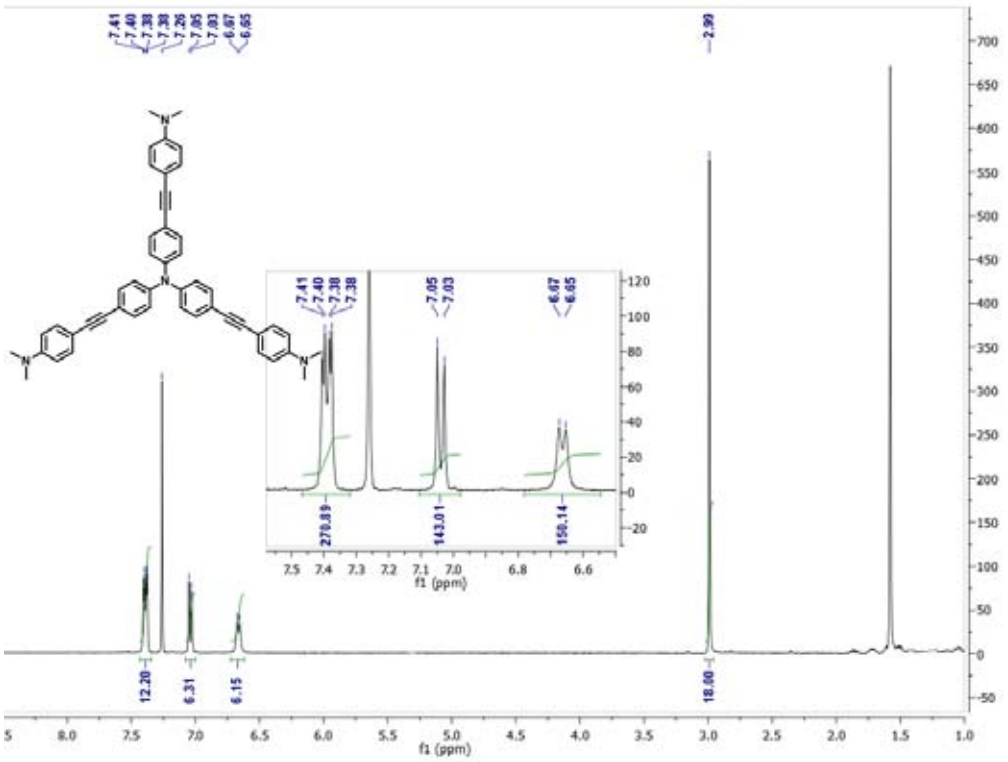

Figure A.13 ^{1}H NMR of **3N^{0}** in $CDCl_3$.

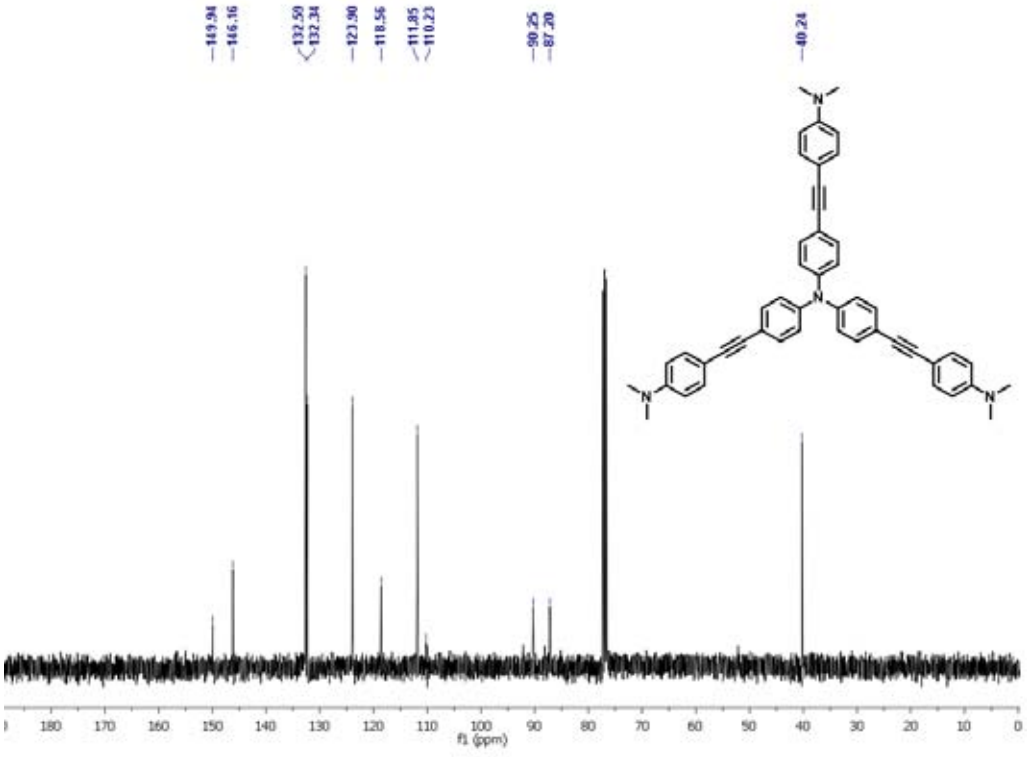

Figure A.14 ^{13}C NMR of **3N^{0}** in $CDCl_3$.

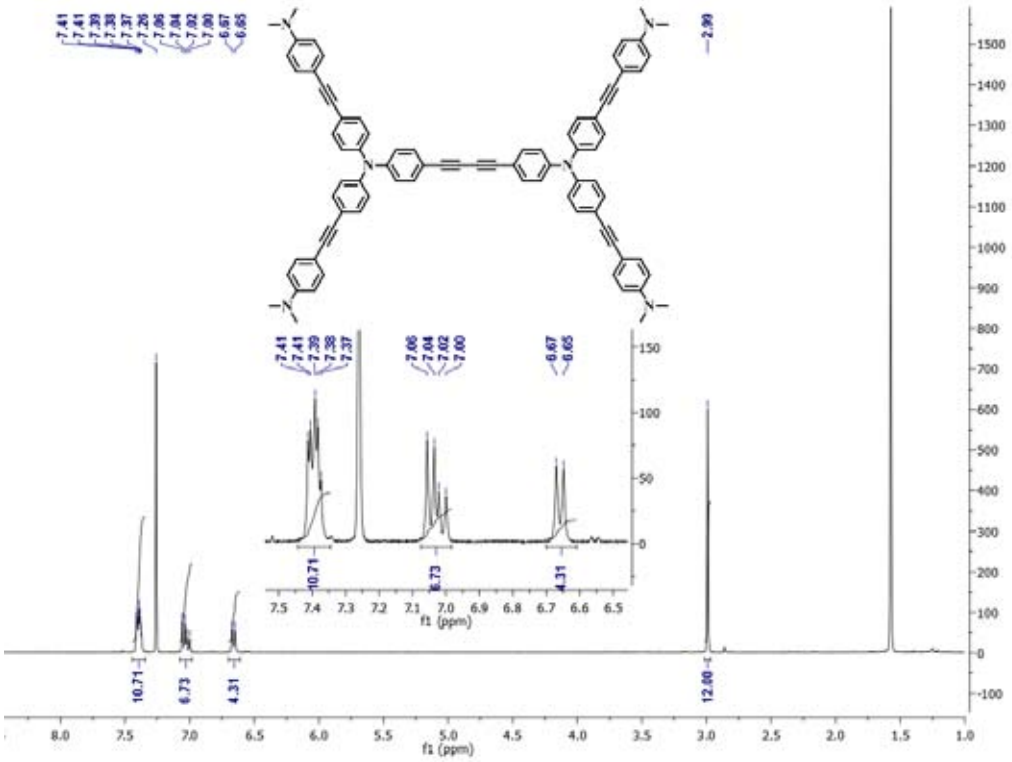

Figure A.15 ^{1}H NMR of **4N^{0}** in $CDCl_3$.

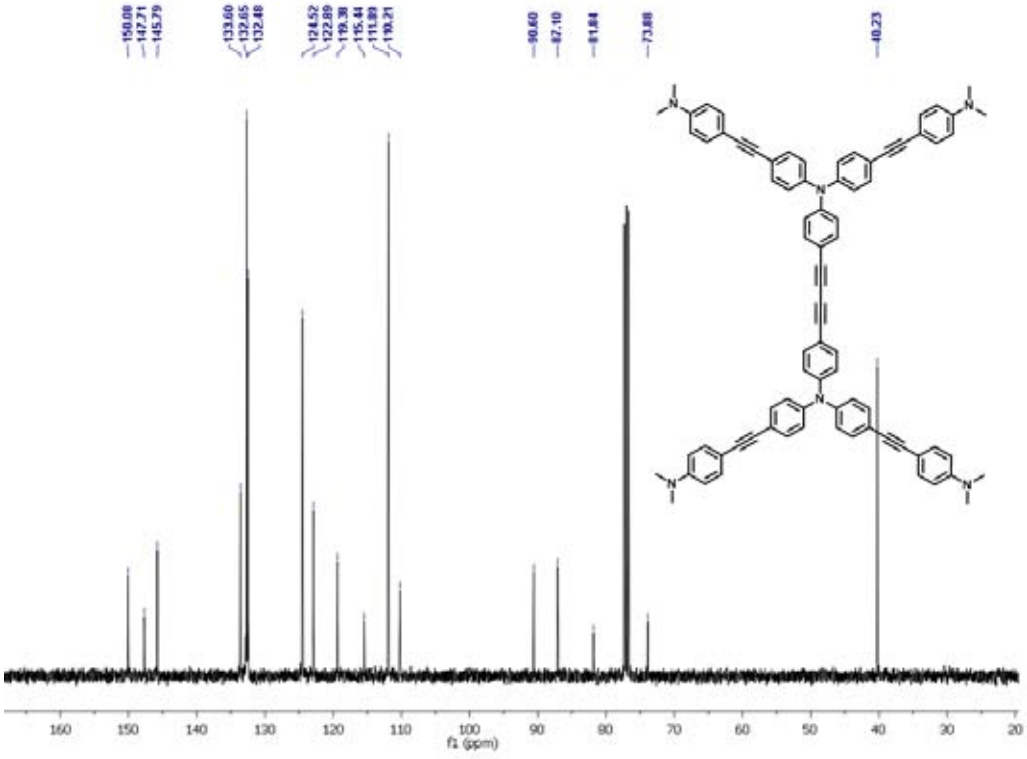

Figure A.16 ^{13}C NMR of **4N^{0}** in $CDCl_3$.

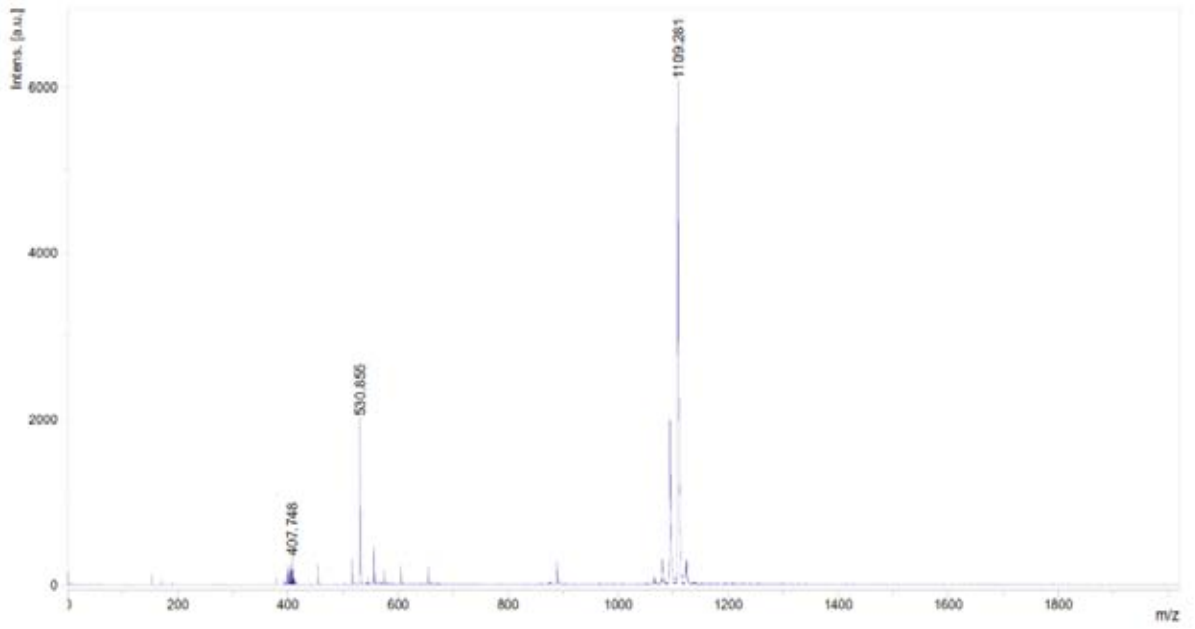

Figure A.17 MALDI-TOF-MS of **4N^0.**

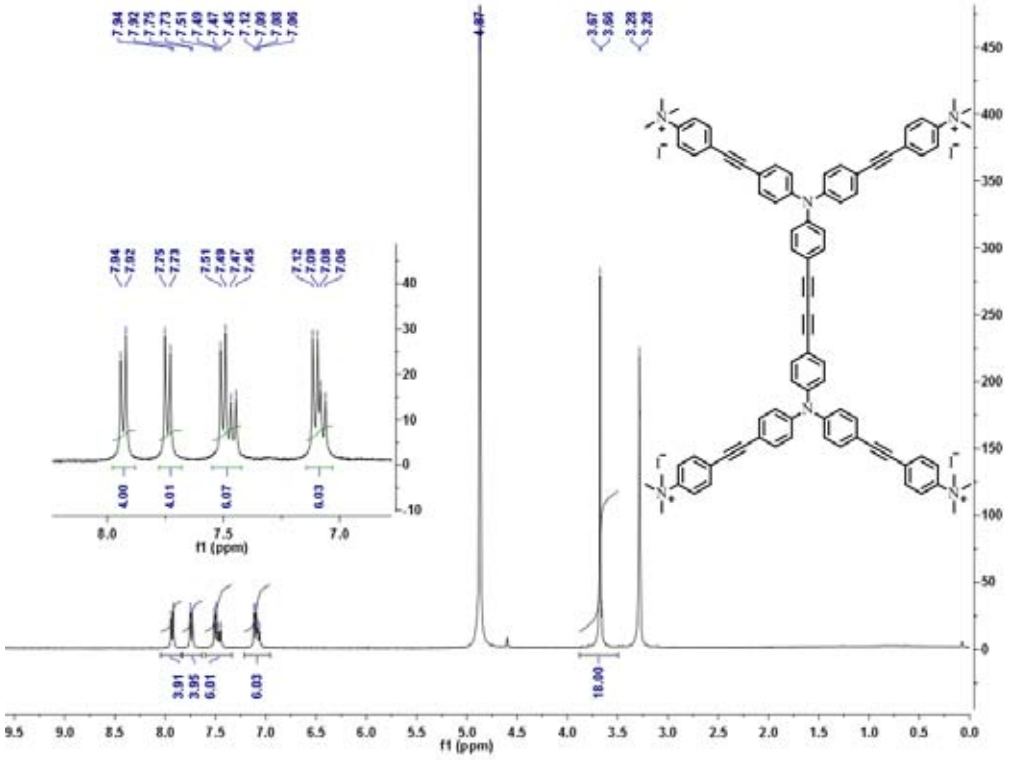

Figure A.18 ^{1}H NMR of **4N$^+$I$^-$** in CD_3OD.

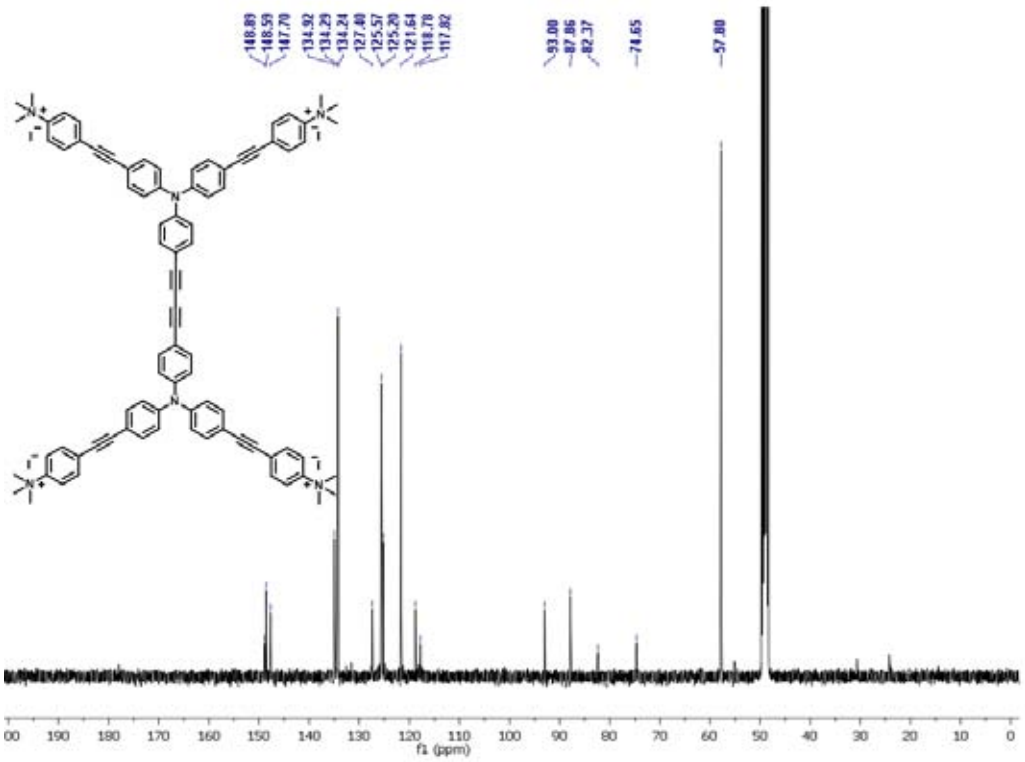

Figure A.19 ^{13}C NMR of $\mathbf{4N^+I^-}$ in CD_3OD.

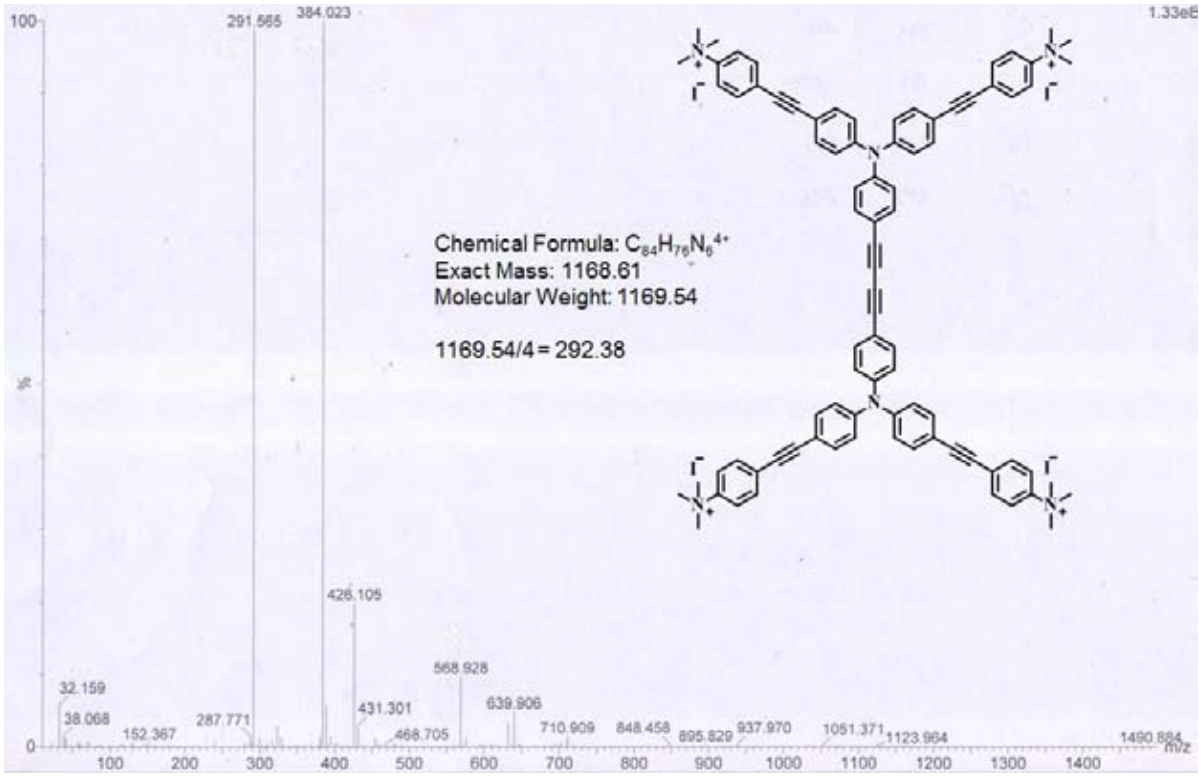

Figure A.20 ESI-MS of $\mathbf{4N^+I^-}$ in CH_3OH.

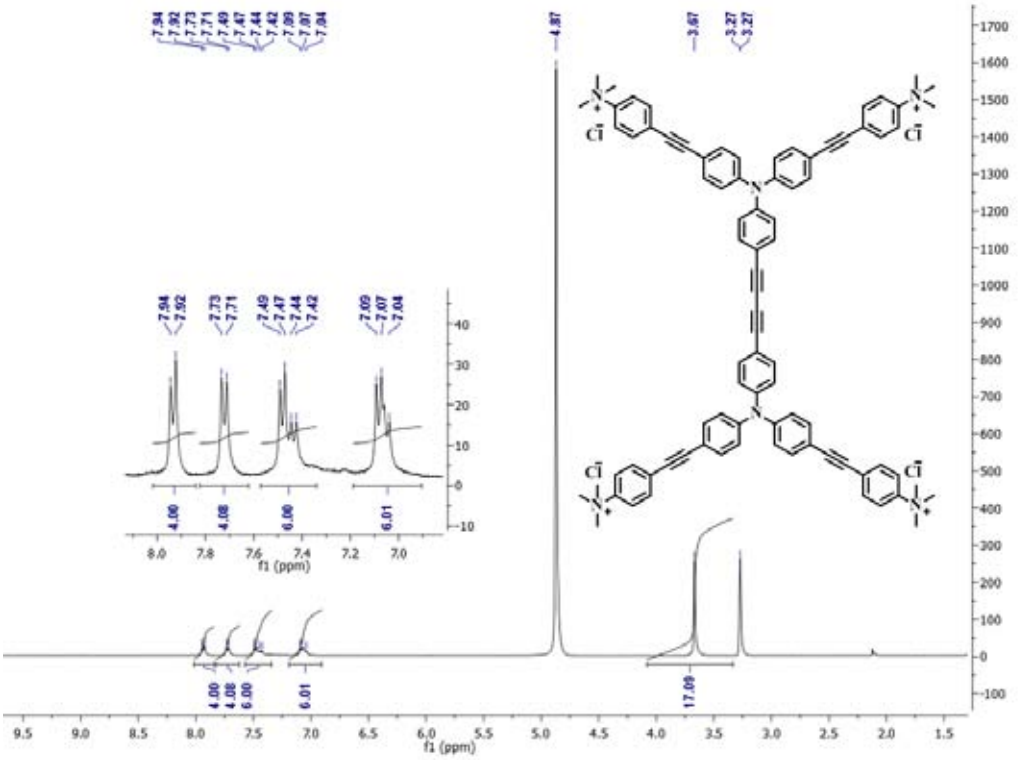

Figure A.21 ^{1}H NMR of **4N^{+}Cl^{-}** in CD_3OD.

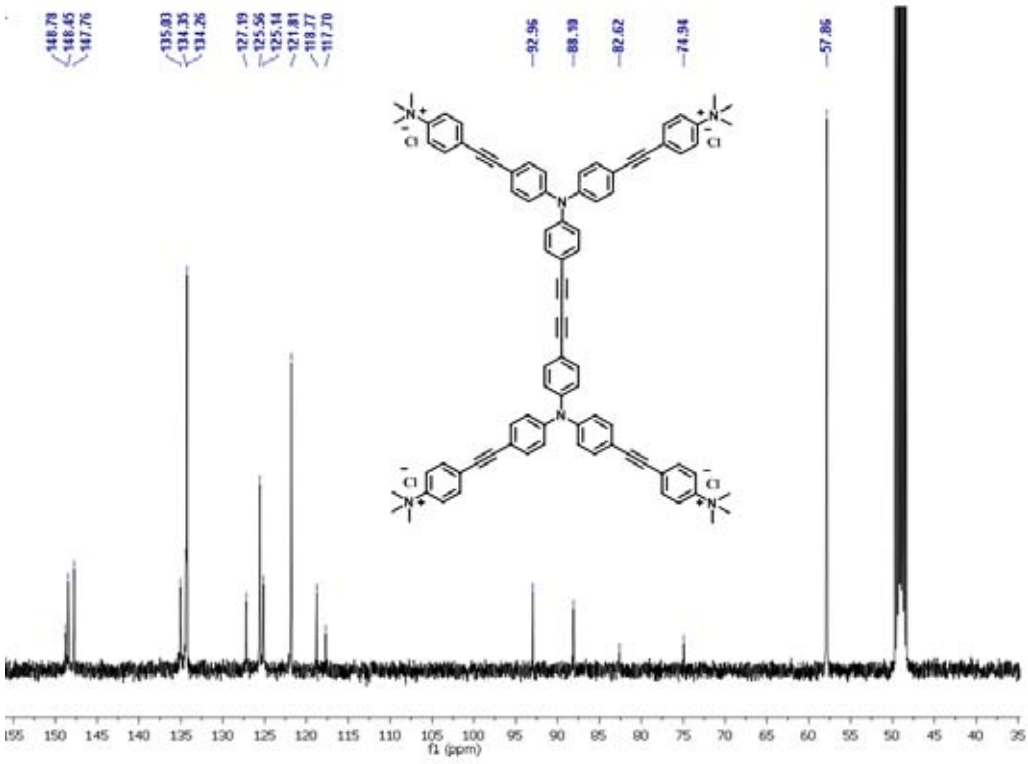

Figure A.22 ^{13}C NMR of **4N^{+}Cl^{-}** in CD_3OD.

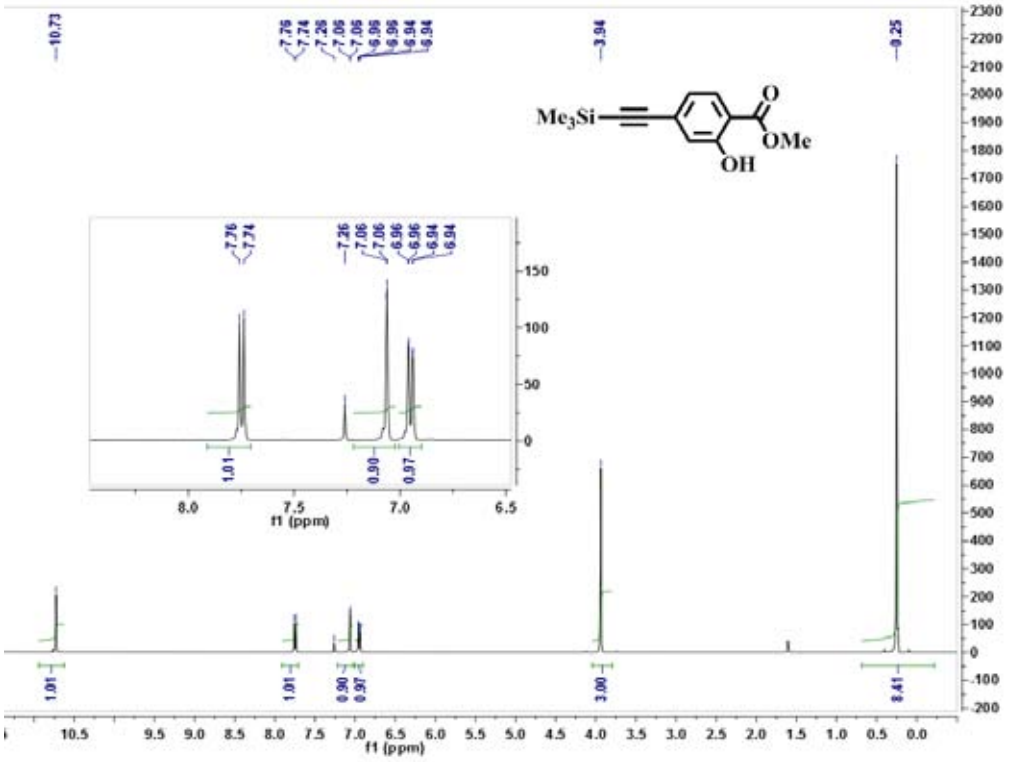

Figure A.23 ^{1}H NMR of methyl 2-hydroxy-4-((trimethylsilyl)ethynyl)benzoate in $CDCl_3$.

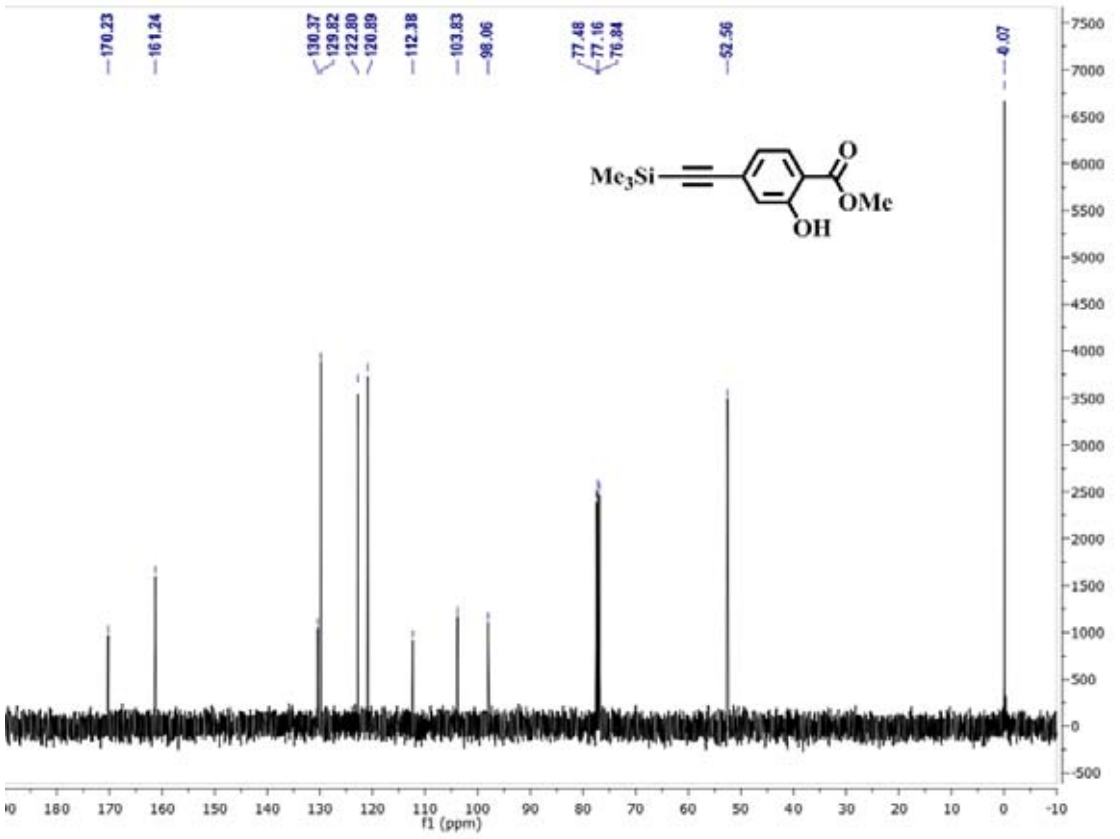

Figure A.24 ^{13}C NMR of methyl 2-hydroxy-4-((trimethylsilyl)ethynyl)benzoate in $CDCl_3$.

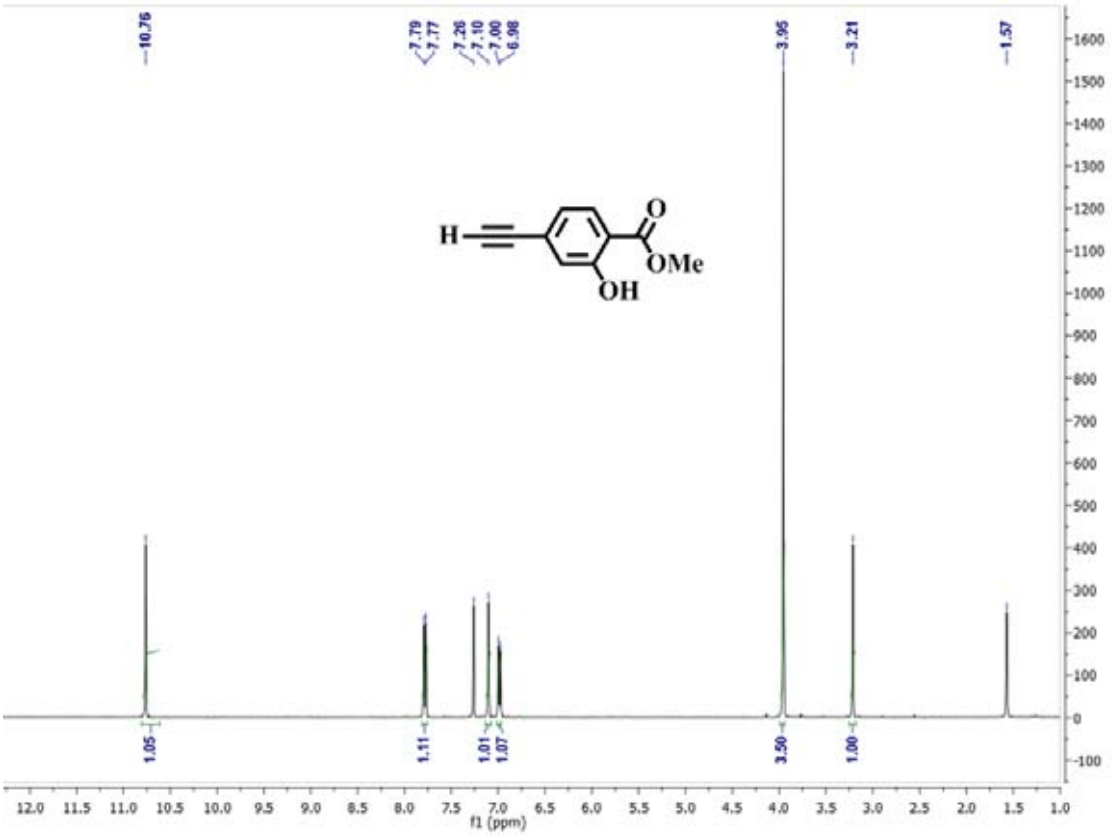

Figure A.25 ^{1}H NMR of methyl 4-ethynyl-2-hydroxybenzoate in $CDCl_3$.

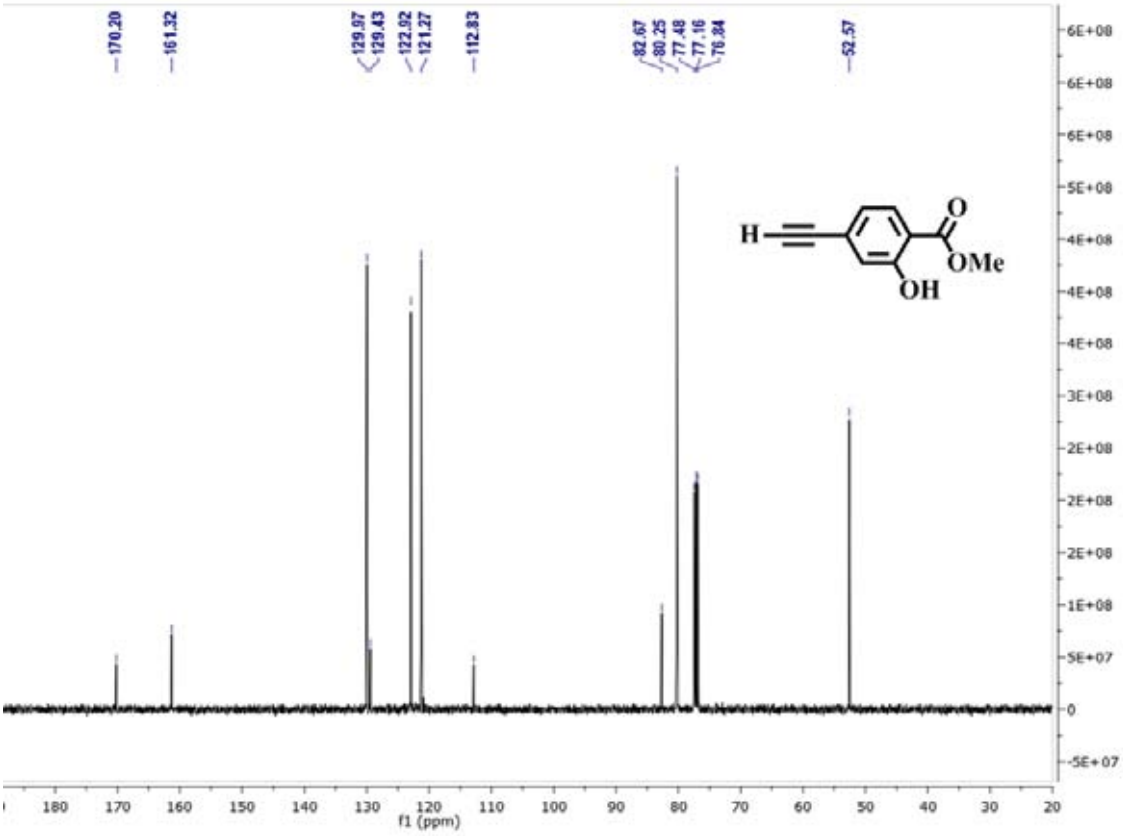

Figure A.26 ^{13}C NMR of methyl 4-ethynyl-2-hydroxybenzoate in $CDCl_3$.

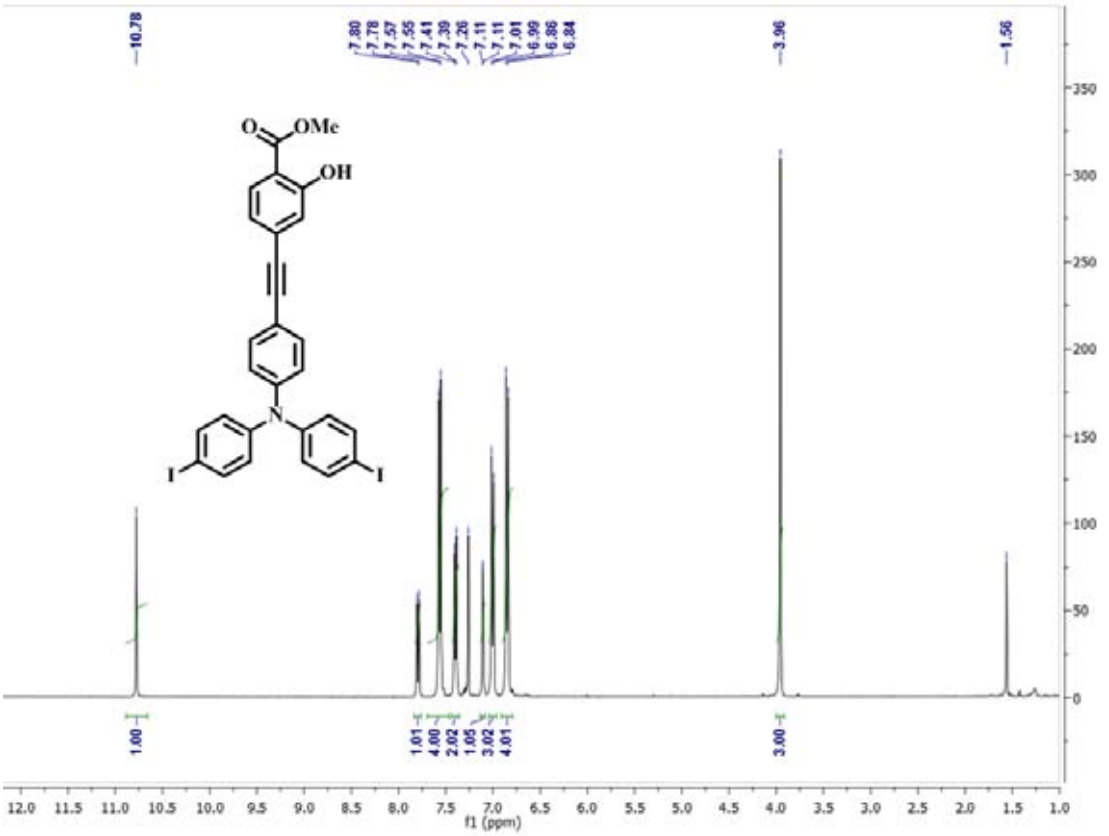

Figure A.27 ^{1}H NMR of **2ISA^{0}** in $CDCl_3$.

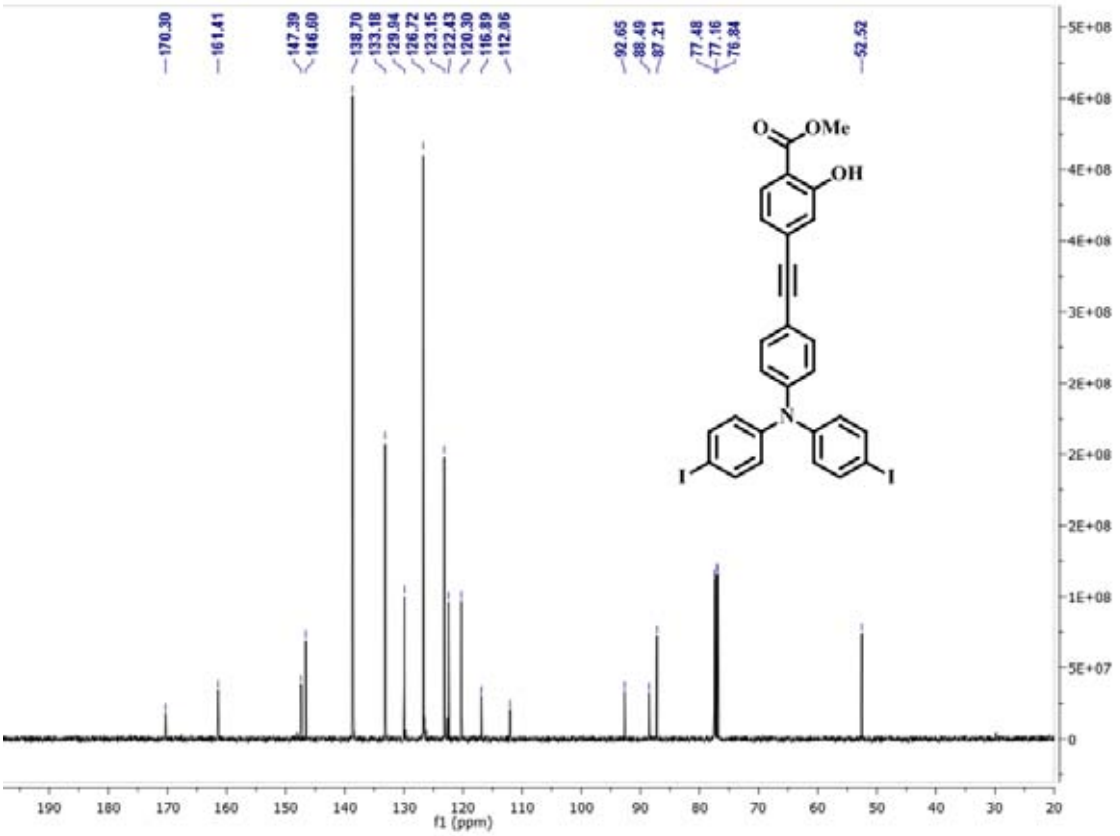

Figure A.28 ^{13}C NMR of **2ISA^{0}** in $CDCl_3$.

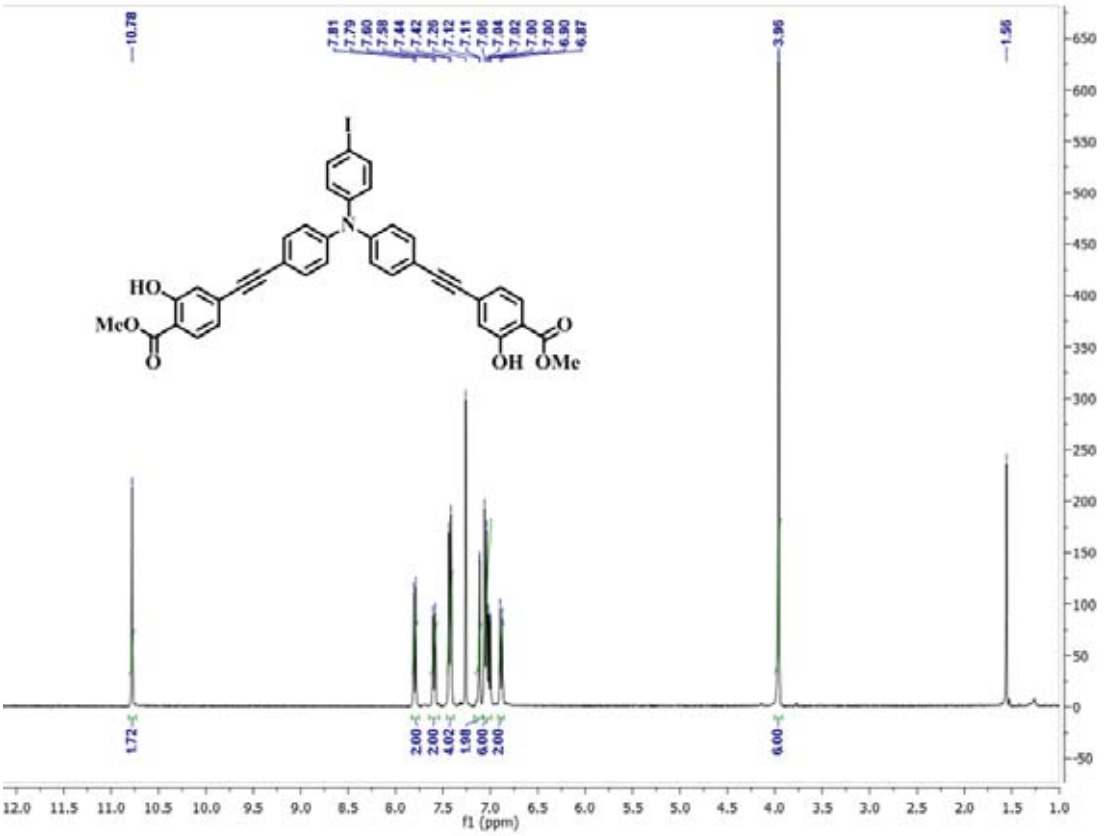

Figure A.29 ^{1}H NMR of **4** in $CDCl_3$.

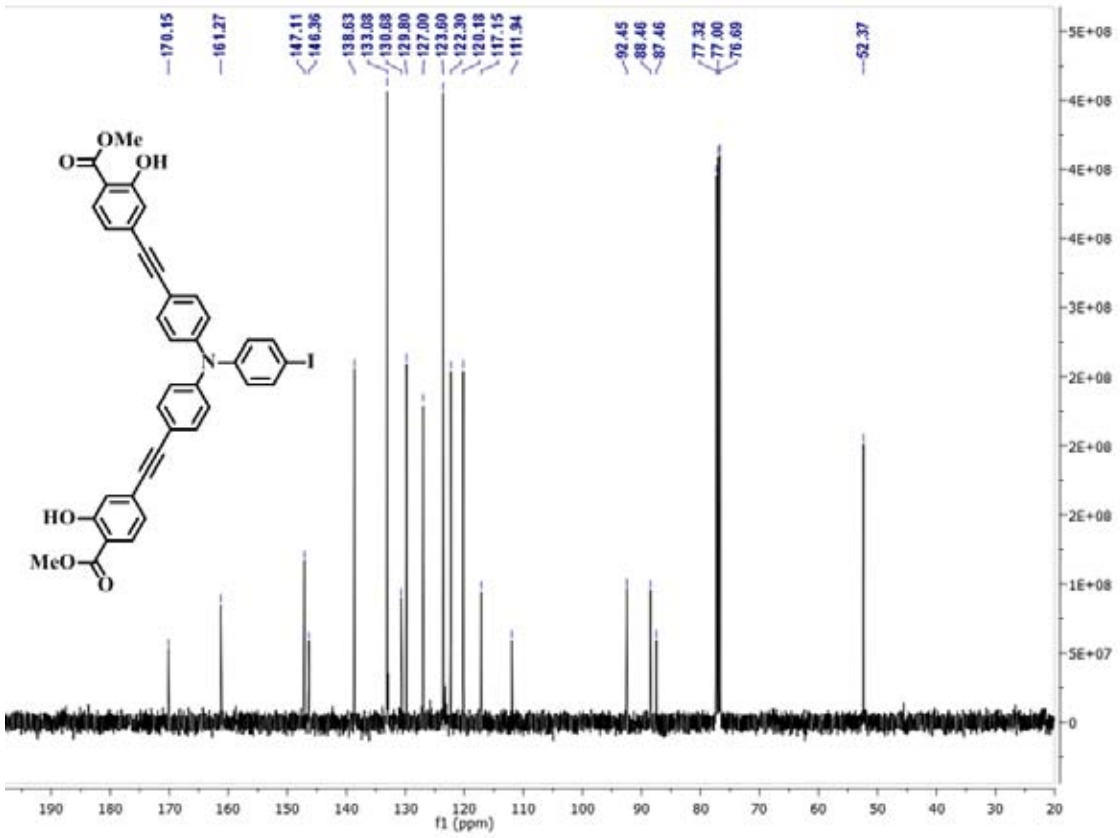

Figure A.30 ^{13}C NMR of **4** in $CDCl_3$.

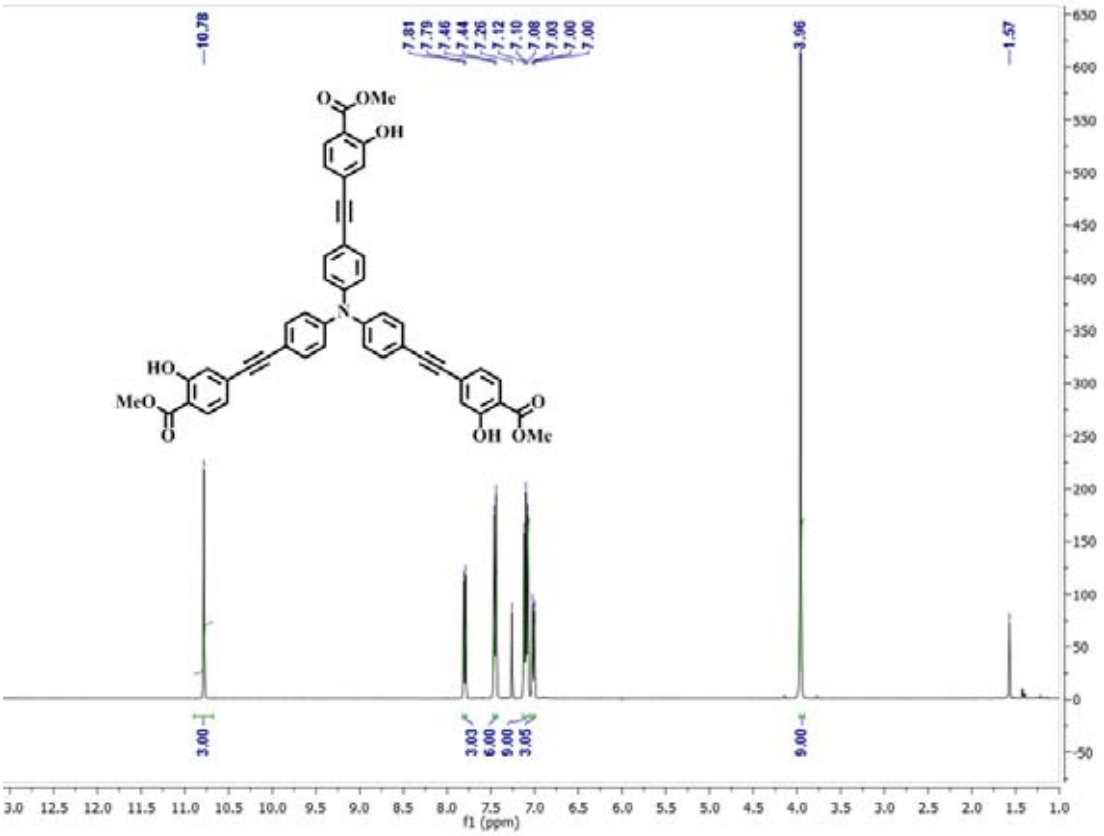

Figure A.31 ^{1}H NMR of **3** in $CDCl_3$.

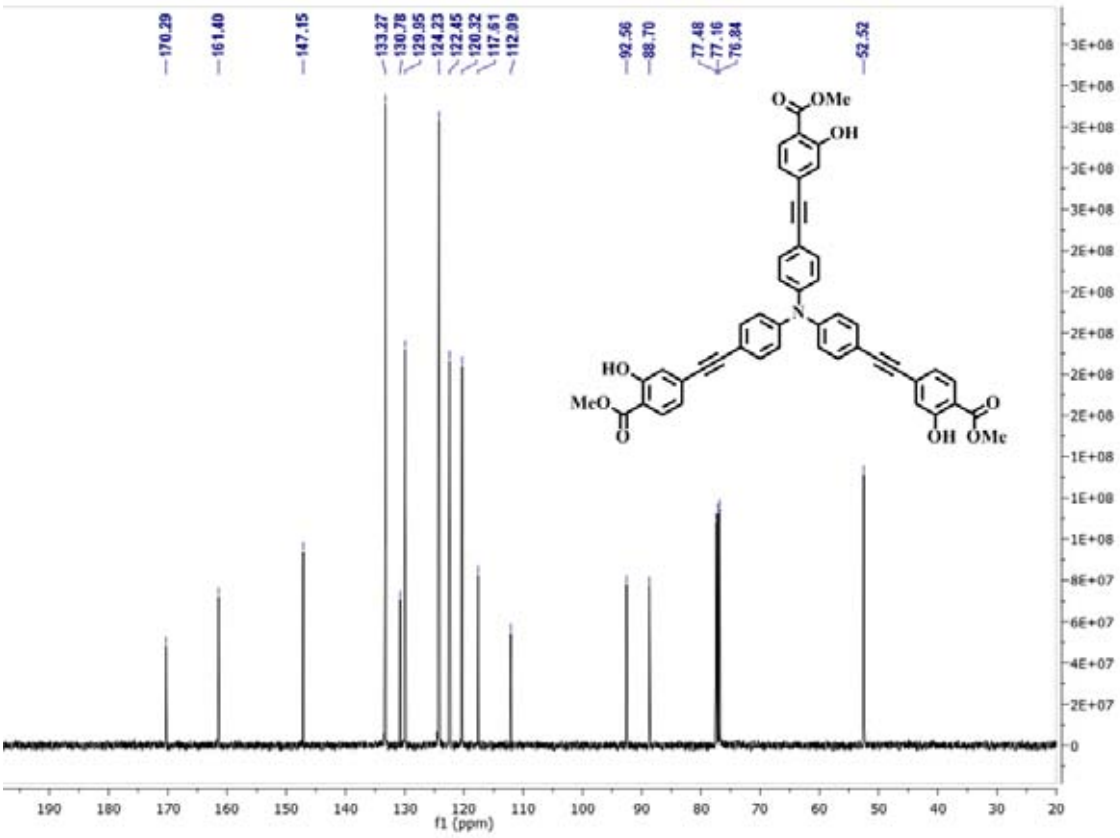

Figure A.32 ^{13}C NMR of **3** in $CDCl_3$.

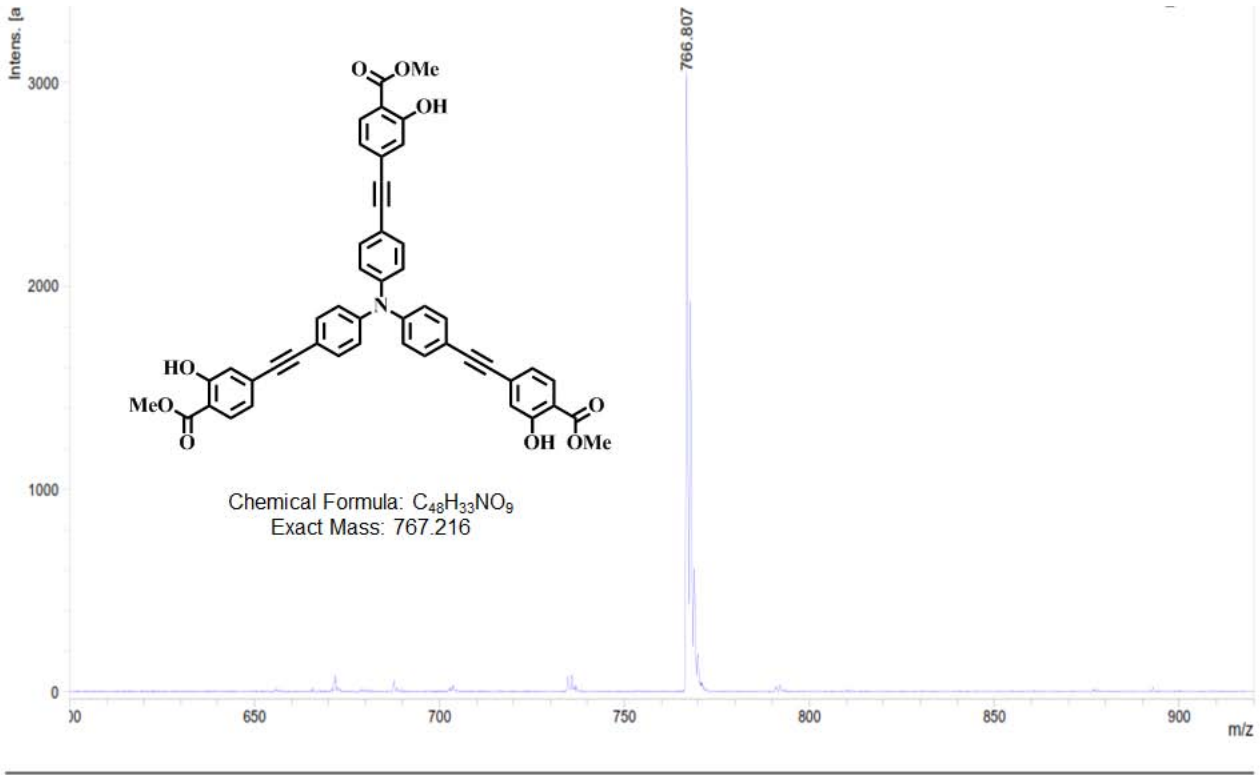

Figure A.33 MALDI-TOF-MS of **3.**

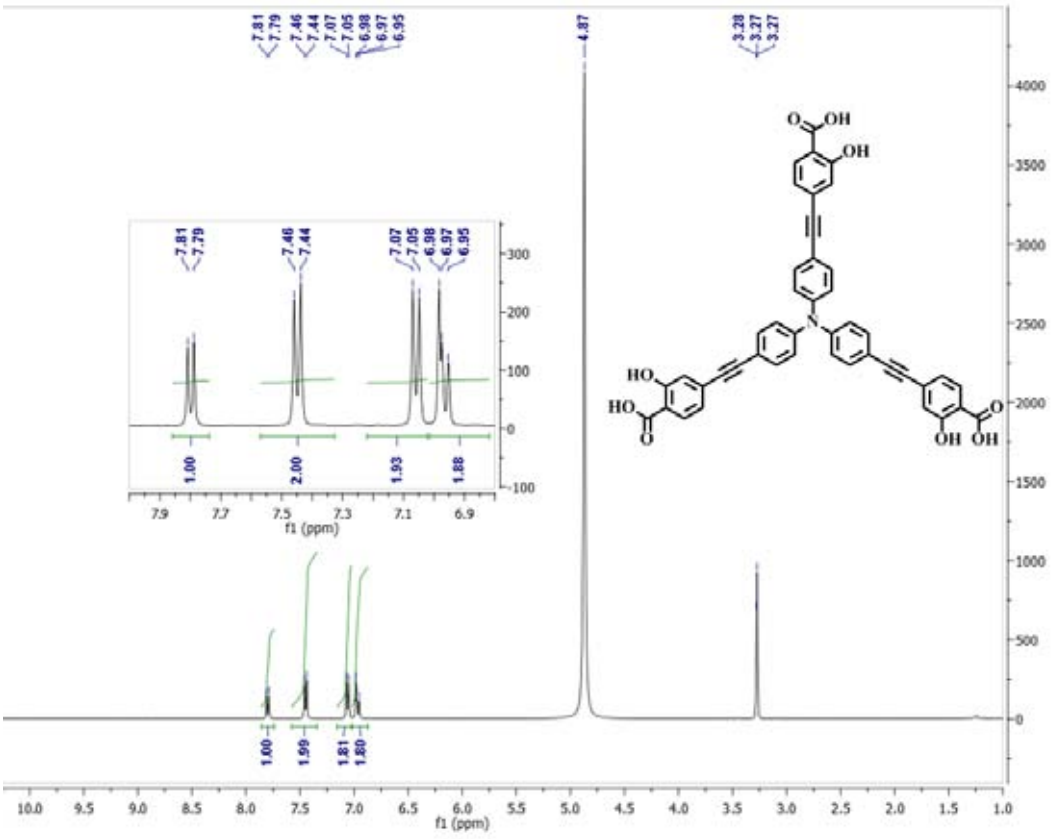

Figure A.34 ^{1}H NMR of **F4** in CD_3OD.

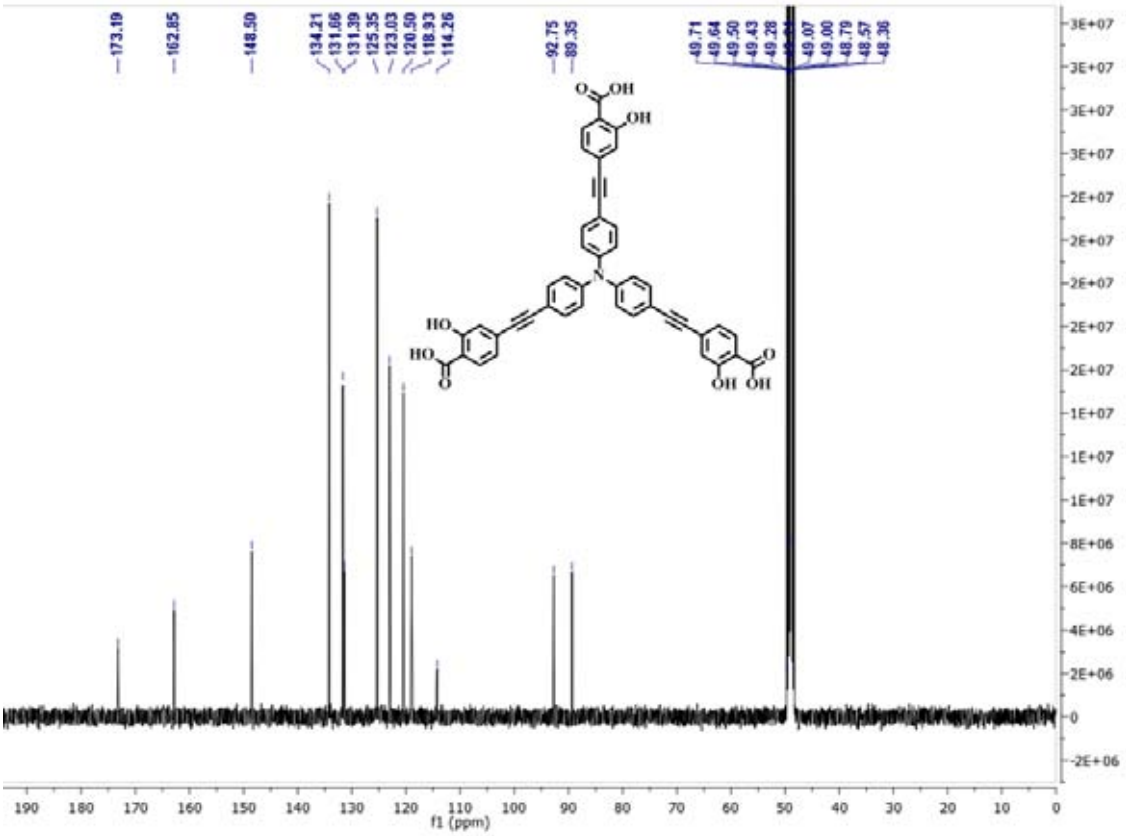

Figure A.35 ^{13}C NMR of **F4** in CD_3OD.

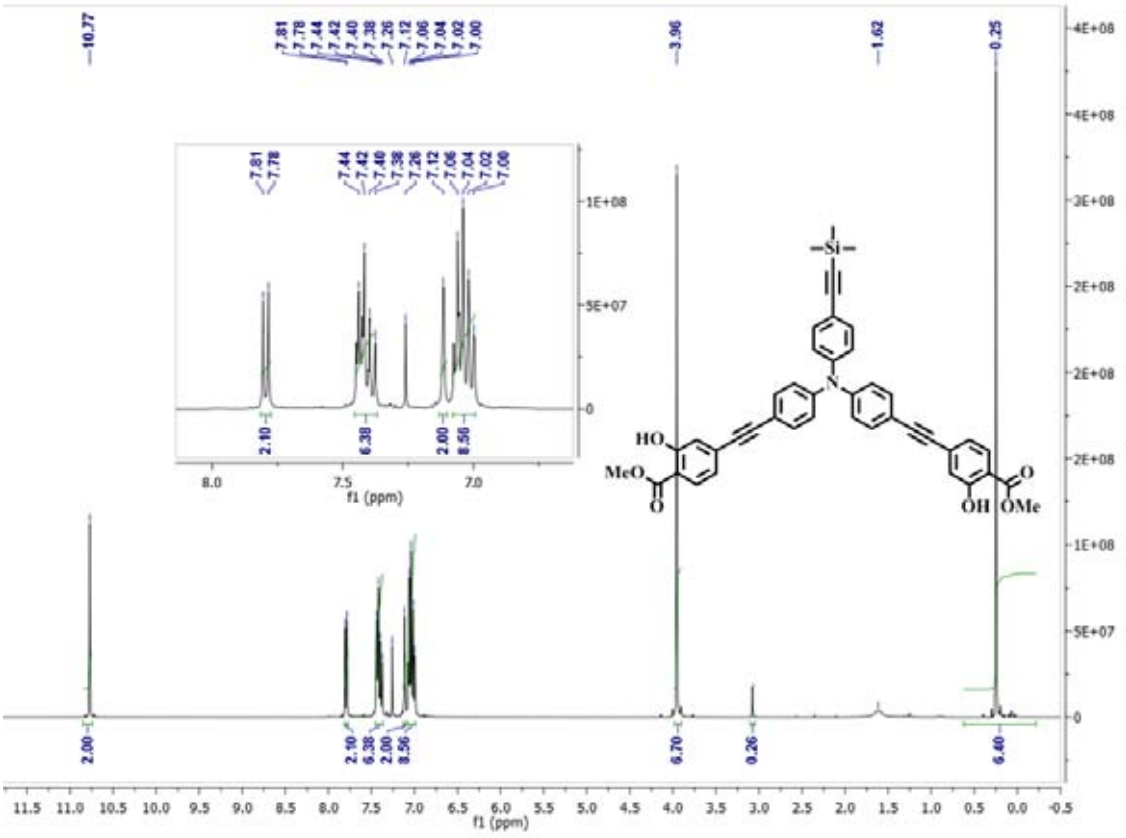

Figure A.36 ^{1}H NMR of **5** in $CDCl_3$.

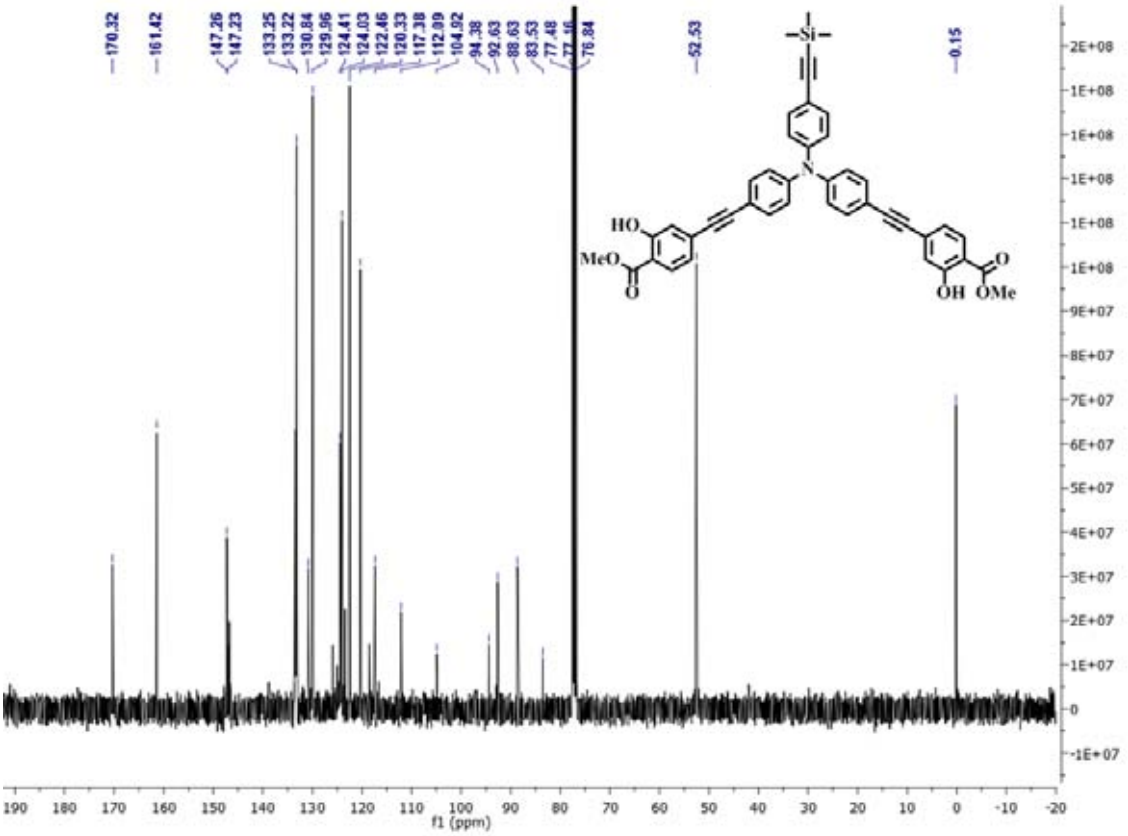

Figure A.37 ^{13}C NMR of **5** in $CDCl_3$.

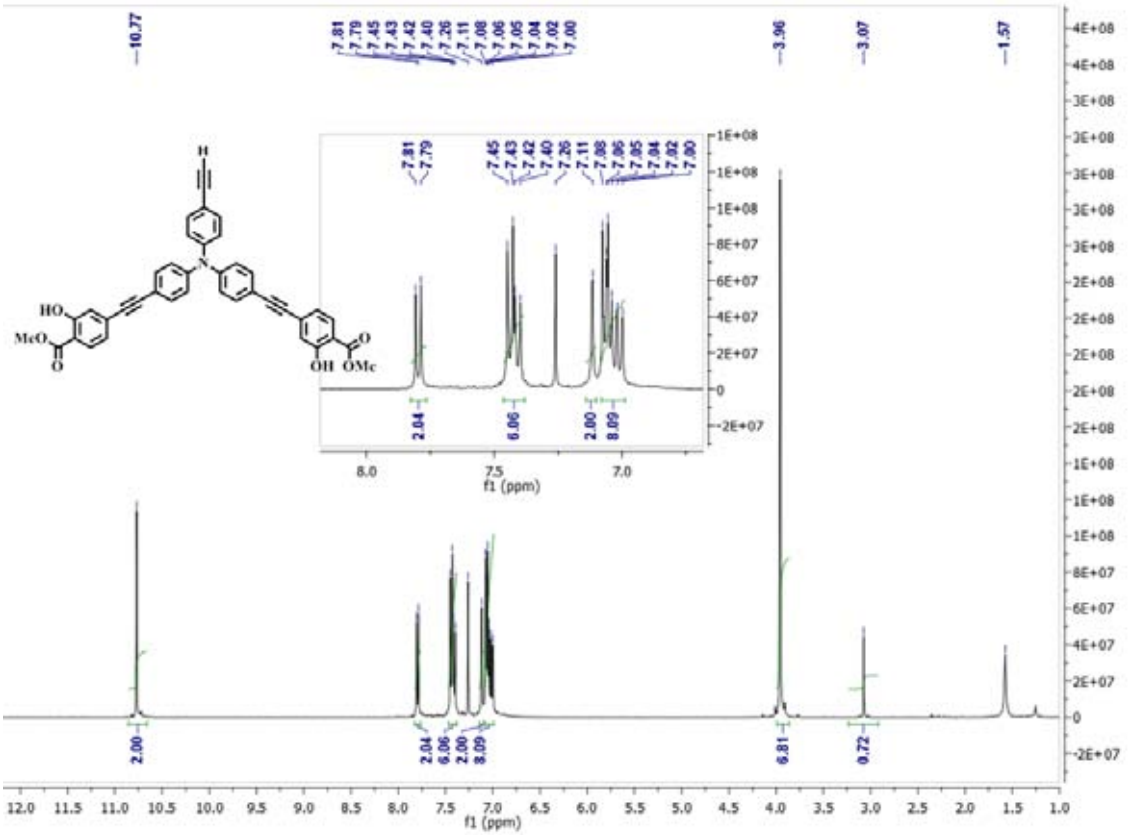

Figure A.38 ^{1}H NMR of **6** in $CDCl_3$.

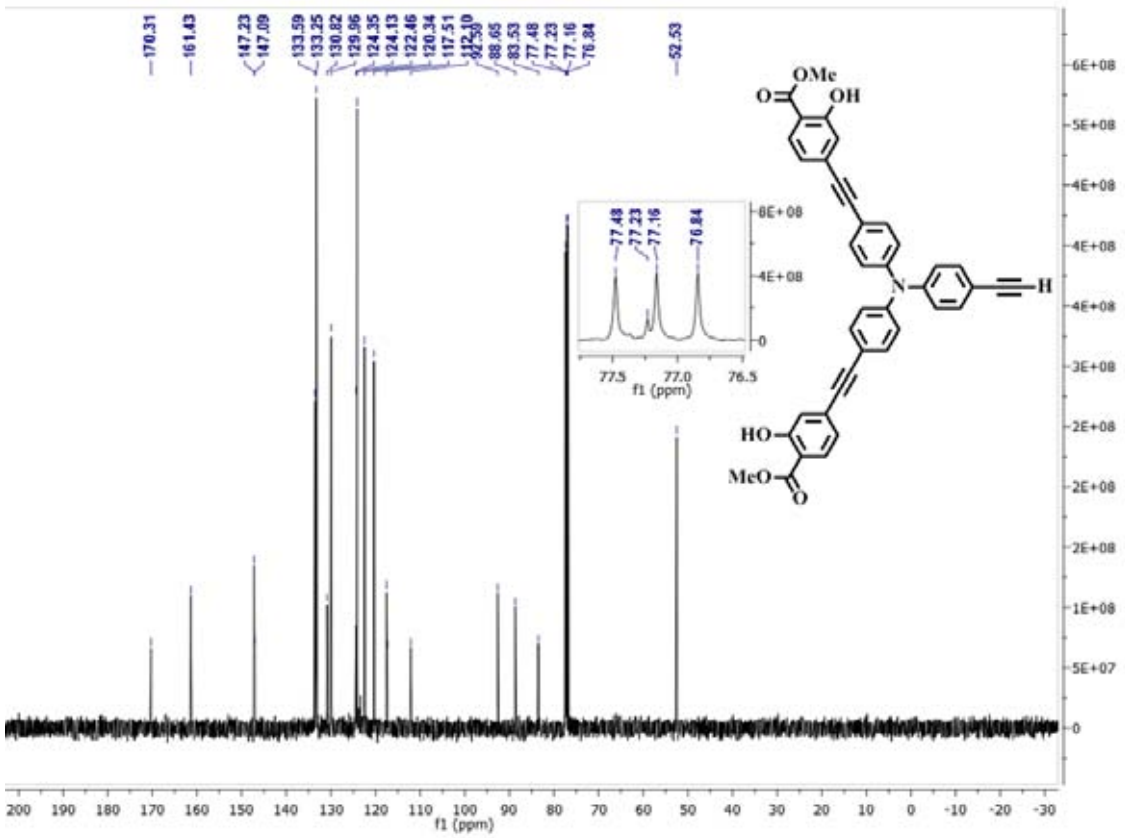

Figure A.39 ^{13}C NMR of **6** in $CDCl_3$.

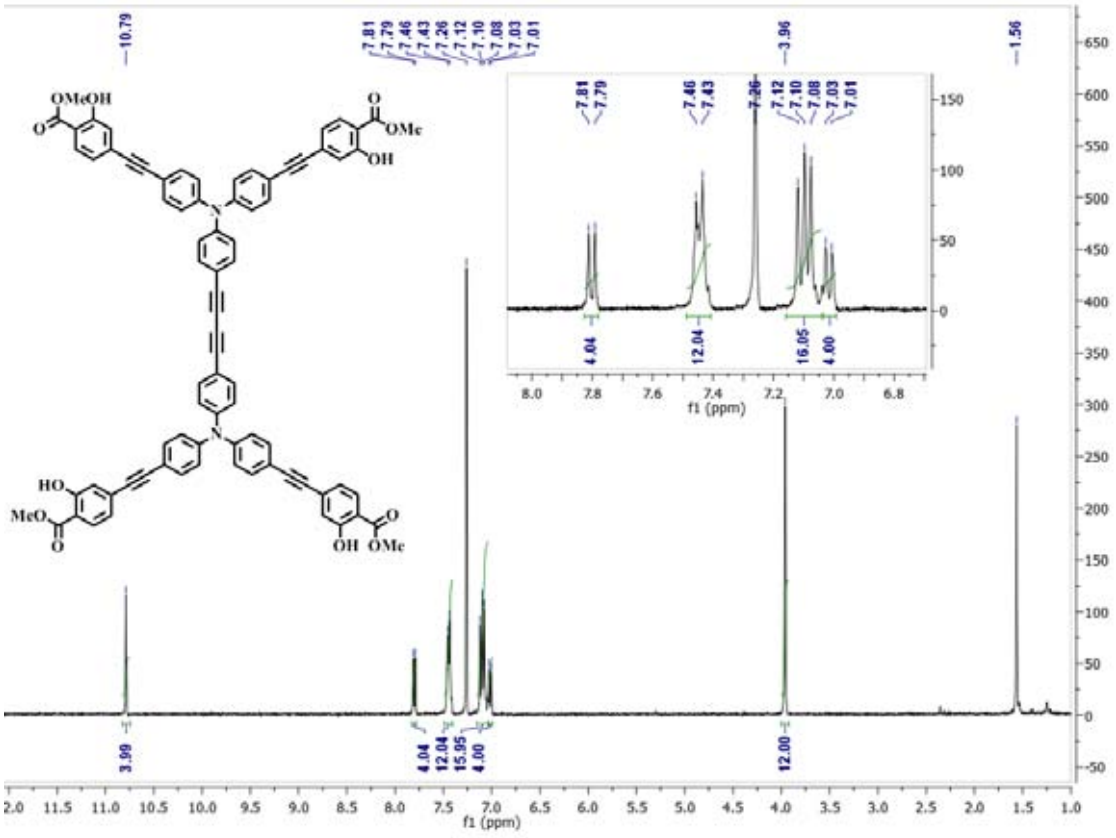

Figure A.40 ^{1}H NMR of **7** in $CDCl_3$.

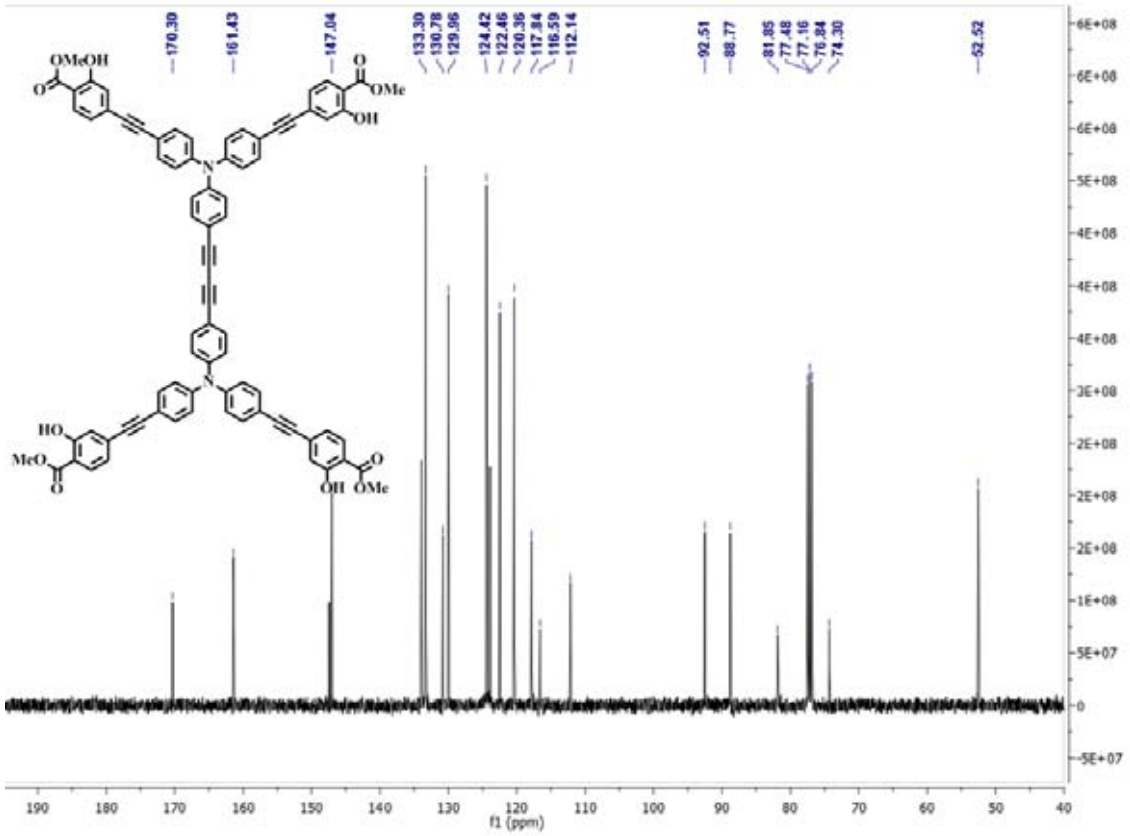

Figure A.41 ^{13}C NMR of **7** in $CDCl_3$.

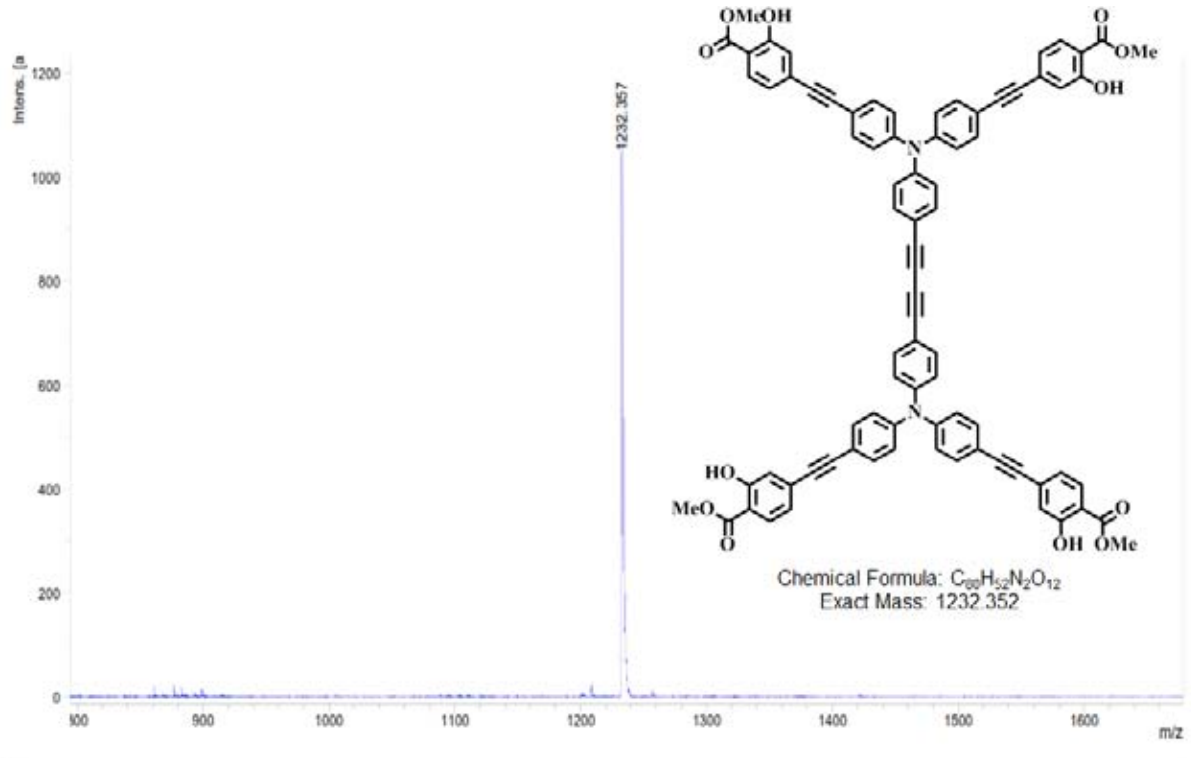

Figure A.42 MALDI-TOF-MS of **7.**

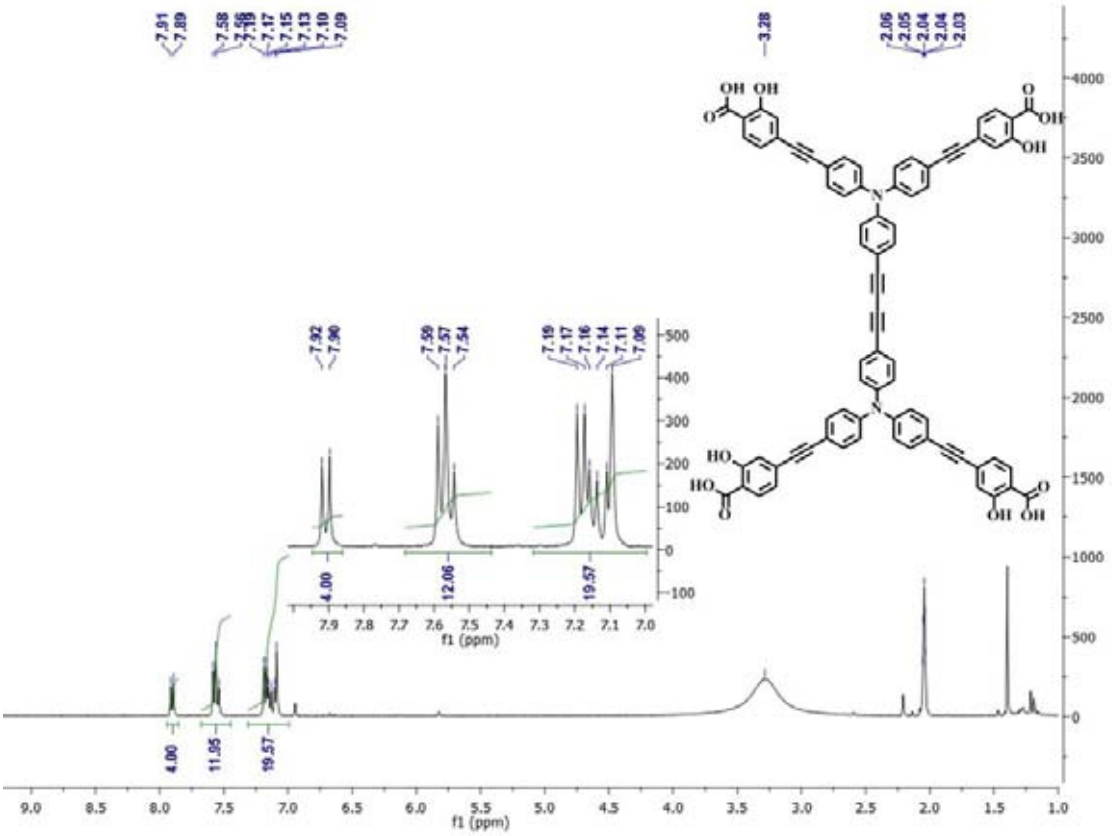

Figure A.43 ^{1}H NMR of **F5** in Acetone-d6.

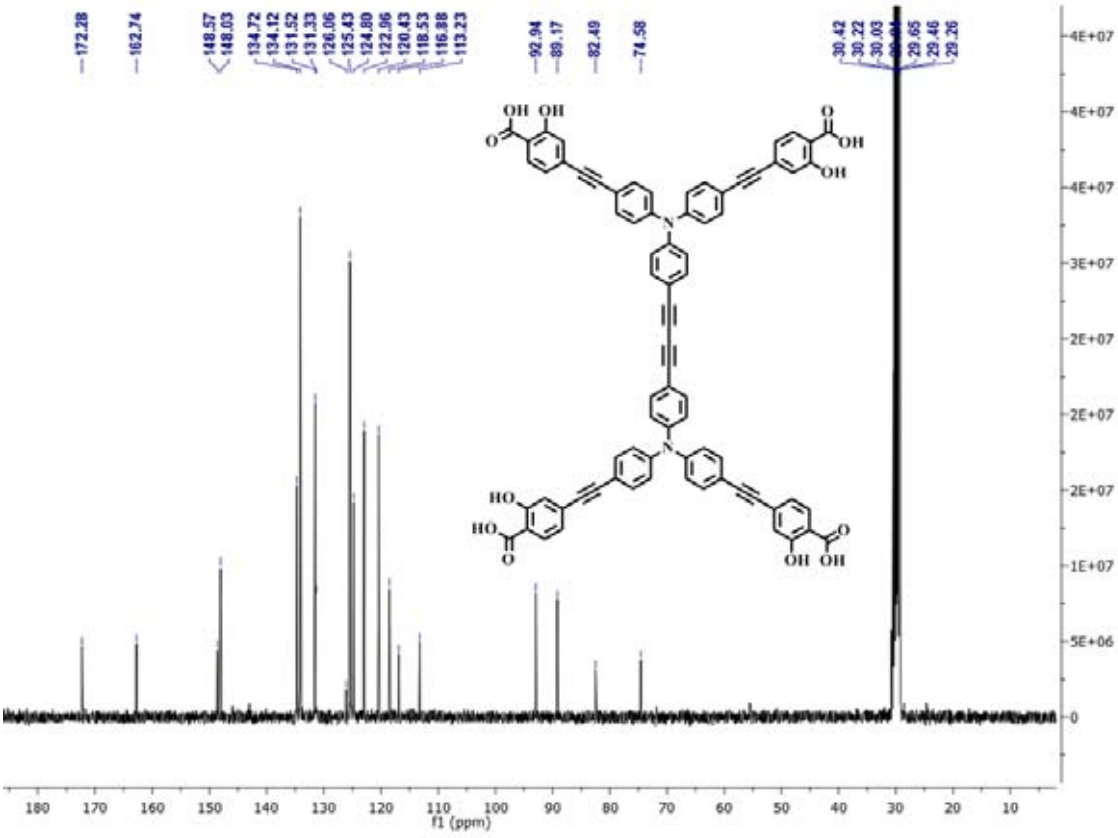

Figure A.44 ^{13}C NMR of **F5** in Acetone-d6.

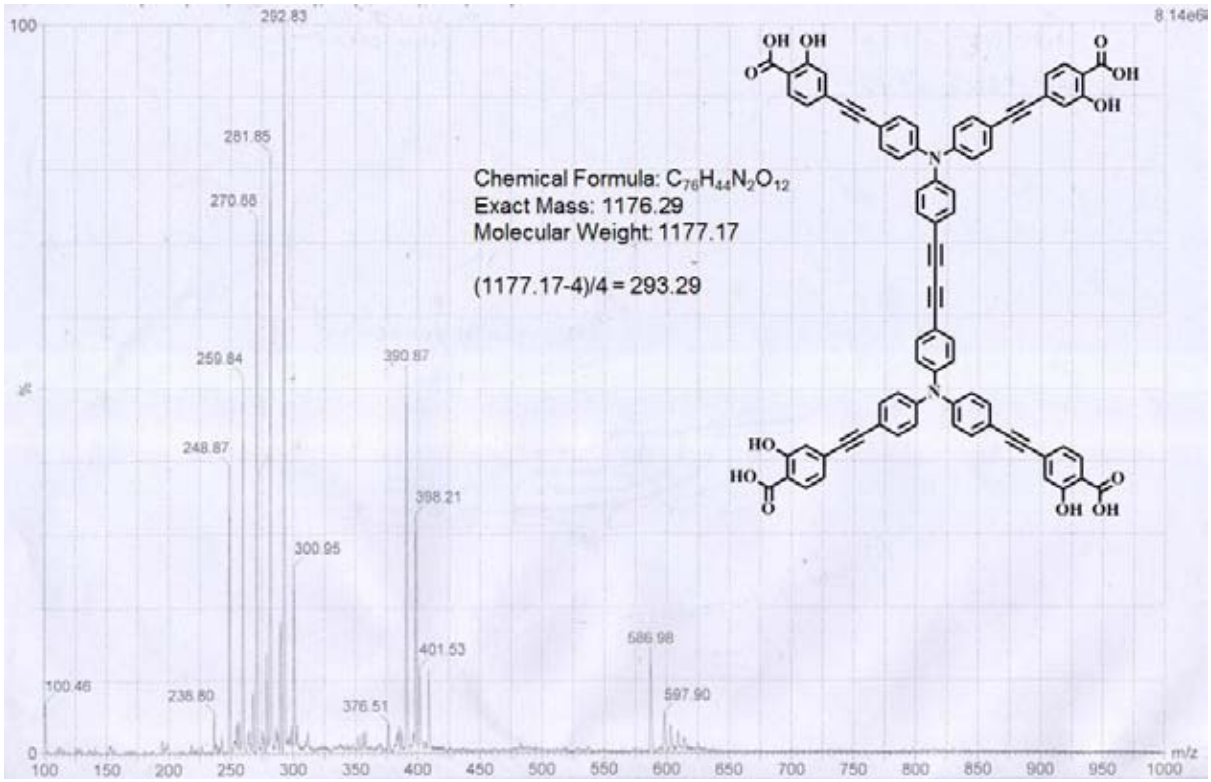

Figure A.45 ESI-MS of **F5** in CH_3OH.

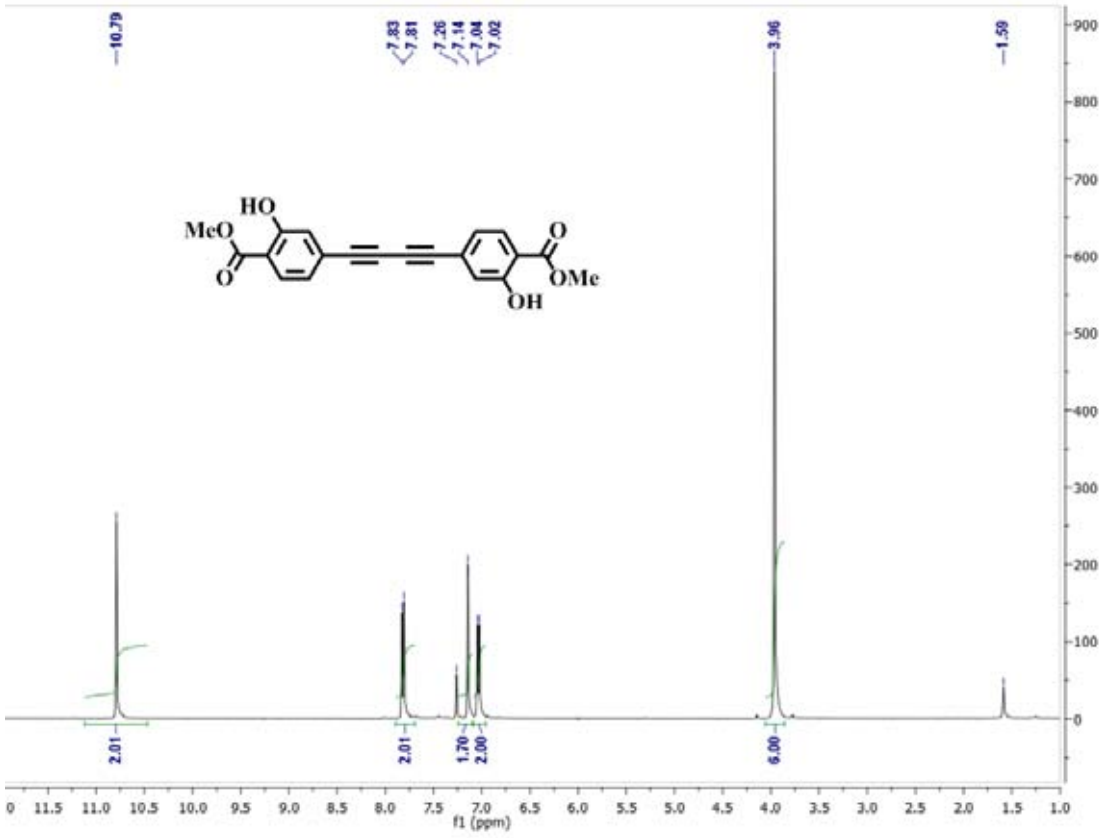

Figure A.46 ^1H NMR of **1** in $CDCl_3$.

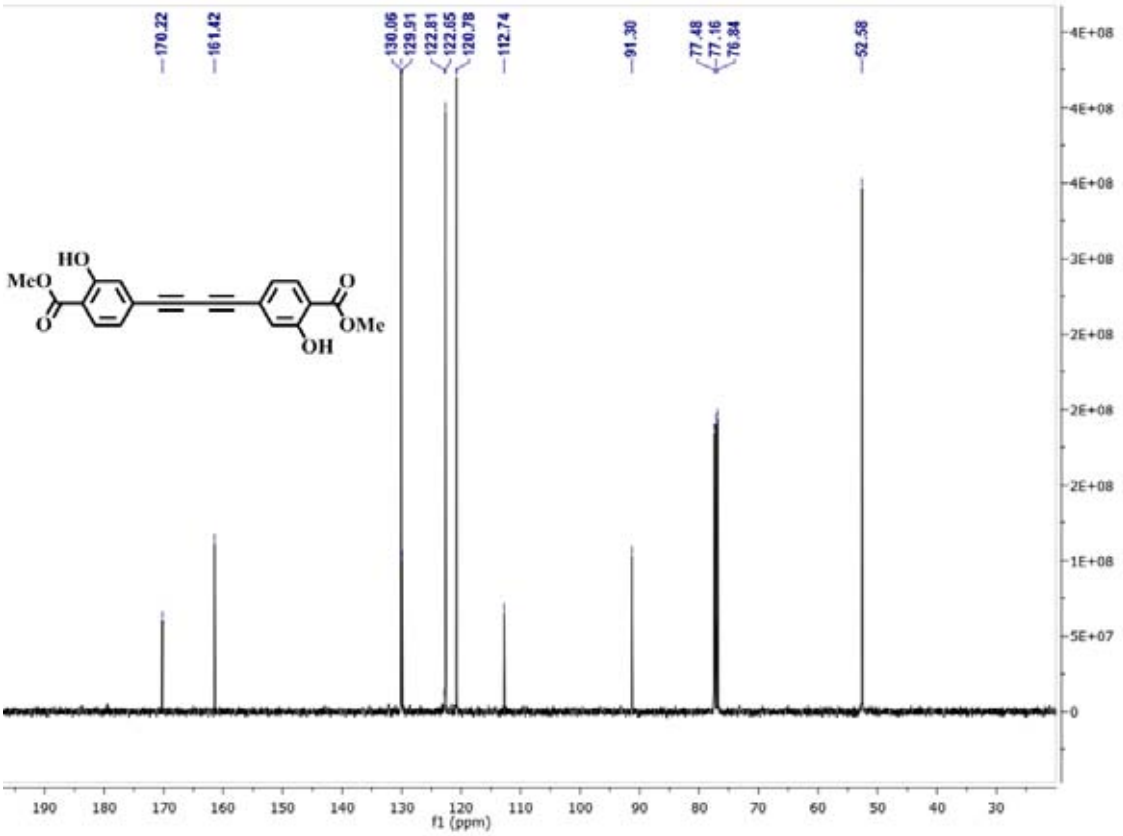

Figure A.47 ^{13}C NMR of **1** in $CDCl_3$.

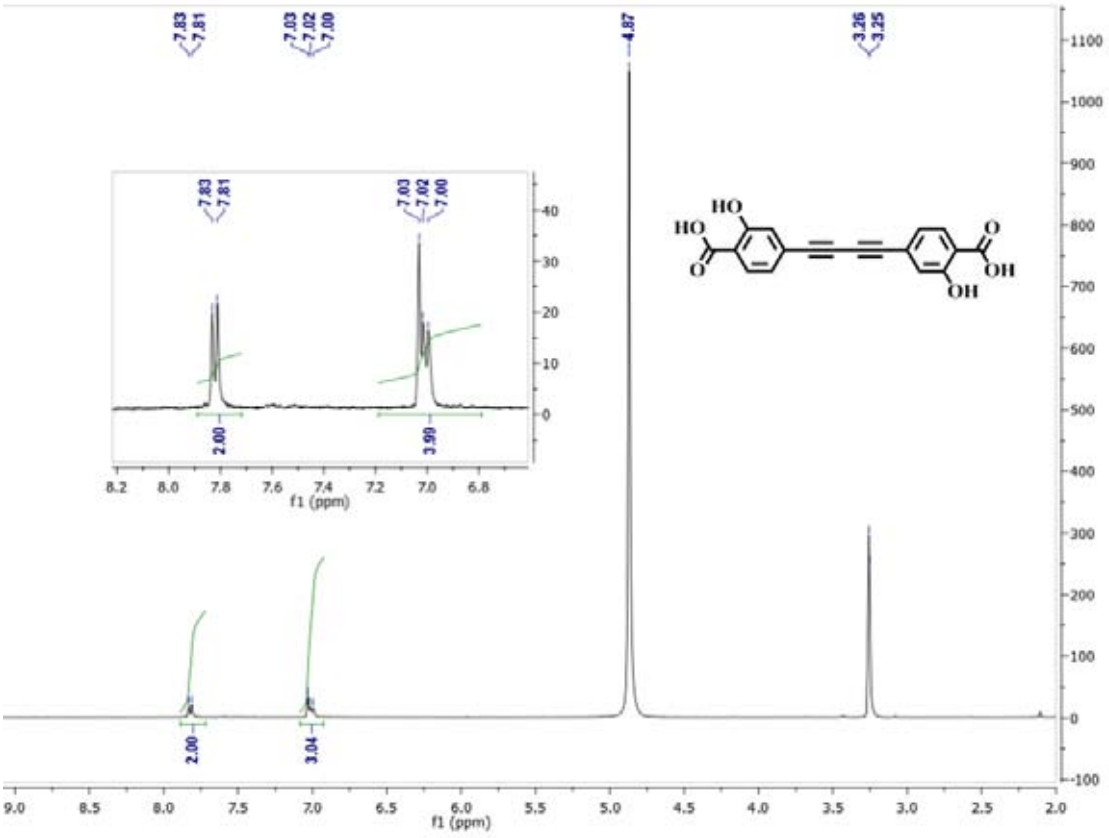

Figure A.48 ^{1}H NMR of **F3** in CD_3OD.

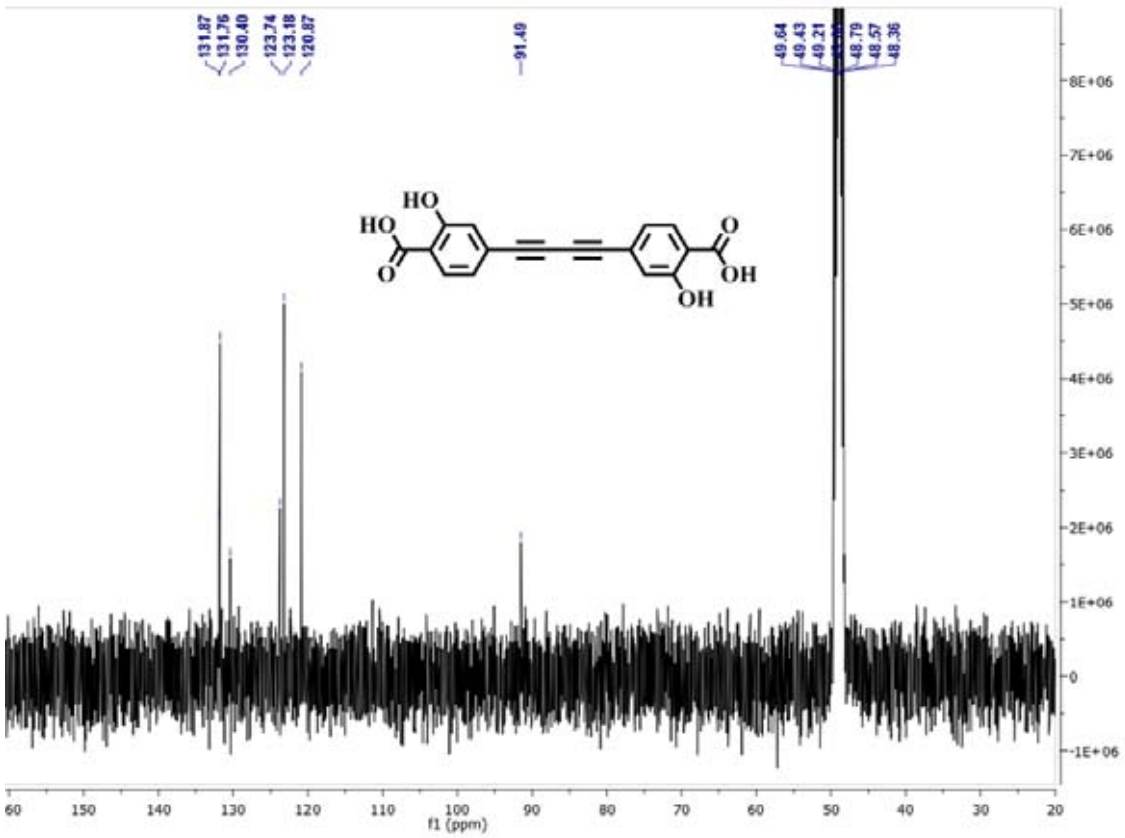

Figure A.49 ^{13}C NMR of **F3** in CD_3OD.

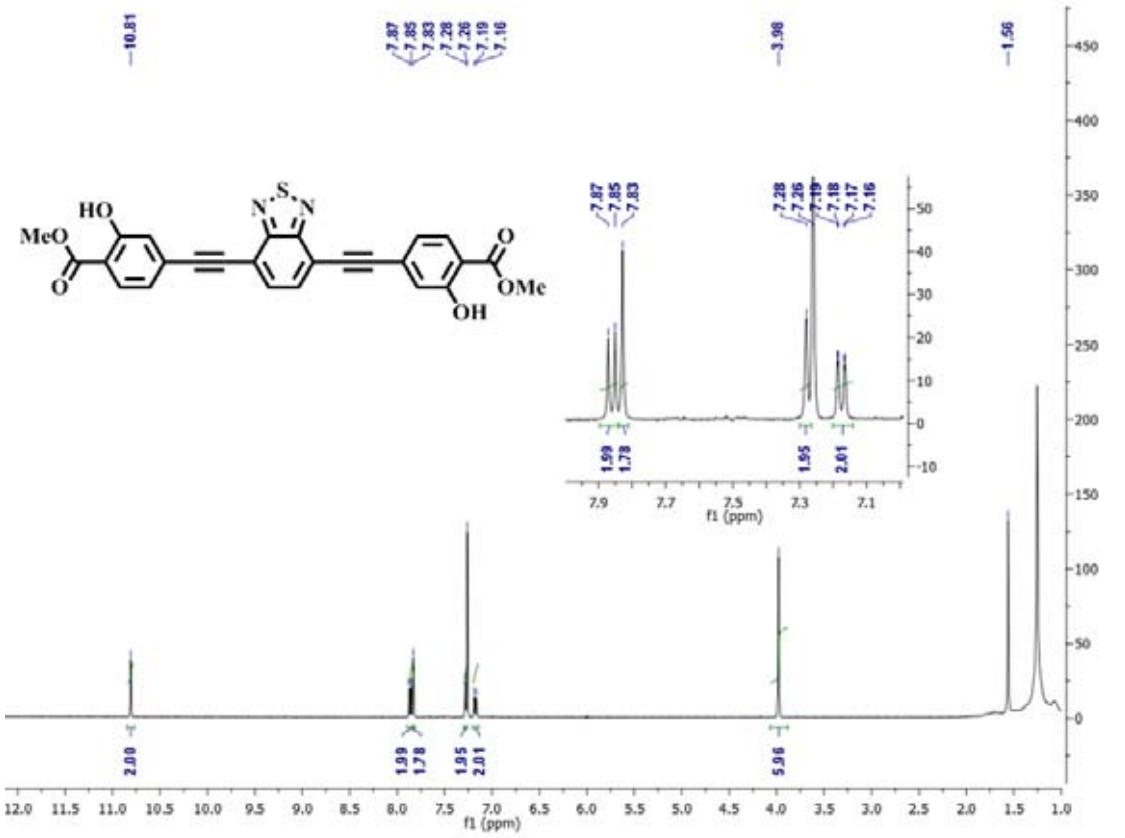

Figure A.50 ^{1}H NMR of **2** in $CDCl_3$.

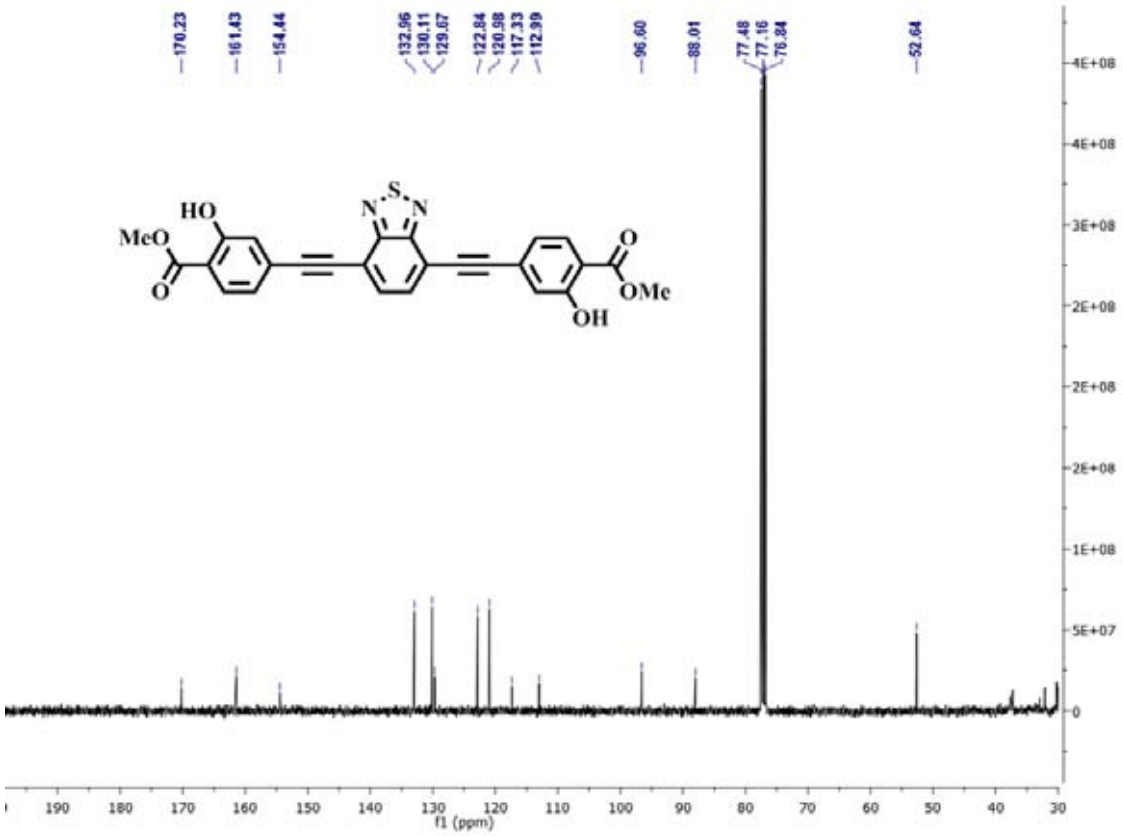

Figure A.51 ^{13}C NMR of **2** in $CDCl_3$.

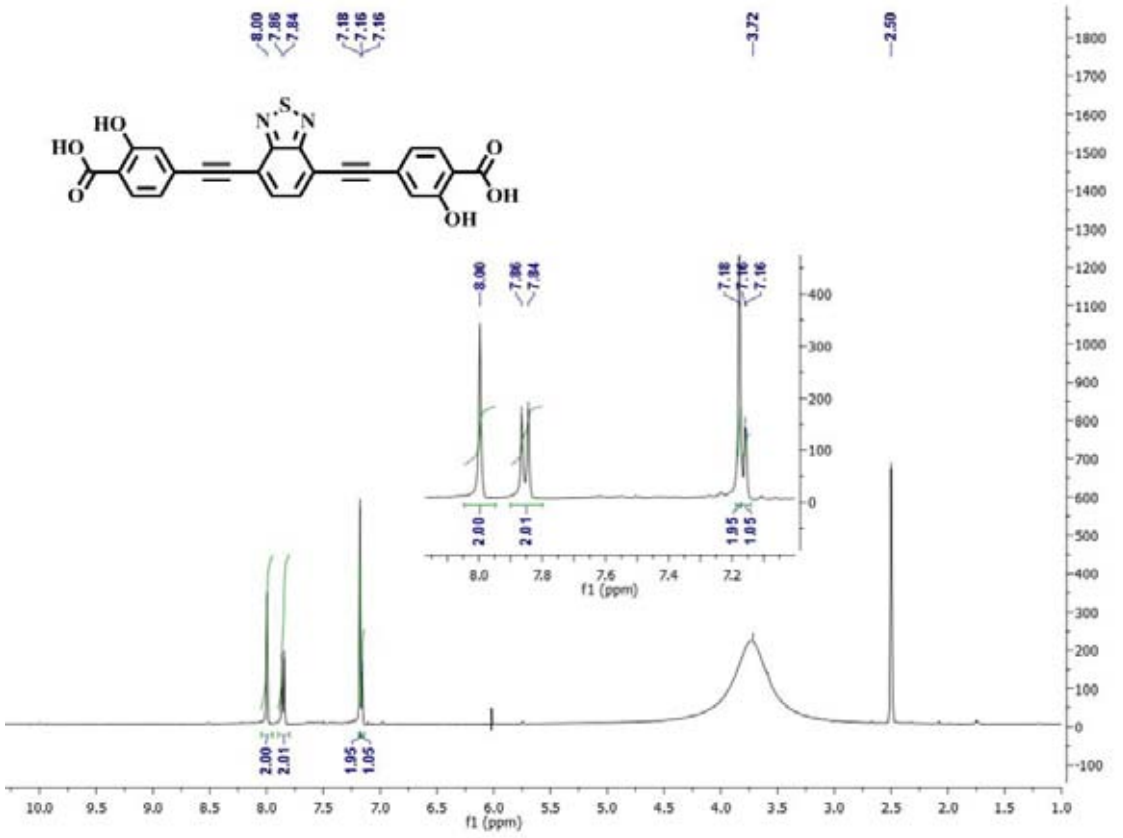

Figure A.52 ^{1}H NMR of **F2** in DMSO-d6.

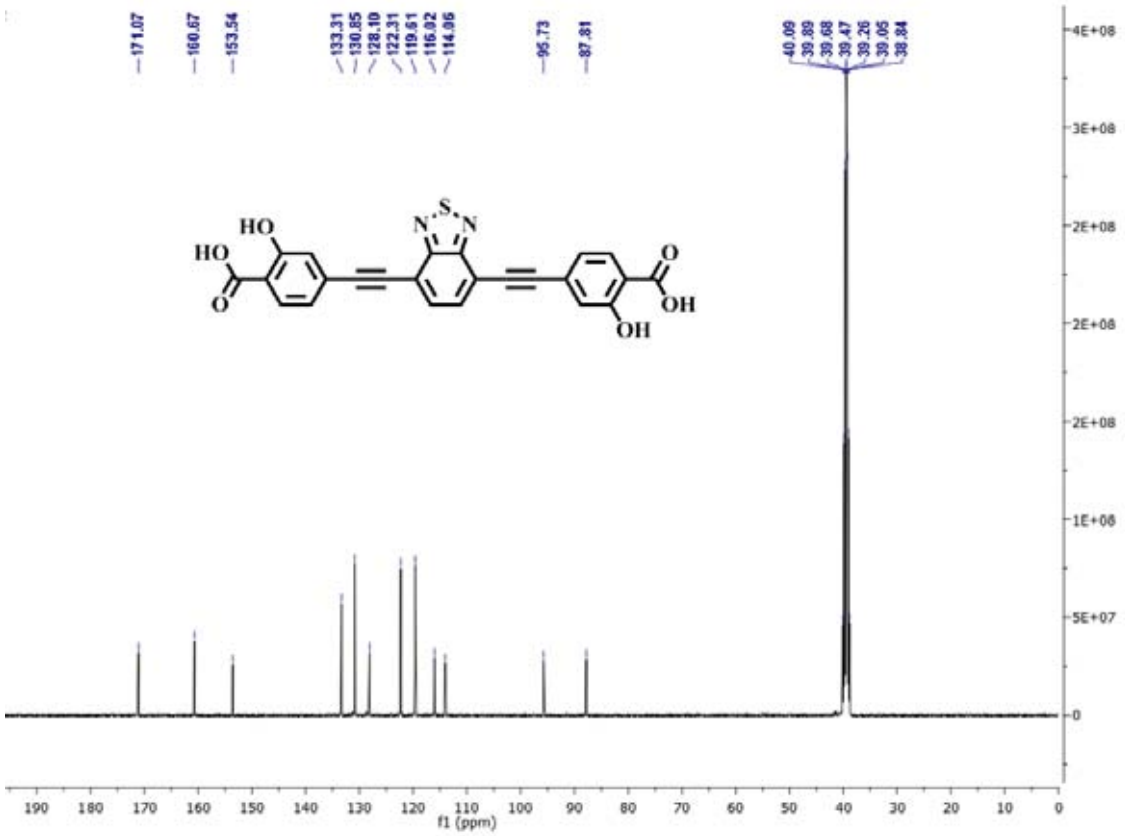

Figure A.53 ^{13}C NMR of **F2** in DMSO-d6.

VITAE

Ms. Nattaporn Kimpitak was born on January 23rd, 1984 in Ratchaburi, Thailand. She graduated with high school degree from Ratchaborikanukroh School, Ratchaburi. She graduated with Bachelor Degree of Science, majoring in Chemistry from Silpakorn University in 2006. In 2008, she has been a graduate student in Petrochemistry and Polymer Science and become a member of Material Advancement via Proficient Synthesis Group under supervision of Assoc. Prof. Dr. Mongkol Sukwattanasinitt and she further received a Master Degree in field Petrochemistry and Polymer Science from Chulalongkorn University. During the course of study, she received the scholarship from the ADB under the Petroleum & Petrochemical Technology Consortium and 100th anniversary of Chulalongkorn University Fund.

Her present address is 98/1 Moo. 10 Jedeehak, Muang, Ratchaburi, Thailand 70000.